FLUORO AND OXOFLUORO ANIONS OF IODINE(V), TELLURIUM(IV), SELENIUM(IV) AND ANTIMONY(III)

by: W.D. Moffett

A thesis submitted to the School of Graduate Studies in partial fulfillment of the requirements for the degree of Ph.D. in Chemistry

UNIVERSITY OF OTTAWA
OTTAWA, CANADA, 1974

ABSTRACT

The synthesis and characterization by x-ray powder photography and Raman and infrared spectroscopy of M_2TeOF_4, $KTe(OH)F_4$ and $M_2TeO_2F_2$ compounds is described. The M_2TeOF_4 compounds are shown to be isomorphous with M_2SbF_5 compounds. The unit cells of M_2TeOF_4 compounds are shown to be nearly the same as those of the corresponding M_2SbF_5 compounds indicating the anion volumes are very similar. The vibrational spectra of the $M_2TeO_2F_2$ compounds show evidence of anion bridging. The Raman and infrared spectra are shown to be consistent with C_{4v} $TeOF_4^{2-}$ and $Te(OH)F_4^-$ ions, and a C_{2v} $TeO_2F_2^{2-}$ ion with the oxygens in equatorial positions. The Raman spectra of TeF_5^- and $Te(OH)F_4^-$ ions in aqueous hydrofluoric acid are reported and assigned, and the hydrolysis constant K_h, for the equilibrium:

$$TeF_5^- + H_2O \overset{K_h}{\rightleftharpoons} Te(OH)F_4^- + HF$$

has been evaluated from Raman peak intensities. There is no evidence for $TeOF_4^{2-}$ or $TeO_2F_2^{2-}$ in solution.

The infrared and Raman spectra of $CsIO_2F_2.1/3H_2O$, $CsIO_2F_2.HIO_2F_2.2H_2O$ and $Co(NH_3)_6(IO_2F_2)_3.H_2O$ have been obtained and interpreted. The compounds are shown to be hydrates and to contain the $IO_2F_2^-$ ion with some departure from the expected C_{2v} symmetry. The Raman spectrum of the $IO_2F_2^-$ ion in aqueous hydrofluoric acid is reported and assigned, and the hydrolysis constant

K_h for the equilibrium:

$$IO_2F_2^- + H_2O \overset{K_h}{\rightleftharpoons} IO_3^- + 2HF$$

has been evaluated from Raman peak intensities. The synthesis of $MIOF_4$ salts is described. The $MIOF_4$ products contain some MIO_2F_2 as impurity. The Raman and infrared spectra of $CsIOF_4$ are reported and assigned. Solutions of HIO_3 in hydrofluoric acid show the presence of IO_3^- and $IO_2F_2^-$ as well as their parent acids, and IF_5. $IO_2F_2^-$ and HIO_2F_2 have been characterized by Raman and NMR spectroscopy in solution. The Raman spectrum of HIO_2F_2 is found to be consistent with a species having C_s symmetry. The Raman and NMR spectra of IF_5 in acetonitrile show the existence of an adduct $IF_5.CH_3CN$. Dissolution of IF_5/H_2O in acetonitrile gives the IOF_4^- ion as well as its parent acid $HIOF_4$. Part of the Raman spectrum of $HIOF_4$ is assigned.

The vibrational spectra of Cs_2SbF_5 and $Co(NH_3)_6Sb_2F_9$ are reported and assigned. Solutions of SbF_3 in hydrofluoric acid show the absence of SbF_5^{2-} up to 48% HF. The Raman spectrum of a solution of SbF_3 in water shows the presence of the SbF_4^- ion.

The vibrational spectra of $KSeO_2F$ are reexamined and found to be consistent with polymeric SeO_2F^- as suggested. Dissolution of SeO_2 in hydrofluoric acid gives H_2SeO_3 and $SeOF_2$ in addition to unidentified oxofluoroselenium(IV) species, most likely SeO_2F^- and $HSeO_2F$.

The stretching frequencies in the vibrational spectra

of the C_{4v} fluoro and oxofluoro species AXF_4E (X = F, OH or O) are correlated, and the observed trends discussed in relation to the stereochemistry of the species. The C_{2v} species are also discussed.

ACKNOWLEDGEMENTS

I am very greatful to Professor J.B.Milne for his continued help and encouragement during the course of the Ph.D. programme.

I would also like to thank Drs. A.R.Davis and R.J. Gillespie for the use of their Raman spectrometers.

TABLE OF CONTENTS

LIST OF FIGURES

LIST OF TABLES

LIST OF SYMBOLS

c_x	Initial concentration of species (mole l^{-1})
M_x	Partially corrected concentration
a_x	Molar activity
$a_{H_2O}(N)$	Activity of water in mole fraction scale
$f_{\pm x}$	Molar activity coefficient

CHAPTER I

Introduction

Since the preparation of the first compound of the inert gases, $XePtF_6$, by Bartlett[1] in 1962, and the subsequent discovery and characterization of the fluorides and oxyfluorides of xenon[2], there has been a renewed interest in the analogous ions and molecules formed by the heavier elements of groups VII, VI and V. In particular iodine, tellurium, selenium and antimony have been studied quite extensively. The penultimate valence state is of special importance due to the presence of the formally non-bonding lone pair of electrons in the valence shell of the species formed. The Valence Shell Electron Pair Repulsion (VSEPR) theory of Gillespie[3] has had some degree of success in predicting the shape of these species, although there remains some degree of uncertainty regarding the role of the $4S^2$ or the $5S^2$ lone pair[4-6]. The alternate Molecular Orbital theory of bonding has also failed to provide a complete understanding of the bonding[7].

This introductory chapter reviews the fluoro and oxofluoro species of xenon, iodine, tellurium, selenium and antimony in their penultimate valence states. The discussion follows an order based on isoelectronic species. Thus all the hexafluoro species AX_6E are dealt with together, and then the pentafluoro species AX_5E, and so on through AOX_4E, AOX_3E, AO_2X_2E and AO_2XE. (A = Xe,I,Te,Se or Sb. O = oxygen. X = halogen, usually F. E = lone valence electron pair)

Fluoro Species

Xenon hexafluoride is prepared by the direct combination of the elements whereby the synthesis follows a stepwise pattern through XeF_2 and XeF_4 [8]. XeF_6 is one of the most thoroughly investigated small molecules of recent years, and the nature of its gas phase symmetry seems to have been solved[9]. Vibrational spectra in the gas phase show 3 distinct Xe-F stretching vibrations[10,11], an observation inconsistent with O_h symmetry. VSEPR theory predicts a C_{2v}, C_{3v} or C_{5v} symmetry for XeF_6 [3]. In the solid phase this compound has been shown to be polymeric[12], and so elucidation of the molecular parameters depends upon electron diffraction measurements on the gas phase[13,14]. These show the molecule to have approximately C_{3v} symmetry having a mean Xe-F bond distance of 1.890 Å, but a radial distribution function for these bonds shows this value to be a composite of non-equivalent bonds. However, any of the structures predicted by VSEPR theory are eliminated on the basis of the observed small dipole moment of $\leqslant 0.03$ D[15]. Goodman[16] and Claasen et al[9] account for the observed vibrational spectra of XeF_6 at various temperatures by an equilibrium mixture of 3 electronic isomers. The explanation proposed by Bartell and Gavin[17] involves a pseudo Jahn-Teller distortion.

Salts of the isoelectronic hexafluoroiodate(V) ion $M^{I}IF_6$, are well known, and their structure has been examined by vibrational[18-21] and Mossbauer spectroscopy[22]. The most recent investigation on the cesium and rubidium salts has shown their structure to be consistent with a distorted octahedral IF_6^- having

a symmetry no greater than C_{2v}[23]. Christe[23] has also isolated a new adduct having the formula $IF_5.3CsF$. Klamm et al[21,24] have observed the vibrational and ^{19}F NMR spectra of Et_4NIF_6 in CH_3CN.

Salts of the isoelectronic tellurium(IV) ion TeF_6^{2-}, have not been investigated in any detail. The literature contains 3 reports of the anion: the pyridinium salt claimed by Aynsley and Hetherington[25], the thiouronium salt which was prepared from aqueous solution by Aynsley and Campbell[26], and the $(NO)_2TeF_6$ salt prepared by Seel and Massat[27]. However, Edwards and Mouty[28] report that the co-ordination of tellurium(IV) cannot be increased over the pentafluoro species. Downs and Adams[29] also report failure to prepare salts of the TeF_6^{2-} ion or to observe it in solution. The other hexahalotellurate(IV) ions are well known, the ions being characterized both in solid salts and in solution[4,30-34]. There is some question as to the shape of the $TeCl_6^{2-}$ ion: some authors report it to be octahedral[4,31,32], while others observe vibrational spectra consistent with some distortion[30]. The $TeBr_6^{2-}$ and TeI_6^{2-} ions have been investigated by quadropole resonance[33] and crystal structure determinations[6,34] which establish the anions to have regular octahedral structures. Again, however, Downs and Adams[30] are not in agreement with these conclusions.

The antimony(III) ion SbF_6^{3-} eludes characterization. There appears to be no report of this ion in the literature, Downs and Adams[29] failing to observe it under what they consider to be the most advantageous conditions. The ready synthesis of the other hexahalo species is well documented[30-32]. Thus the hexahaloantimonate

ions show a greater resemblance to tellurium than to xenon or iodine in that the hexafluoroantimonate(III) ion has not been observed, and the other hexacoordinate halo species all have regular octahedral structures, the $5s^2$ lone pair remaining stereochemically inactive[35,36].

The trisoxalatoantimonate(III) ion is of particular note due to its shape: the use of bidentate ligands has frozen out a pentagonal bipyramidal structure with one vacant site[37,38]. Thus in this 7 electron pair system the stereochemical role of the formally non-bonding lone pair is apparent. The crystal structure of antimony trifluoride has revealed a distorted octahedral arrangement of the fluorines around the antimony[39]. Of course, 3 of these Sb-F bond distances are significantly longer than normal single Sb-F bonds by a value of 0.7 Å. Other bridged or polymeric antimony species do not have this distorted octahedral coordination. An x-ray crystal structure determination on the bridged species $Co(NH_3)_6Sb_2F_9$, prepared as part of this thesis[40], has shown the anion to consist of two square pyramids sharing a corner[41]. A ^{121}Sb Mossbauer spectrum has been reported for this compound, Ballard et al[42] finding the measured isomer shift indicates involvement of the lone pair in the bonding. The existence of the polymeric species KSb_2F_7 has recently been confirmed[43,44], and it has been shown by Ryan and Mastin[44] to have square pyramidal and trigonal pyramidal components arranged in an infinite chain.

Selenium(IV) has a formally non-bonding lone pair, $4s^2$, and Seel and Massat[27] report isolation of the nitrosonium salt of the hexafluoroselenate(IV) ion, $(NO)_2SeF_6$, using selenium tetra-

chloride as starting material.

$$SeCl_4 + 6FSO_2NO = (NO)_2SeF_6 + 4NOCl + 6SO_2$$

In the reaction of NO_2F with SeF_4, however, Aynsley et al[45] succeeded only in preparing the pentafluoro species $(NO_2)SeF_5$. Some hexacoordinate ions of the other halogens have been isolated in salts, for example $(NH_4)_2SeBr_6$[46]. A crystal structure determination on K_2SeCl_6 has also shown the anion to be a regular octahedron[4]. Hendra and Jovic[47] have prepared many salts of the $SeCl_6^{2-}$ anion, and they have observed it in solutions of SeO_2 in concentrated HCl.

Thus very little information about the role of the lone valence electron pair in fluoro anions of the heavier main group elements can be gleaned from the hexafluoro species due to the lack of any structural information on TeF_6^{2-} and SeF_6^{2-}, and the lack of reports of the SbF_6^{3-} anion. As a result considerable attention has been focused on the pentafluoro species, AX_5E.

Pentafluoro species are known for all five elements, Xe(VI), I(V), Te(IV), Se(IV) and Sb(III). VSEPR theory predicts a square pyramidal structure for AX_5E species[3]. This predicted structure is distorted from a regular square pyramid in two ways: firstly the angle between the apical F_a and the basal fluorines F_b is closed

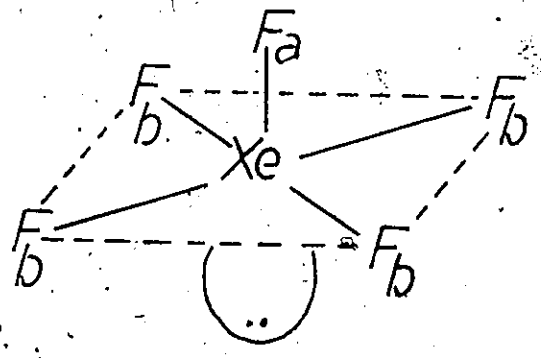

$Xe\text{-}F_a < Xe\text{-}F_b$

$\angle(F_aXeF_b) < 90^\circ$

down to less than 90°. This is due to the greater repulsive effect of the lone pair on the basal bond pairs compared to the bond pair which is trans to it. Secondly, again as a result of the greater lone pair - bond pair repulsion, the central atom basal fluorine bonds are longer and weaker than the apical bond which is trans to the lone pair. The structure of XeF_5^+ in a number of salts[49-51], as well as in XeF_6 itself[52,53] has been investigated and found to be square pyramidal with the distortion as predicted. The bond angle and distances are given in Table I.

TABLE I

Molecular Parameters for AF_5E Species

	XeF_5^+ a	IF_5 b	TeF_5^- c	SbF_5^{2-} d
R,Å (apical)	1.76	1.84	1.86	1.916
r,Å (basal)	1.82	1.87	1.95	2.075
β, (degrees)	80.4	81.9	78.8	79.4

a ref 47, b ref 55, c ref 28, d ref 69

The existence of the neutral molecule IF_5 has been known for a long time[54], and its structure has been investigated by electron diffraction[55], vibrational spectroscopy[56-59] and ^{19}F nmr[60].

All of these indicate a square pyramidal structure. This configuration has also been observed for the IF_5 entity in the adduct $IF_5.XeF_2$ [61]. The electron diffraction study of Robiette et al[55] shows IF_5 is isostructural with XeF_5^+, and their molecular parameters are given in Table I.

Moving one position to the left in the periodic chart, the isoelectronic ion TeF_5^- has been the subject of an extensive investigation. Salts of this ion have been prepared in liquid SeF_4 [63].

$$TeO_2 + MF + SeF_4 = MTeF_5 + 2SeOF_2$$

The original method of preparation from aqueous HF [62] has also been shown to yield pure salts[64]. A hydrate $Ba(TeF_5)_2.H_2O$ is reported as having been isolated from aqueous solution[65]. The vibrational spectra of TeF_5^- have been investigated in solution in acetonitrile and in nitromethane[29], and in salts, both as the powder[66] and a single crystal[58]. A single crystal x-ray determination by Edwards and Mouty[28] has established the anion to be square pyramidal, the lone pair again occupying the position trans to the apical fluorine. The molecular parameters reported by these authors are given in Table I.

Salts containing the isoelectronic antimonate(III) ion SbF_5^{2-} were first prepared in 1871[67], and later by Bystrom and Wilhelmi[68]. The original crystal structure of these authors on $(NH_4)_2SbF_5$ was verified by Ryan and Cromer[69]. Once again, as for TeF_5^-,

the anion is square pyramidal, the F(apical)-Sb bond distance being shorter than the basal bond distances and the (F_aSbF_b) angle is closed down from 90°. The observed molecular parameters are given in Table I. Vibrational spectroscopy has been used to observe the ion in solution in acetonitrile[29]. Birchall and Della Vale[70] have observed the ^{121}Sb Mossbauer spectrum of the ion in the potassium salt finding a lower S electron density at the nucleus than in the corresponding chloro salt. These authors account for this in terms of the $5s^2$ electron pair involvement in the bonding of the pentafluoroantimonate(III).

The reaction of liquid SeF_4 with an alkali metal fluoride gives salts of the SeF_5^- ion[71]. Christe[66] has recently observed the vibrational spectra of $CsSeF_5$, finding the results consistent with the anion having C_{4v} symmetry. An x-ray powder photograph on the potassium salt indicates it to be isostructural with $KTeF_5$ [72].

Oxofluoro Species

The most highly coordinated oxyfluoride of xenon(VI) is $XeOF_4$, and this molecule has been shown to exist as a discrete species[73]. VSEPR theory predicts a square pyramidal structure for $XeOF_4$ with O axial. The square pyramid will be distorted with the (OXeF) angle being less than 90° due to the greater repulsive effect of the lone pair on the basal bond pairs. However, the anomalous structure of $XeOF_4$ is well established, the (OXeF) angle being in fact 91.8° [74]. The complete molecular parameters are given in

Table II.

TABLE II

Molecular Parameters for AOF_4E Species

	$XeOF_4$ [a]	IOF_4^- [b]
R, Å (apical)	1.703	1.72
r, Å (basal)	1.900	1.965
β, (degrees)	91.8	88.5

a ref 74, b ref 75

The infrared and Raman spectra of the compound are consistent with C_{4v} symmetry[73].

The isoelectronic ion IOF_4^- was first postulated by Klamm and Meinert[24] when hydrolysis of IF_6^- in acetonitrile revealed the presence of a Raman band at 890-900 cm^{-1}, the IO characteristic stretching frequency. Ryan and Asprey[75] recently isolated the cesium salt from a solution of CsF and IF_5 in acetonitrile and an unidentified oxygen source. The crystal structure determination by these authors has found the molecular parameters recorded in Table II. The (OIF) angle is closed down to 88°, and this trend of the angle closing down as we move to the left in the periodic chart has not been observed for the isoelectronic pentafluoro species, see Table I.

The literature contains no reports of the isoelectronic ion $TeOF_4^{2-}$, and apart from the early work of Prideaux and Millott[76], oxyfluorides of tellurium(IV) have received little attention[72].

There is no report of the preparation or observation of oxofluoro anions of antimony(III), although the existence of oxofluoro anions of antimony(V) and tellurium(VI) in the higher oxidation states is well documented[77-80]

The preparation of $XeOF_3^+$ by Bartlett et al[81] in salts with SbF_6^- and $Sb_2F_{11}^-$ and their investigation by Raman spectroscopy has shown the structure of $XeOF_3^+$ to be consistent with a distorted trigonal pyramidal configuration: two fluorines being axial and the third sharing the equatorial plane with the oxygen and the lone pair. This is the structure VSEPR theory would predict for such a species[3].

In their preparation of the isoelectronic IOF_3, Aynsley et al[82] felt that this species must contain ionic IO_2^+ and the well known IF_6^-. However, a crystal structure determination by Viers and Baird[83], and more recently by Edwards[84], shows IOF_3 to have the

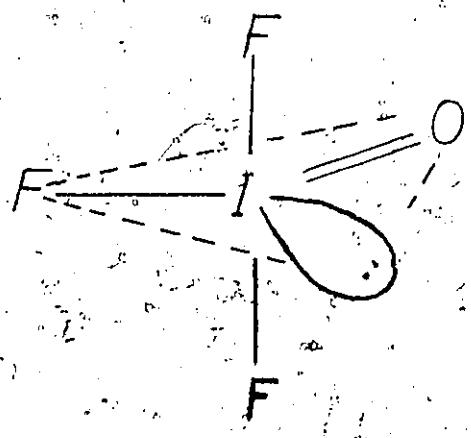

expected trigonal pyramidal configuration with two of the fluorines in the axial positions. These crystal structure determinations show many intermolecular IO and IF contacts considerably less than the sum of the van der Waals radii.

The selenium analogue, $SeOF_3^-$, has been characterized by Paetzold and Aurich[85] and these authors report the structure of a distorted trigonal bipyramid to be consistent with the vibrational spectra. Again, two of the fluorines are axial while the remaining three positions are occupied by the oxygen, the lone pair and the third fluorine. A crystal structure determination has been done on the analogous chloro anion, $SeOCl_3^-$, as the 8-hydroxyquinolium salt by Cordes[86], this author finding the anion to be polymeric, essentially consisting of a distorted square pyramidal configuration about the selenium. Each selenium is surrounded by one oxygen and five chlorine atoms. The Se-O bond distance is similar to that observed for other compounds. However, the Se-Cl distances vary quite considerably, two of them being 2.23 and 2.27Å, similar to that observed for a number of other selenium-chlorine compounds[87], two are 2.96 and 2.99Å, and the fifth chlorine atom is at a distance of 3.3Å, only just shorter than the sum of the non-bonding radii, 3.86Å.

The existence of pentacoordination about the selenium in this case indicated the possibility of isolating a salt of the $SeOCl_4^{2-}$ anion. Cordes and Bi-Cheng Wang[88] prepared the dipyridinium salt of this ion again finding the coordination about the selenium a little unusual. Selenium-chlorine distances vary from 2.244 to 2.990Å. The four Se-Cl bonds in each $SeOCl_4^{2-}$ unit can be grouped

into three catagories: bonds of 3.0Å which can be characterized as some type of ion-dipole association[89], those of 2.24Å, normal single bonds, and bonds of intermediate distance, 2.5Å. Thus the immediate environment about the selenium could be classified as a trigonal pyramidal $SeOCl_3^-$ unit, the axial chlorines at 2.5Å and the equatorial Cl at 2.24Å, the oxygen and the lone pair occupying the equatorial plane.

There is no report of the analogous $SeOF_4^{2-}$ ion in the literature, and the preparation of $KSeOF_3$ by Paetzold and Aurich[90] always favoured this lower coordinated species due to the large excess of $SeOF_2$, which was used as solvent.

$$KF + SeOF_2 = KSeOF_3$$

Alkali metal salts of $SeOCl_3^-$ were first reported by Wise[91] and are reported to contain discrete anions by Paetzold and Aurich[85], in sharp contrast to the observed coordination in the 8-hydroxyquinolinium salt[86].

Reaction of $XeOF_4$ with XeO_3 yields the xenon(VI) dioxide difluoride first prepared by Houston[92].

$$XeOF_4 + XeO_3 = 2XeO_2F_2$$

The examination of this compound by Houston and others[93] by vibrational spectroscopy has shown its structure to be consistent with a discrete molecular species having C_{2v} symmetry. Thus the mol-

ecule has a pseudo trigonal bipyramidal structure where the 2 F atoms are axial and the oxygens and the lone pair share the equatorial plane. This is the structure VSEPR theory predicts for a XY_2Z_2E species[3]. There is some question as to the monomeric nature of XeO_2F_2 in the solid.

The isoelectronic $IO_2F_2^-$ ion has been isolated from aqueous solution as the potassium salt, and Helmholtz and Rodgers[94] have reported its crystal structure. Their determination shows this anion to have a pseudo trigonal bipyramidal structure exactly analogous to that proposed for XeO_2F_2.

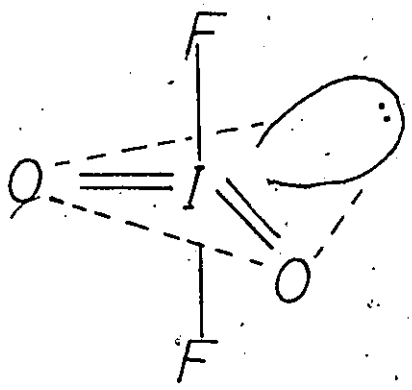

The two fluorine atoms are axial while the oxygen atoms and the lone valence electron pair occupy the three equatorial positions. The (FIF) angle is 180° and the (OIO) angle approximately 100°. In addition these authors report two IO...I nearest neighbour distances of 2.82 and 2.85Å, considerably shorter than the sum of the van der Waals radii, 3.5Å. The recent vibrational spectra of Carter and Aubke[95] support the earlier report of the splitting of the (IO_2) stretches in the infrared spectrum[96]. The appearance of more bands

than are allowed for C_{2v} symmetry could, of course, be explained by some polymerization over oxygen bridges.

Although the isoelectronic selenium ion $SeO_2F_2^{2-}$ is reported by Mitra and Kundu[97] as the hydrated zinc salt, $ZnSeO_2F_2.6H_2O$, no structural information is recorded. These authors have also reported the isolation of the parent acid, $H_2SeO_2F_2$. Prideaux and Millott[98] report an oxyfluoride with a melting point of 18°C having the composition $SeO_2.5HF$. A more recent study[99] on this SeO_2-HF system reports the composition of this compound to be $SeO_2.4.5H_2F_2$.

The lower oxofluoro cation XeO_2F^+ has been characterized by ^{19}F nmr and vibrational spectroscopy[100], and a trigonal pyramidal geometry is found to be consistent with the results.

Iodyl fluoride is obtained by the disproportionation of IOF_3 at 110°C [82,101-103].

$$2IOF_3 = IO_2F + IF_5$$

The ready hydrolysis of this compound to iodic and hydrofluoric acids is noted[101]. Carter and Aubke[95] find evidence for the existence of IO_2^+ non-bridged groups in iodyl fluoride by examination of the vibrational spectra. The number of bands they observe however, leaves some doubt as to the monomeric nature of the compound. TeO_2 is isoelectronic to IO_2^+ and it has been shown to be polymeric[137]. The adduct of IO_2F with AsF_5 has been suggested to contain IO_2^+

and AsF_6^- entities rather than the alternate $IO_2F_2^-.AsF_4^+$ formulation[96]. The infrared spectra of several authors does not support the existence of IO_2^+ in this compound[95,96]. Carter and Aubke[95] prefer a complex either a bridging oxygen as has been observed for $NbF_5.SeOF_2$ [105], or a AsF_6^- anion any a polymeric I-O-I bridged counter cation.

The analogous selenium ion has been prepared by Paetzold and Aurich[106], who have isolated the potassium salt from a melt at 300°C.

$$SeO_2 + KF = KSeO_2F$$

From their observed vibrational spectra, and in particular the frequency of the Se-F stretching vibrations, these authors conclude the SeO_2F^- species is polymeric. This is in sharp contrast with the fluorosulfinite ion which has been found to be monomeric[107].

Oxo Species

XeF_4 and XeF_6 are hydrolyzed by water to give XeO_3 [108,109]. Conductivity and Raman experiments suggest XeO_3 exists in solutions in concentrations up to 11M[110]. In basic solution, however, $HXeO_4^-$ is reported to be the predominant species[111]. The Raman spectrum of XeO_3 is found to be consistent with a molecule having C_{3v} symmetry, the shape predicted by VSEPR theory[3].

The vibrational spectra of iodate salts have been investigated widely[112-114]. Conductivity[112,114] and Raman[112,115]

experiments have been used to investigate the nature of aqueous solutions of iodic acid. At high concentrations, up to 6M, complex species are reported to exist in solution[116]. The crystal structure of iodic acid reveals a large degree of intermolecular association[117].

Tellurium dioxide is polymeric [137]. Tellurous acid H_2TeO_3 is readily dehydrated to the dioxide[118]. Both acid and normal salts are known, and their vibrational spectra have been investigated[119].

Selenium dioxide is also polymeric[120], and while selenous acid is very soluble in water, Raman studies indicate the presence of H_2SeO_3 and $HSeO_3^-$ only[121]. Acid and normal salts are well known and their vibrational spectra have been investigated[122].

Antimony trioxide is polymeric, the lattice consisting of Sb_4O_6 units[123]. Dissolution of the trioxide in either acids or bases yields antimonous salts[111].

****

This present study was undertaken to investigate the nature of the aqueous fluoride chemistry of iodine(V), tellurium(IV), selenium(IV) and antimony(III). The systematic study of the fluoro and oxofluoro anions of these elements should add to our understanding of the stereochemical role of the lone valence electron pair in these species.

As a general rule inorganic fluorine chemists exclude water, as far as possible, from systems under study and products showing hydrolysis are avoided. It was felt, however, that the aqueous fluorine chemistry of tellurium(IV), iodine(V) and antimony

(III) and selenium(IV) would prove fruitful since the possibility of many oxofluoro species should provide a variation in the coordination of the central atom. This diversity of coordination should lead to a better understanding of the stereochemical role of the lone valence electron pair.

Furthurmore, between the traditional interest in oxo anion behaviour in aqueous solutions and, more recently, interest in fluoro anion equilibria in 100% HF, equilibria in aqueous hydrofluoric acid have been little studied. Thus, the hydrolysis equlibria of both fluoro and oxofluoro anions in aqueous solution are included in this study.

The order in which the elements studied are dealt with in the following chapters is based upon the completeness of the work. Thus, tellurium is dealt with first since the fluorine and oxyfluorine chemistry of this element is most understood. Iodine is dealt with next, and then antimony and selenium. The latter two elements are considered together since the work on them is of a somewhat preliminary nature.

CHAPTER II

Experimental

1.Materials and Apparatus

Metal Fluorides

Cesium fluoride, 99% (Ozark-Mahoning); rubidium fluoride, 99% (K&K); and potassium fluoride, 98% (B.D.H.) were used after drying for 12 hrs under vacuum. Barium fluoride, 99% (Fisher) and silver fluoride, 99% (Ozark-Mahoning) were used similarily. Antimony trifluoride, 99% (Ozark-Mahoning) was used after vacuum sublimation.

Tetraalkylammonium Fluorides

These were prepared by literature methods[124,125]. Tetramethylammonium fluoride was prepared by dehydration of the trihydrate[124] (Eastman Chemicals), by heating at 130°C under vacuum. Tetraethylammonium fluoride pentahydrate was formed on neutralization of 10% tetraethylammonium hydroxide (Eastman), by 10% hydrofluoric acid[124]. Attempted preparation of anhydrous tetraethylammonium fluoride by the method of Hayami et al[125], used by Downs and Adams[29], yielded only the monohydrate. The products were verified by fluoride analysis. Analysis. Calcd for $Et_4NF.H_2O$: F, 10.27. Found: 10.2.

Heavy Metal Oxides and Oxoacids

Antimony trioxide (J.T.Baker, analysed) was used directly.

Figure 1

Apparatus for the Preparation of Iodine Pentafluoride

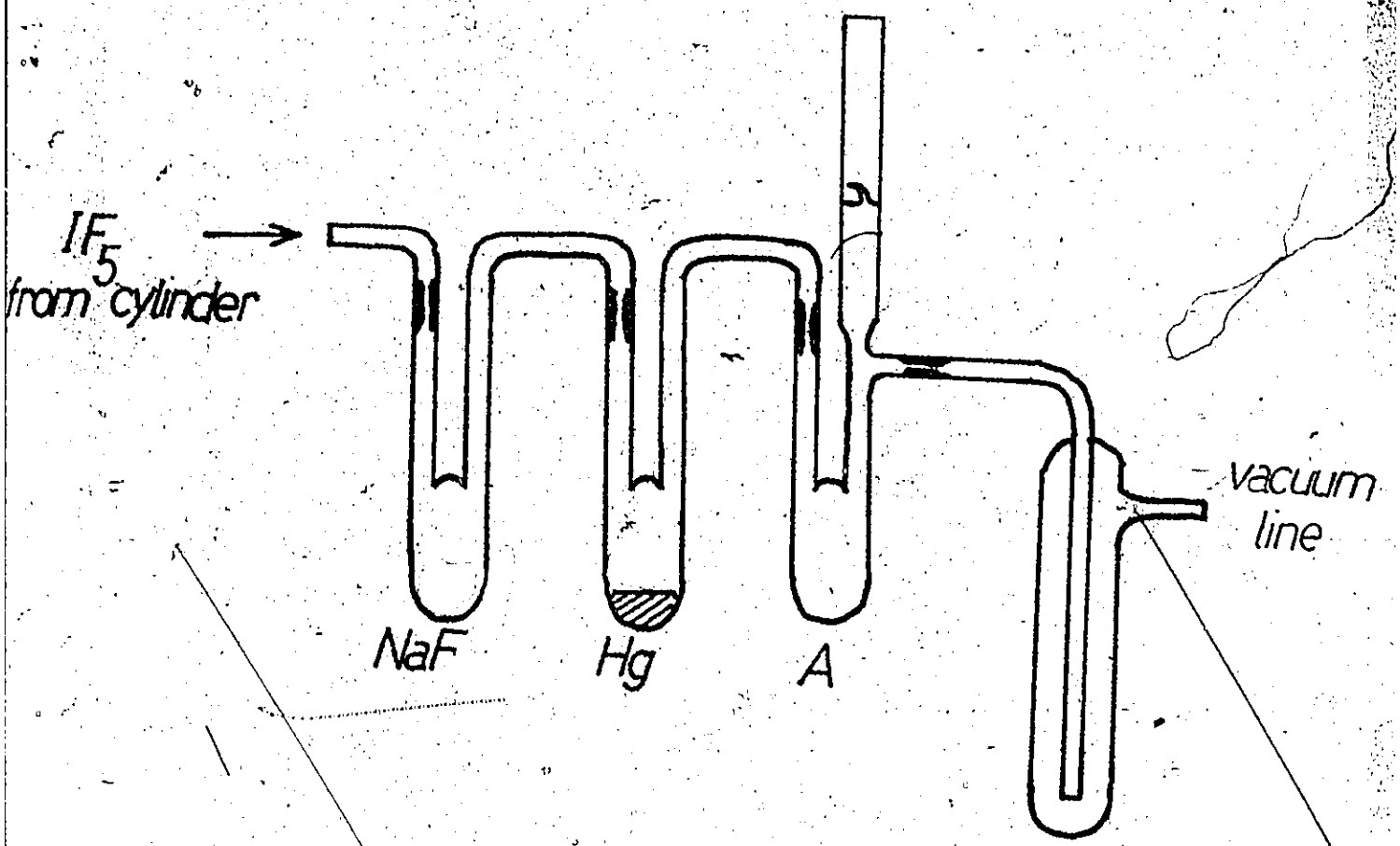
IF_5
from cylinder
NaF
Hg
A
vacuum
line

Tellurium dioxide, 99% (Fisher) and selenium dioxide, 99.9%, (Alfa Inorganics) were used after drying for 12 hrs under vacuum. For some of the Raman experiments, selenium dioxide was obtained by dehydration of freshly prepared selenous acid in a vacuum desiccator. Iodic acid, 99% (B.D.H) was used directly.

Sulfur Dioxide

Matheson high purity grade was used directly.

Iodine Pentafluoride

Iodine pentafluoride, 98% (Matheson) was purified by trap-to-trap distillation from NaF, to remove traces of HF, and from Hg, to remove traces of iodine, under vacuum in the all-glass apparatus shown in Figure 1. The product thus obtained was stored in a glass break-seal container, A, at 0°C until required. Over a period of several weeks there was no apparant decomposition or attack on the glass.

Hydrofluoric Acid

48% HF (J.T.Baker) was used directly after standardization with NaOH using phenolphthalein as indicator.

100% HF (Matheson, anhydrous) was used after a single vacuum distillation. For the manipulation of HF a monel vacuum line equipped with Kel-F traps (Argonne National Laboratory) and sealed diaphram monel Hoke valves was used. The pressure in the line was measured by a monel Bourdon-type gauge 0-1500 mm ±5mm, (Helicord).

Figure 2

Schematic Diagram of the Monel Vacuum Line

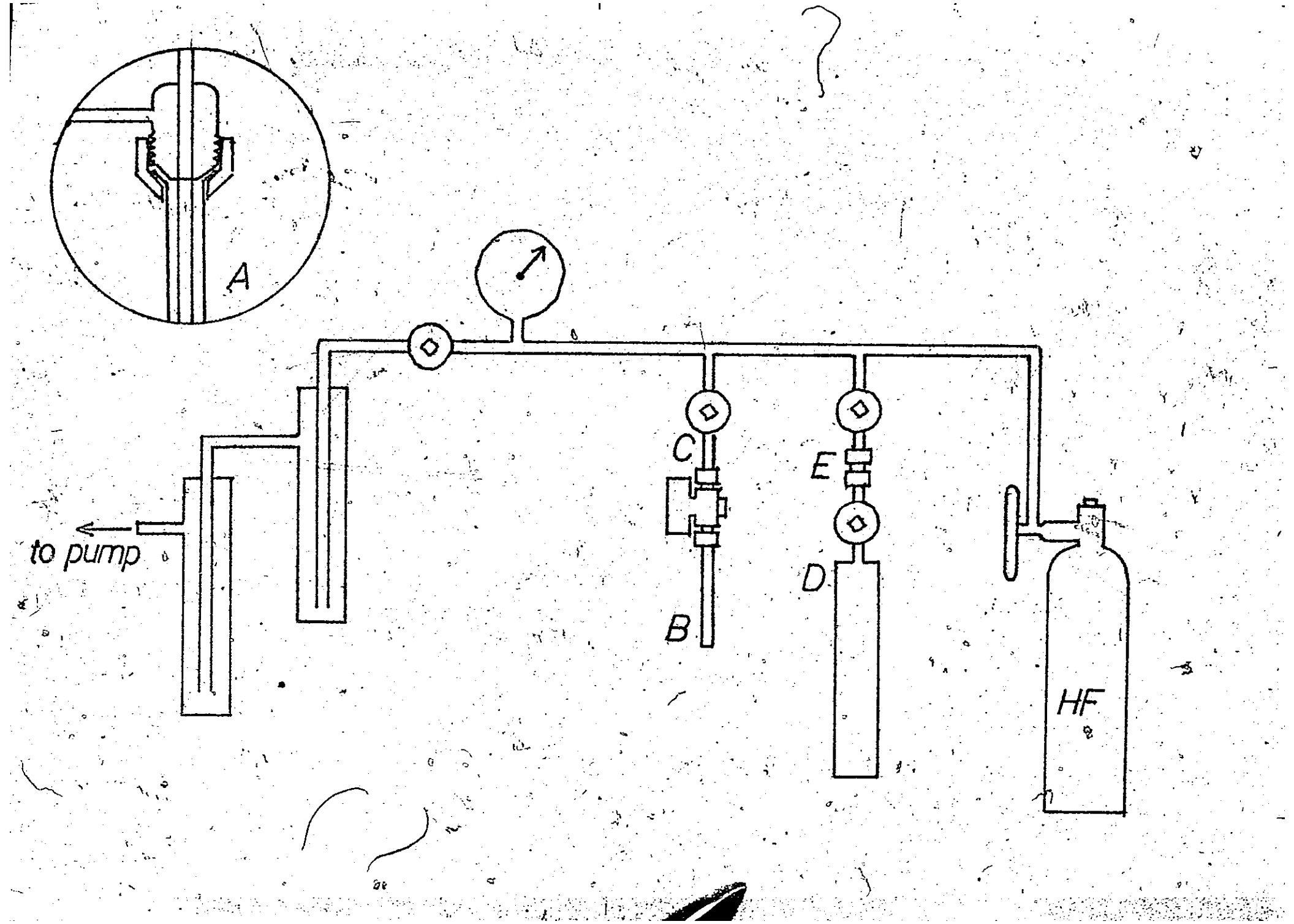
A
to pump
C
B
E
D
HF

A schematic diagram of the vacuum line is shown in Figure 2. The Kel-F traps are attached to the line by means of a flare-type fitting, insert A. The Kel-F trap at D, which could be closed by a Hoke valve and could be removed from the line via a 3/4" brass Swagelock fitting, E, served as a reaction vessel. For the Raman experiments, the sapphire cell B, was connected to the outlet C using an all-Teflon needle valve equipped with 1/4" Teflon Swage-lock ports (Nupro). The Kel-F inserts for the nmr studies were also attached at the same outlet by means of a 3/16" brass Swagelock.

Selenium Oxychloride

Selenium oxychloride (J.T.Baker, analysed) was used after a single vacuum distillation.

Potassium Chloride

99.8% potassium chloride (B.D.H., Analar) was used after drying for 12 hrs under vacuum.

Acetonitrile

Acetonitrile (Eastman, anhydrous) was dried by refluxing over P_2O_5 followed by distillation.

Dimethylsulfoxide

DMSO (Fisher) was dried over molecular sieves for 12 hrs and then distilled at reduced pressure.

Pyridine

Pyridine (Fisher) was used directly.

2.Infrared and Raman Spectra

Infrared Specrta

Infrared spectra were taken as mulls in Nujol or Fluorolube, using CsBr plates, on a Beckmann IR 20A spectrometer. The spectra were calibrated by reference of the Nujol peaks to standard polystyrene peaks. All reported frequencies are ± 3 cm^{-1}.

Ráman Spectra

Raman spectra were recorded on a Jarell-Ash series 300 spectrometer. For some of the solid spectra a Spex Industries double monochromator was used. A Spectra-Physics argon ion laser was used in both cases, and detection was by a cooled photomultiplier tube. A spike filter was used to remove plasma lines from the solid spectra. Solid samples were contained in 1 mm o.d. pyrex tubes, and for solutions, a cylindrical sapphire cell 10 cm long x 5 mm i.d. (Tyco, Sapphikon Division) was used. For solutions up to 48% HF this was closed with a plastic cap, and for solutions above this concentration an all-Teflon needle valve equipped with 1/4" Teflon Swagelock ports was used. Slit widths were generally 5 cm^{-1} for solid samples and 10 cm^{-1} for solutions. Integrated peak intensities were measured with a planimeter and were accurate to within ±3%. All integrated peak intensities were referenced to ν_1 of ClO_4^- (925 cm^{-1}) = 100.

3. X-Ray Powder Photography

The x-ray powder photographs were taken in Lindemann tubes, 0.5 and 0.3 mm, using Cu K irradiation. Debye-Scherrer cameras of 11.5 and 5.75 cm were used. Film shrinkage and other errors were allowed for by referencing the sample reflexes to those of KF. All intensities were estimated visually and were referenced to the strongest line being equal to 100. An insufficient number of h 0 0, 0 k 0, and 0 0 l reflexes were observed to carry out Nelson-Riley plots.

4. ^{19}F Nuclear Magnetic Resonance

Spectra were taken on a Varian Associates HA-100 spectrometer. The temperature was regulated by a Varian Temperature Controller and was accurate to $\pm 5^{\circ}C$. Samples were contained in Kel-F tubes which could be inserted into glass NMR tubes. Shifts were referenced to $CFCl_3$ as an external standard. Solute transfers were made in the dry-box, and the Kel-F tubes were attached to the line as described in Section 1. The tubes were heat-sealed under vacuum.

5. Chemical Analysis

Fluoride

Analysis for fluoride was done by titration with La^{3+} using a F^--sensitive electrode. Interferences due to complexing of the fluoride by Sb(III), Te(IV) or Se(IV) were avoided by removal of the heavy metal from solution. This was accomplished by precipitation with H_2S. After removal of the precipated heavy metal the

solution was neutralized with dilute NH_4OH and reduced in volume on a hot plate.

The tetraalkylammonium fluorides were analysed directly. It was found that fluoride analysis by titration with La^{3+} was not possible in the presence of iodate(V). The titration of 2:1 $KF-HIO_3$ mixtures as well as the fluoroiodates gave reasonably sharp end points, but the results were 20% too high. Distillation from dilute H_2SO_4 solution failed to separate the iodine which distilled over with the fluoride. Thus Weinland's[126] original method was adopted and the total number of acid equivalents determined by titration with standard NaOH using phenolthalein as indicator.

Tellurium and Selenium

These were determined volumetrically using $KMnO_4$ and back-titrating with ferrous ion[127].

Iodine

This was analysed as iodate(V) by reduction with KI and titration of the liberated iodine with $Na_2S_2O_3$ [127].

Ammonia

The ammonia in the hexamminecobaltsalts was analysed by treatment of the salt with an excess of a strong base and distillation of the liberated ammonia into a known excess of standard acid. The excess acid was then determined volumetrically[127].

Cobalt

This was analysed spectrophotometricaly using standard solutions of $Co(NH_3)_6Cl_3$ for calibration. Solutions of $Co(NH_3)_6Cl_3$ in dilute HCl were shown to obey the Beer-Lambert law over the concentration range 20-120 mg/100 mls at λ_{max} = 570 nm.

6.Preparation of the Compounds

(i) Antimony(III) Compounds

M_3SbF_6: Attempted preparation of salts of the hexafluoroantimonate(III) ion from solutions according to the hypothetical equation in CH_3CN

$$3MF + SbF_3 = M_3SbF_6 \quad (M = Cs, Rb, K, Et_4NF \text{ and } Me_4NF)$$

yielded only M_2SbF_5 and MF as shown by the infrared spectra (540 cm^{-1}) and x-ray powder photographs. A similar reaction employing SO_2 as solvent yielded the MSO_2F salts indicating SO_2 to be a better fluoride acceptor than SbF_3.

A melt of CsF and Cs_2SbF_5, though providing solution at 300°C, proved unsuccessful.

Preparations attempted from aqueous HF also gave only the familiar pentafluoroantimonate salts.

$Co(NH_3)_6Sb_2F_9$: Hexamminecobalt nonafluoroantimonate(III) was prepared from a 0.2M solution of $Co(NH_3)_6F_3$ and a solution of Sb_2O_3 in 48% HF. The $Co(NH_3)_6F_3$ solution was prepared by dissolving 0.01 moles of $Co(NH_3)_6Cl_3$ in water and adding a saturated solution of

of AgF, 0.03 mole . The precipated AgCl was filtered off and the resulting solution was concentrated to 50 ml on the vacuum line. 0.01 mole of Sb_2O_3 was dissolved in a minimum ammount of 48% HF and the resulting solution was filtered to remove any suspended particles. Addition to the $Co(NH_3)_6F_3$ solution yielded a good crop a dark orange crystals on cooling in dry ice. The crystals were collected at the pump, washed with a few mls of ice-cold ethanol and dried under vacuum. Analysis. Calcd for $Co(NH_3)_6Sb_2F_9$: NH_3, 17.73. Found: 17.89. Sb, 42.32. Found: 42.15. F, 29.71. Found: 29.47.

$M^I_2SbF_5$: These salts were prepared by standard methods [70] and analysed for fluoride.

(ii) Tellurium(IV) Compounds

M_2TeF_6: Two of the literature methods claiming salts of the hexafluorotellurate anion were attempted. The proceedure for the preparation of the pyridinium salt[25] yielded only the pentafluorotellurate, $PyHTeF_5$. Analysis. Calcd for $PyHTeF_5$: F, 31.39. Found: 31.9. Similarly, the literature method for the dithiouronium salt[26] yielded only the familiar pentafluorotellurate. The product was verified by its infrared spectrum. Seel and Massat[27] report the preparation of $(NO)_2TeF_6$, but their procedure was not attempted.

Preparations were attempted from aqueous HF using tetraalkylammonium salts but these too yielded the pentafluorotellurates. Seemingly, the HF itself is a better fluoride acceptor

forming HF_2^-, and resulting in the failure to increase the coordination of the tellurium.

A 1:1 molar mixture of MF and $MTeF_5$ (M = Cs and Me_4N) was shaken for several days in an acetonitrile solution but also failed to produce the hexafluorotellurate species.

M^ITeF_5: The pentafluorotellurate(IV) salts were prepared by standard methods[64] and analysed for fluoride.

$KTe(OH)F_4$: 6.4 g TeO_2 (0.040 mole) and 4.0 g $KHCO_3$ (0.040 mole) were weighed into a Teflon dish and 6.2 ml of 28.0M HF added (0.016 mole). 20 mls of water were added and the mixture was heated to give solution. After filtering to remove any suspended particles, the solution was allowed to cool. The large crystals which separated were collected by suction filtration and recrystallized once from water. The product was dried in a vacuum desiccator over $CaCl_2$. Analysis. Calcd for $KTe(OH)F_4$: F, 29.26. Found: 29.34. Te, 49.13. Found: 49.14.

A second recrystallization proved impossible since dissolution in water was accompanied by some hydrolysis. However, dissolution in dilute HCl solution (Te:Cl = 1:1) yielded back $KTe(OH)F_4$ on crystallization, indicating the stability of the $Te(OH)F_4^-$ ion in dilute acid solution.

The compound was also prepared by forced hydrolysis in acetonitrile:

$$KTeF_5 + H_2O + KF = KTe(OH)F_4 + KHF_2$$

Equimolar amounts of the reactants: $KTeF_5$, H_2O and KF were refluxed for 2 hrs in a glass apparatus. An infrared spectrum of the dried filtered product showed the Te-OH stretching frequency (698 cm^{-1}) and the characteristic bands of KHF_2 at 1200 and 1475 cm^{-1}.

$CsTe(OH)F_4$ and $NaTe(OH)F_4$: Attempts to prepare the cesium salt by the analogous method yielded a mixture of the pentafluorotellurate and the hydrolysed product which could not be separated by recrystallization. It was also not possible to prepare the sodium salt by the above method since even highly concentrated solutions failed to crystallize.

Cs_2TeOF_4 and K_2TeOF_4: Cs_2TeOF_4 was prepared by mixing TeO_2, $CsTeF_5$ and CsF in the proportions 1:1:3 in a platinum boat.

$$TeO_2 + CsTeF_5 + 3CsF = 2Cs_2TeOF_4$$

A typical reaction had 0.277 g TeO_2(0.00173 mole), 0.617 g $CsTeF_5$ (0.00174 mole) and 0.791 g CsF (0.00523 mole). All materials were handled in the dry box. The boat was then transferred to a quartz tube and heated slowly in a stream of dry nitrogen to 500°C, at which temperature a clear colourless melt was formed. Further heating to 900°C had no effect upon the products. A white crystalline product was obtained on cooling. Analysis. Calcd for Cs_2TeOF_4: F, 15.65. Found: F, 15.7.

An x-ray powder photograph of the product showed no CsF, $CsTeF_5$ or TeO_2 lines.

K_2TeOF_4 was prepared in an analogous manner with a melt forming at 550°C.

$$TeO_2 + KTeF_5 + 3KF = 2K_2TeOF_4$$

The product was again stable to higher temperatures. Again an x-ray powder photograph revealed the absence of the starting materials.

An attempted preparation of Cs_2TeOF_4 by refluxing the reactants in DMSO for 24 hr showed no evidence of change in the starting materials.

$Cs_2TeO_2F_2$ and $Rb_2TeO_2F_2$: $Cs_2TeO_2F_2$ was prepared by mixing TeO_2 and CsF in the ratio 1:2.

$$TeO_2 + 2CsF = Cs_2TeO_2F_2$$

The reactants were handled in the dry box and placed in a platinum boat. The boat was slowly heated in a stream of dry nitrogen, to 800°C at which temperature a clear colourless melt was formed. Furthur heating to 900°C had no effect upon the reaction. A typical reaction had 1.60 g TeO_2 (0.01 mole) and 3.04 g CsF (0.02 mole). A white crystalline product was obtained on cooling. An x-ray powder photograph revealed the absence of the starting materials CsF and TeO_2, as well as $CsTeF_5$ and Cs_2TeOF_4.

The rubidium salt was prepared in an exactly analogous

manner.

$$TeO_2 + 2RbF = Rb_2TeO_2F_2$$

Attempted preparation of the barium salt according to the reaction

$$TeO_2 + BaF_2 = BaTeO_2F_2$$

failed due to the absence of solution even on heating to 900°C. At this temperature the characteristic red colour of a melt of pure TeO_2 was observed unlike the $M_2TeO_2F_2$ melts. This retention of TeO_2 in high temperature melts containing fluoride is in sharp contrast to the sublimation of SeO_2 at 300°C under similar conditions (see later, p 38). In addition attempted preparation of $BaTeO_2F_2$ from aqueous solution failed.

Finally attempted preparation of $M^I_2TeO_2F_2$ (M = Cs, Rb, K or Et_4N) from aqueous solution failed, the pentafluorotellurates being formed instead.

M^ITeO_2F: Attempted preparation of the dioxofluorotellurate(IV) salts from melts according to the reaction

$$M^IF + TeO_2 \rightarrow M^ITeO_2F \quad (M = Cs, Rb)$$

yielded only a mixture of TeO_2 and M^ITeO_2F as indicated by the

infrared spectrum. This is in sharp contrast with the analogous monofluorodioxoselenates which are readily prepared[106].

$Co(NH_3)_6(TeF_5)_3$:

This compound was prepared from a 0.2 M solution of $Co(NH_3)_6F_3$ and a solution of TeO_2 in 48% HF. $Co(NH_3)_6F_3$ (0.01 moles) prepared as described above for the $Co(NH_3)_6Sb_2F_9$ preparation was added to 0.01 moles of TeO_2 which had been dissolved in 20 mls of 48% HF. On cooling, the mixture yielded a good crop of orange crystals. The crystals were collected at the pump, washed with a few mls of cold ethanol and dried under vacuum. Analysis. Calcd for $Co(NH_3)_6Sb_2F_9$: Te, 47.19. Found, 46.13. Co, 7.11. Found, 7.02. NH_3, 12.31. Found, 12.20. F, 34.39. Found, 34.22.

(iii) Iodine(V) Compounds.

$CsIOF_4$ and $KIOF_4$:

Preparations of these salts were attempted in three different ways. The first of these involved the reaction of the alkali metal fluoride with the corresponding iodate or difluoroiodate, and IF_5 which was also the solvent for the reaction. Secondly, a series of reactions employing the stoichiometric amount of all the reactants was tried using CH_3CN as solvent. Lastly, reactions in which the product was obtained by deliberate hydrolysis of IF_5 and an alkali metal fluoride in CH_3CN were tried.

Stoichiometric amounts of KF and KIO_2F_2 were allowed to react in an excess of IF_5 according to the hypothetical reaction equation

$$KF + KIO_2F_2 + IF_5 = 2KIOF_4 \quad (IF_5 \text{ as solvent})$$

After shaking for several hours at room temperature, the excess IF_5 was pumped off on the vacuum line. The reaction was carried out in an all-glass break-seal container, and a typical reaction had 0.291 g KF (0.005 moles), 1.18 g KIO_2F_2 (0.005 moles), and 37.5 g IF_5 (0.17 moles). An infrared spectrum of the product, which appeared to be homogeneous, revealed the presence of KIF_6 (636 cm^{-1}) and KIO_2F_2 (810 cm^{-1}) in addition to some $KIOF_4$ (888 cm^{-1}). The spectrum of this mixture is given in Chapter IV.

A similar reaction type using KIO_3 and KF was also tried

$$2KF + KIO_3 + 2IF_5 = 3KIOF_4 \quad (IF_5 \text{ as solvent})$$

A typical reaction had 0.47 g KF (0.0081 moles), 0.856 g KIO_3 (0.004 moles) and 37.5 g IF_5 (0.17 moles). Once again the excess IF_5 was removed on the vacuum line after the reactants appeared to give a homogeneous product. An infrared spectrum of the product of this reaction showed the presence of KIF_6 and KIO_2F_2.

It was felt that a series of reactions using the stoichiometric amount of all reagents in CH_3CN as solvent might prove fruitful. Thus 2.94 g KF (0.05 moles), 5.41 g KIO_3 (0.025 moles) and 11.25 g IF_5 (0.05 moles) were shaken together in CH_3CN for 24 hrs according to the hypothetical equation

$$KIO_3 + 2KF + 2IF_5 \xrightarrow{CH_3CN} 3KIOF_4$$

The reaction apparatus was an all-glass break-seal type which allowed the product to be filtered. The solvent was then pumped off on the vacuum line yielding a soluble and an insoluble product. An infrared spectrum of both products indicated the presence of the desired salt $KIOF_4$, in addition to a small amount of KIO_2F_2. There was no evidence for any KIF_6 in the product. Analysis. Calcd for $KIOF_4$: F, 29.46. Found 33.23 (28.42). I, 49.19. Found: 49.65. The fluoride analysis was done by titration with La^{3+} using a fluoride sensitive electrode. However, in the course of the work on the salts of $IO_2F_2^-$ (see later) it was discovered that fluoride analysis obtained in this way were ~20% too high. However, a correction factor for the analysis was obtained from the ratio of the apparant fluoride analysis on $CsIO_2F_2.1/3H_2O$ and $CsIO_2F_2.HIO_2F_2.2H_2O$ determined by titration with La^{3+}, to the fluoride analysis determined from the total number of acid equivalents[126]. This correction factor is 0.85 and the corrected analysis for $KIOF_4$ is given in parenthesis. Thus the analysis on the above product finds I too high and F too low. This result is consistent with some KIO_2F_2 in the product. Calcd for KIO_2F_2: F, 16.10, I, 55.04. This method of obtaining the fluoride analysis is, of course, open to question. If the error is due to the insolubility of $La(IO_3)_3$ then the correction factor obtained from the 2:1 fluoride to iodate systems will tend to over-compensate for this in the 4:1 case. However, the "corrected" value would then be the lower limit of the analysis and the true fluoride value will lie somewhere between the observed and corrected values. The observed analysis is consistent with ~10% of the product being KIO_2F_2. Calcd for 10% impurity due to KIO_2F_2: F, 28.12. I, 49.78.

Ryan and Asprey[75] report isolation of several crystals of $CsIOF_4$ from a solution of CsF and IF_5 in CH_3CN and an unidentified oxygen source

$$CsIF_6 + \left\{ \begin{matrix} H_2O \\ SiO_2 \end{matrix} \right\} \xrightarrow{CH_3CN} CsIOF_4$$

Thus, a series of experiments involving deliberate hydrolysis of $CsIF_6$ was begun since the apparent solubility of $CsIOF_4$ indicated the possibility of obtaining a product which was not contaminated with $CsIO_2F_2$. The appropriate quantities of the reagents were mixed in the dry box and then refluxed in dry CH_3CN for ½ hr in the apparatus shown in Figure 3. A typical reaction had 5.0 g CsF (.033 moles), 10 g IF_5 (.045 moles) and 0.6 g H_2O (.033 moles), in 100 mls of dry acetonitrile. The hot solution was filtered rapidly by forcing it through the medium porosity frit A, using an overpressure of dry nitrogen. The solution was allowed to cool in the bulb B, where a small quantity (ca 500 mg) of crystals was deposited. The cooled solution was then sucked back into the bulb C, and the crystals pumped dry on the vacuum line. Analysis. Calcd for $CsIOF_4$: F, 21.00. Found, 17.32 (15.20). The corrected value for the fluoride analysis is again given in parenthesis, and this low fluoride analysis suggests the presence of $CsIO_2F_2$ in the product. Calcd for $CsIO_2F_2$: F, 11.51.

A second preparation where it was attempted to increase the yield of the product was attempted by repeated dissolution of the material in bulb C, and repeated filtering. However, this always increased the amount of $CsIO_2F_2$ in the product, and gave a

Figure 3

Apparatus for the Preparation of $CsIOF_4$

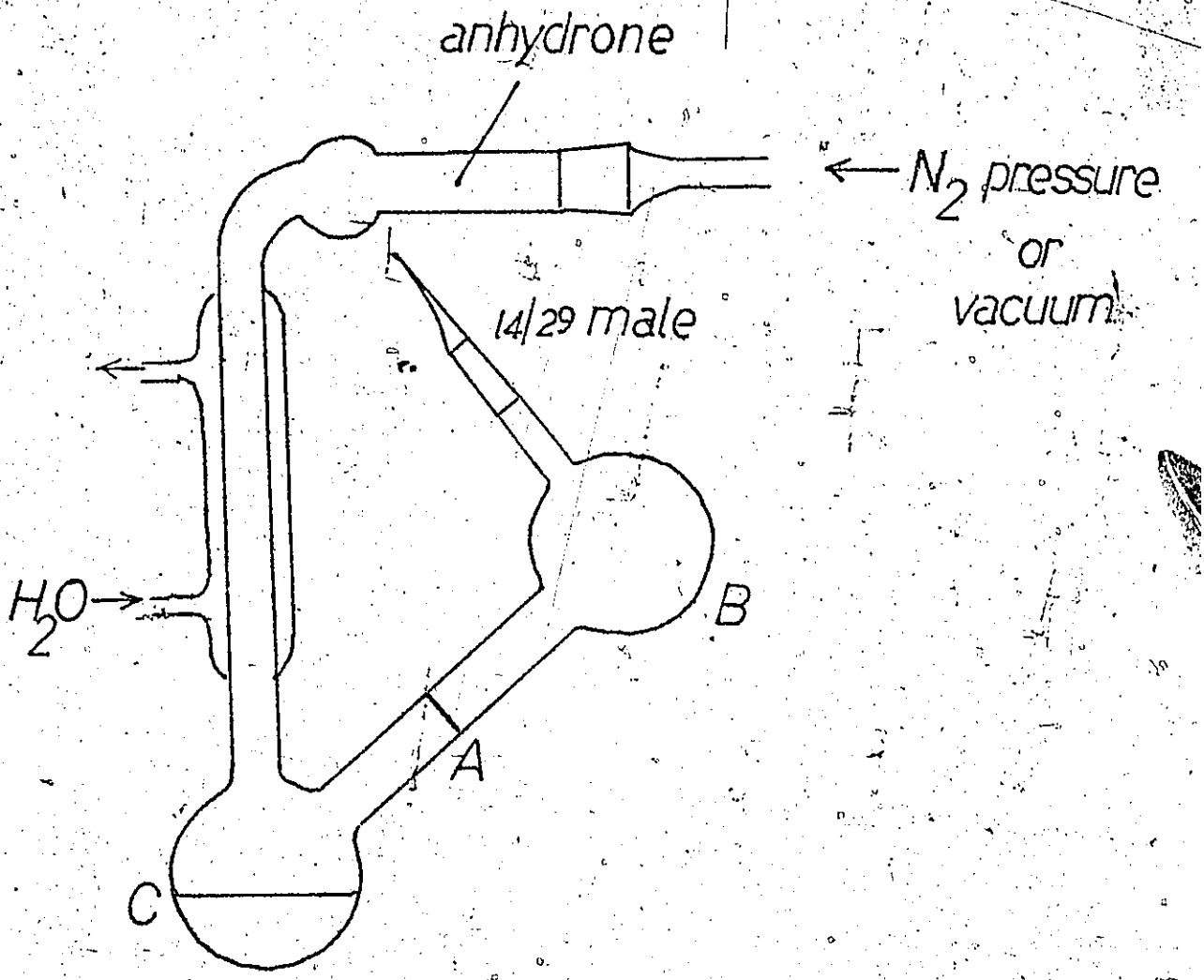
anhydrone
N_2 pressure
or
vacuum
14/29 male
H_2O
B
A
C

brown colouration to the CH_3CN which is indicative of some disproportionation to molecular iodine and I(VII).

The existence of some $CsIO_2F_2$ in all of the products obtained by deliberate hydrolysis suggested that a possible oxygen source other than the water added was present. Since SiO_2 has been shown to be shown to be an effective oxygen source in the decomposition of IF_7 and XeF_6 [128], an experiment was tried in plastic apparatus using finely ground SiO_2 powder as a potential oxygen source. The solvent used was CH_3CN.

$$2KF + 2IF_5 + SiO_2 \xrightarrow{CH_3CN} 2KIOF_4 + SiF_4$$

$$SiF_4 + 2KF = K_2SiF_6$$

Stoichiometric quantities of KF and IF_5 were mixed in the dry box with a two-fold excess of SiO_2 powder in a plastic bottle. The bottle was protected from the atmosphere by a drying tube of magnesium perchlorate, and 100 mls of dry CH_3CN were added. The reactants were stirred for 18 hrs at 60°C, and the solid product was then filtered and pumped dry on the vacuum line. An infrared spectrum of the product did not show the presence of $KIOF_4$ or the expected K_2SiF_6, but instead revealed the presence of SiO_2 and KIF_6.

KIO_2F_2:

The method of Helmholtz and Rodgers [94] was used.

$CsIO_2F_2.1/3H_2O$:

A 2:1 molar ratio of CsF and HIO_3 were dissolved in hot 15% HF and large crystals deposited on cooling. This proceedure is essentially that of Weinland and Koppen[126] for the preparation of $CsIO_2F_2$. In this work this proceedure always yielded the hydrate $CsIO_2F_2.1/3H_2O$. Analysis. Calcd for $CsIO_2F_2.1/3H_2O$: I, 37.79. Found. 37.82. F, 11.32. Found, 11.41 (calculated from the number of acid equivalents). Crystallization from hot (95°C) 15% HF also yielded the hydrate. Attempts to dehydrate the compound by heating at 90°C under vacuum for 12 hrs caused some decomposition to $CsIO_3$, as evident from an infrared spectrum.

$CsIO_2F_2.HIO_2F_2.2H_2O$:

This compound was prepared from 40% HF by the method of Weinland and Koppen[126]. Analysis. Calcd for $CsIO_2F_2.HIO_2F_2.2H_2O$: I, 45.02. Found, 44.87. F, 13.48. Found, 13.50 (calculated from the number of acid equivalents). Although the product was formed as well-developed crystals, it was not possible to store it for extended periods due to the loss of both HF and H_2O.

$Co(NH_3)_6(IO_2F_2)_3.H_2O$:

$Co(NH_3)_6F_3$ (0.01 moles) was prepared as previously described. HIO_3 (0.03 moles) was dissolved in 30 mls of 48% HF and the resulting solution was filtered. Addition to the $Co(NH_3)_6F_3$ solution yielded a good crop of orange crystals on cooling in ice. The crystals were filtered, washed with a few mls of ethanol, then ether, and dried under vacuum.

Analysis. Calcd for $Co(NH_3)_6(IO_2F_2)_3H_2O$: I, 49.46. Co, 7.66. Found: I, 50.06. Co, 7.88.

(iv) Selenium(IV) Compounds

$KSeO_2F$:

This was prepared by the method of Paetzold and Aurich[106], using the apparatus shown in Figure 4. SeO_2 and KF were weighed out in the dry box and transferred to a platinum boat. The mole ratio of SeO_2 to KF was 1:1. The boat was then heated slowly to 300°C in a stream of dry nitrogen in the tube furnace. The outlet of the tube was protected by a trap containing concentrated H_2SO_4, B. A typical reaction had 2.5 g SeO_2 (.012 moles) and 1.33 g KF (.023 moles). A clear colourless melt was formed at ca 300°C, but heating above this temperature caused decomposition of the product.

$M^I_2SeO_2F_2$:

A melt of 2:1 mole ratio of KF to SeO_2, tried according to the hypothetical reaction

$$2KF + SeO_2 = K_2SeO_2F_2,$$

failed to give solution at 300°C, and continued heating above this temperature caused some of the SeO_2 to sublime out of the tube.

Dissolution of a 2:1 mole ratio of KF and SeO_2 in 48% HF yielded crystals of $KSeO_2F$, as shown by the infrared spectrum.

Similarly, a hot 2:1 mole ratio solution of CsF and SeO_2 gave $CsSeO_2F$ on cooling. The product was verified by fluoride

analysis. Analysis. Calcd for $CsSeO_2F$: F, 7.23. Found: F, 7.42.

Attempted preparation of $Cs_2SeO_2F_2$ from a solution of CsF and SeO_2 in DMSO according to the hypothetical reaction

$$2CsF + SeO_2 \xrightarrow{DMSO} Cs_2SeO_2F_2$$

failed. The reactants were shaken for 12 hrs in DMSO until they appeared to give a homogeneous product. This product was then filtered and the solvent pumped off on the vacuum line. The reaction had 1.49 g SeO_2 (.0134 moles) and 4.074 g CsF (.0267 moles). An x-ray powder photograph on the product revealed the presence of CsF, and an infrared spectrum of the product gave the familiar spectrum of SeO_2F^-. It is unlikely that any SeF_4 (b.p. ca 100°C) could have boiled out of the solution, and so the presence of CsF in the product suggests that the above reaction does not occur.

Figure 4

Tube Furnace for the Preparation of $KSeO_2F$

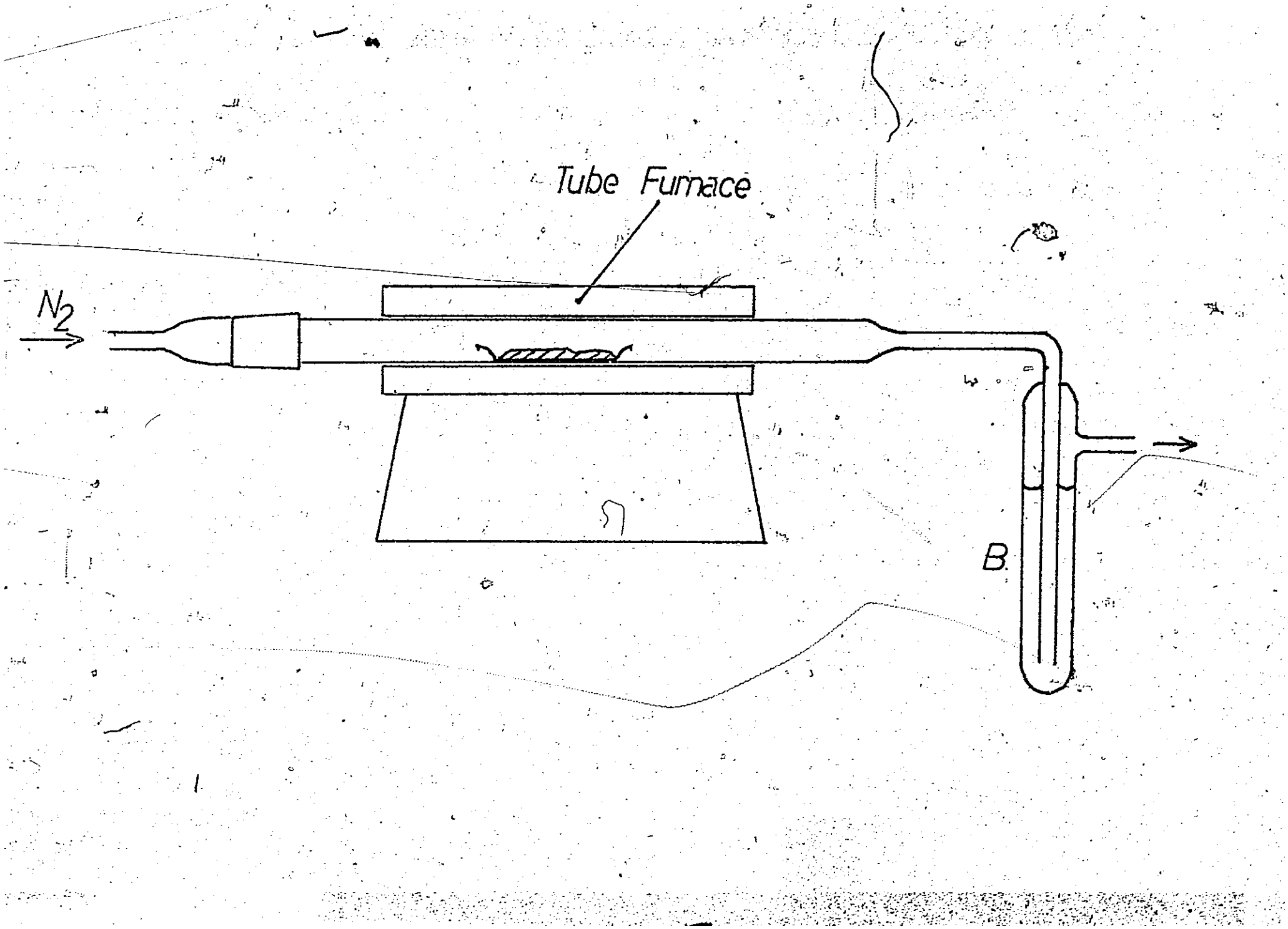
Tube Furnace
N_2
B

CHAPTER III

Fluoro- and Oxofluoro- Anions of Tellurium(IV)

The fluoro and oxofluoro anions formed by tellurium in its penultimate oxidation state are given in Table III, along with the known species in the highest oxidation state.

TABLE III

TeF_6	TeF_4
TeF_7^- a	TeF_5^- g,h
TeF_8^{2-} a	(TeF_6^{2-}) ? h, j
$TeOF_5^-$ b	$TeOF_4^{2-}$ h
$Te(OH)_{6-n}F_n$ c,d,e (n = 1,6	$Te(OH)F_4^-$ h
$TeO_3F_2^{2-}$ c	$TeO_2F_2^{2-}$ h
TeO_3F^- c	
$F_5TeOTeF_5$ c	

a ref 131, b ref 132, c ref 133, d ref 134, e ref 135
g ref 58, h this thesis, j refs 25,26,27

All of the known oxofluorotellurate(IV) species have been synthesized and characterized as part of this thesis. The well known pentafluorotellurate(IV) ion has been investigated both as a salt and

in aqueous solution in this work. The failure to isolate salts of the hexafluorotellurate(IV) ion, or indeed to observe it in solution, means that the evidence for this species remains sparse.

X-Ray Powder Photography

$CsTeF_5$ and $KTeF_5$:

Although the single crystal x-ray determination on $KTeF_5$ reported by Edwards and Mouty[28], gives complete information on the structure of the TeF_5^- ion in the crystal, the x-ray powder data for both $CsTeF_5$ and $KTeF_5$ obtained in this work are given in Table IV.

Cs_2TeOF_4 and K_2TeOF_4:

The determined x-ray data for both of these salts are given in Table V. An examination of the powder photographs shows the compounds to be isomorphous with the isoelectronic antimony(III) salts, Cs_2SbF_5 and K_2SbF_5. The pentafluoroantimonate(III) salts belong to the orthorhombic crystal system, and the cell parameters determined in this work (see Chapter V) agree well with those reported by Bystrom and Wilhelmi[68]. The unit cell dimensions for the two oxotetrafluorotellurate(IV) salts, which clearly also belong to the orthorhombic system, are recorded below along with the values determined for the antimony salts.

The SbF_5^{2-} ion is square pyramidal, the shape predicted by VSEPR theory[3], and the virtual identity of the powder photographs along with the conclusions of the assignment of the vibrational

TABLE IV

X-Ray Powder Photograph Data for TeF_5^- Salts

$CsTeF_5$ — Cu-Kα Irradiation

d(Å)	Intensity
3.999	100
3.805	20
3.596	10
3.394	100
2.504	40
2.424	40
2.522	20
1.996	10
1.842	10
1.759	10
1.6[illegible]	20
1.354	10
1.284	20

$KTeF_5$

d(Å)	Intensity
5.529	50
4.503	80
3.890	80
3.577	50
3.519	50
3.138	20
2.777	20
2.538	10
2.124	100

TABLE IV (Continued)

d(Å)	Intensity
1.945	80
1.805	10
1.471	10
1.771	40
1.600	40
1.515	20
1.402	20
1.589	10

TABLE V

X-Ray Powder Photography Data for Cs_2TeOF_4 and K_2TeOF_4

Cs_2TeOF_4		Cu-Kα Irradiation		
d (Å)	Intensity	Exptl $\sin^2\theta$	Calcd $\sin^2\theta$	hkl
3.531	20	.0477	.0479	002
3.408	100	.0512	.0508	012
			.0508	131
3.303	20	.0545	.0538	200
2.629	50	.0860	.0867	132
2.421	100	.1014	.1014	060
2.288	10	.1135	.1130	222
2.030	30	.1442	.1464	330
2.001	20	.1485	.1493	062
1.956	20	.1554	.1552	260
1.939	30	.1581	.1584	331
1.890	10	.1664	.1662	340
1.783	10	.1869	.1860	072
1.718	30	.2013	.2030	024
1.665	10	.2144	.2153	400
1.573	40	.2401	.2406	430
1.539	40	.2508	.2543	333
1.515	20	.2590	.2593	173
			.2591	370
1.373	10	.3152	.3157	314
1.323	20	.3397	.3392	510
1.285	20	.3599	.3617	512
1.232	20	.3912	.3871	532
1.131	20	.4124	.4097	532
1.032	20	.4647	.4696	533
1.032	20	.5577	.5587	375
0.992	20	.6038	.6035	623
			.6035	117
0.975	20	.6250	.6260	137

TABLE V (Continued)

a = 6.646 Å
b = 14.525
c = 7.042

K_2TeOF_4

Cu-Kα Irradiation

d(Å)	Intensity	Exptl $\sin^2\theta$	Calcd $\sin^2\theta$	hkl
3.710	10	.0432	.0432	130
3.455	40	.0498	.0497	040
3.211	100	.0576	.0570	012
3.119	10	.0611	.0610	200
2.610	10	.0872	.0869	221
2.539	10	.0922	.0930	150
2.317	40	.1107	.1107	240
2.246	40	.1179	.1149	202
2.180	10	.1250	.1242	241
1.885	20	.1673	.1676	170
1.827	10	.1780	.1787	331
1.621	20	.2261	.2268	262
1.386	10	.3092	.3096	154
1.333	10	.3346	.3362	353
			.3362	380
1.226	10	.3952	.3963	470
1.077	10	.5120	.5131	036

a = 6.243 Å
b = 13.825
c = 6.461

spectra, confirm the VSEPR prediction that $TeOF_4^{2-}$ should also be square pyramidal with the oxygen in the apical position[3]. Since Te-O and Te-F bond distances are expected to be shorter than Sb-F(apical) and Sb-F(equatorial) bond distances it is surprising that the unit cells of the tellurium salts are larger than those of the corresponding pentafluoroantimonate(III) salt.

Unit Cell Dimensions (Å)

	a	b	c
K_2SbF_5	6.25	13.68	6.48
K_2TeOF_4	6.24	13.83	6.46
Cs_2SbF_5	6.66	14.53	7.07
Cs_2TeOF_4	6.65	14.53	7.04

standard deviations on these dimensions ± 0.05 Å

In general square pyramidal species have a bond angle between apical and equatorial ligands of less than 90° (see Tables I and II). The one exception to this rule is $XeOF_4$ where the ∠(OXeF) is 91.8° [74]. Moving one group to the left in the periodic chart, the isoelectronic IOF_4^- ion has an ∠(OIF) of 88.5° [75]. This is considerably larger than the isostructural TeF_5^- species[28], where the (F'TeF) angle

is 78.8°. Thus the larger unit cell of the $TeOF_4^{2-}$ salts can perhaps be rationalized in terms of the ∠(OTeF) being greater than ∠(F'SbF) in the SbF_5^{2-} salts.

$KTe(OH)F_4$:

The x-ray powder data for this salt are given in Table VI. It is not apparent from a comparison of the powder photographs for $KTeF_5$ and $KTe(OH)F_4$ that these two isoelectronic salts are isomorphous. Furthurmore, it was not possible to index the reflexes for $KTe(OH)F_4$ to the cubic, tetragonal or orthorhombic systems.

$Cs_2TeO_2F_2$ and $Rb_2TeO_2F_2$:

The x-ray powder data for these two salts is given in Table VII. It was not possible to index the reflexes to the cubic, tetragonal or orthorhombic ststems. Attempts to prepare $BaTeO_2F_2$, which may be isomorphous with KIO_2F_2, a salt of known structure[94], failed. The two salts are isomorphous.

Vibrational Spectra

$KTeF_5$:

The vibrational spectrum of this salt is well known[58,66], the only point of contention being the resolution of ν_4, the symmetric (TeF_4) stretch, and ν_7 the asymmetric stretch. This point will be dealt with in this chapter in the section on solutions, and later in Chapter VI. The infrared spectrum of $KTeF_5$ is given in Figure 6, trace B.

TABLE VI

X-Ray Powder Photography Data for $KTe(OH)F_4$

$KTe(OH)F_4$	Cu-Kα Irradiation
d	Intensity
6.308	40
4.658	10
4.336	10
3.779	100
3.674	100
3.338	40
3.223	30
3.139	30
3.027	100
2.489	100
2.140	20
2.002	40
1.988	40
1.960	20
1.920	20
1.892	20
1.842	20
1.787	40
1.775	20
1.725	10
1.677	10
1.576	40
1.473	10
1.387	10
1.318	10
1.301	10
1.289	10

TABLE VII

X-Ray Powder Photography Data for $Cs_2TeO_2F_2$ and $Rb_2TeO_2F_2$

$Cs_2TeO_2F_2$ Cu-Kα Irradiation

d	Intensity
4.418	5
3.391	100
3.283	60
3.135	20
2.778	10
1.981	50
1.921	50
1.815	5
1.699	30
1.644	10
1.561	20
1.486	10
1.478	10
1.414	10
1.374	20
1.312	10
1.298	20
1.267	20
1.253	10
1.157	20

TABLE VII (Continued)

$Rb_2TeO_2F_2$	Cu-Kα Irradiation
d (Å)	Intensity
3.255	100
3.144	30
2.967	10
2.385	20
2.235	20
1.907	40
1.869	20
1.843	30
1.782	10
1.502	10

Cs_2TeOF_4 and K_2TeOF_4:

Figures 5 and 6, trace C, show representative spectra of these salts. Since the $M^I{}_2TeOF_4$ salts are isomorphous with the $M^I{}_2SbF_5$ salts, which have been shown to contain individual $SbF_5{}^{2-}$ ions[68,69], the $TeOF_4{}^{2-}$ ions must also exist as discrete non-bridging species in both these salts. Furthurmore, $IOF_4{}^-$ and $XeOF_4$ have both been shown to have square pyramidal structures with the oxygen occupying the apical position[74,75]. The isoelectronic $TeOF_4{}^{2-}$ ion will undoubtedly have this C_{4v} structure also, and the infrared and

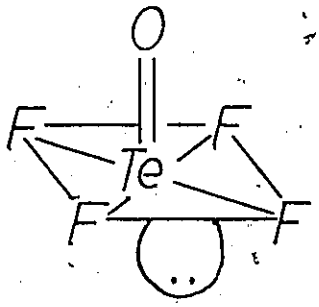

Raman spectra are consistent with this.

In C_{4v} symmetry the normal modes belong to the representation $\Gamma = 3A_1 + 2B_1 + B_2 + 3E$, and of the 9 fundamentals, all are Raman active, while only 6 are infrared active ($3A_1 + 3E$). The assignment for Cs_2TeOF_4 and K_2TeOF_4 is given in Table VIII, and is based upon the following considerations. It may be seen that only 7 fundamentals are observed, but since $\nu_5(B_1)$ in C_{4v} symmetry is very weak and seldom observed, this accounts for one of the absences. It is assumed that $\nu_8(E)$ is not observed due to a coincidence with $\nu_7(E)$. The 4 stretching modes ($2A_1 + B_1 + E$) are

Figure 5

The Raman Spectrum of Cs_2TeOF_4

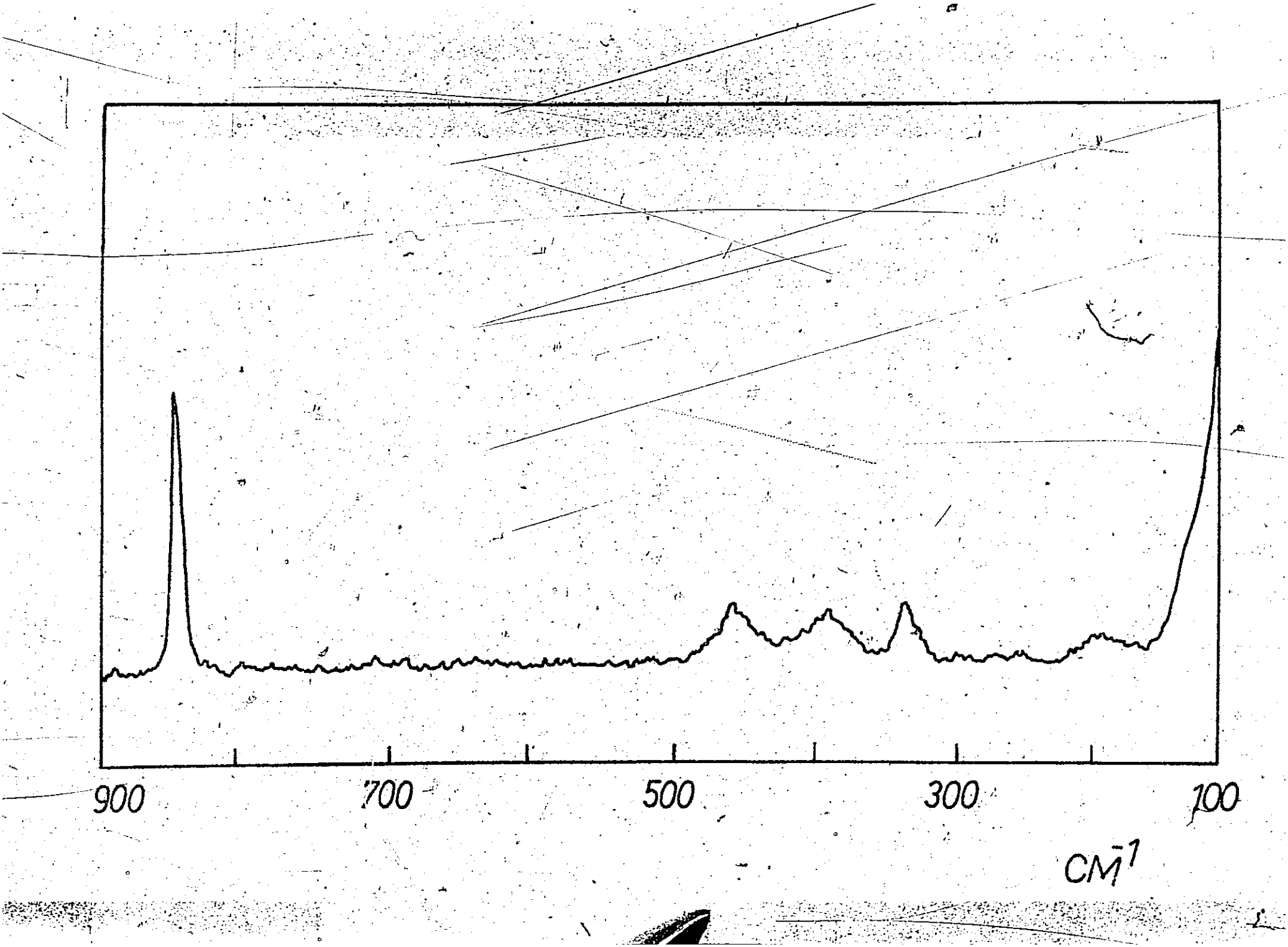
900
700
500
300
100
см⁻¹

Figure 6

The Infrared Spectra of Tellurium(IV) Species

A $KTe(OH)F_4$

B $KTeF_5$

C Cs_2TeOF_4

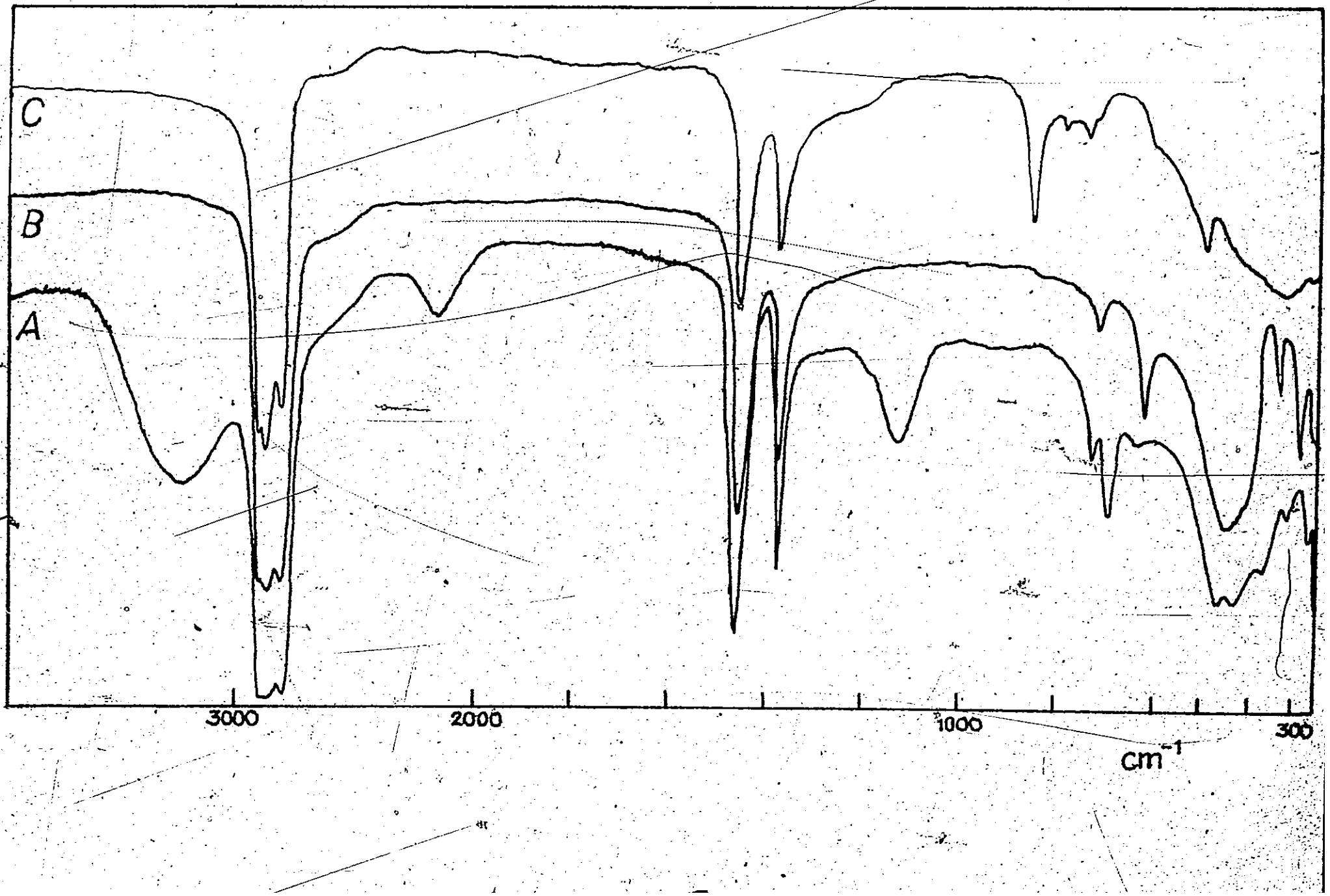
C
B
A
3000
2000
1000
300
cm⁻¹

TABLE VIII

Raman and Infrared Spectra of K_2TeOF_4 and Cs_2TeOF_4

K_2TeOF_4		Cs_2TeOF_4		Assignment (C_{4v})
Ir	Raman	Ir	Raman	
1675 vw				$2\nu_1(A_1)$
1160 vw		1155		$\nu_1 + \nu_7(E)$
847 s	850 vs	840 s	837 vs	$\nu_1(A_1)$
777 w		790 vvw, 770 w		$\nu_2 + \nu_7(E)$
		700 vw,sh		$\nu_4 + \nu_7(E)$
475 s,sh	470 m	480 s,sh	461 m	$\nu_2(A_1)$
			390 m	$\nu_4(B_1)$
305-340 vs,br	344 m	330-360 vs,br	335 m	$\nu_7(E)$
275 br		265		$\nu_3(A_1)$
			190 w	$\nu_6(B_2)$
			129 w	$\nu_5(B_1)$
(340)		(360)		$\nu_8(E)$

expected to be more intense than the deformations, and all should lie above 300 cm^{-1} judging from the spectra of isoelectronic species. Of these 4 stretching bands in the Raman spectrum of Cs_2TeOF_4, the highest frequency band at 837 cm^{-1} must be $\nu_1(A_1)$. This mode always is the highest frequency band in the pentafluoro species, and it lies in the characteristic Te-O stretching region. The peak at 390 cm^{-1} which is Raman active only, must be $\nu_4(B_1)$. Of the remaining 2 bands, that at 461 cm^{-1} is assigned to the symmetric (TeF_4) stretch, $\nu_2(A_1)$ which is expected to be strong in the Raman spectrum, whereas $\nu_7(E)$, the asymmetric (TeF_4) stretching mode, is expected to be strong in the infrared spectrum. The mutual exclusion of these 2 modes has been observed for the isoelectronic $XeOF_4$ [73]. The spectra of other C_{4v} species are given in Table IX. In $TeOF_4^{2-}$ ν_7 lies at a lower frequency than ν_4, which is opposite to that observed for other C_{4v} molecules. Furthur discussion on this point will be found in Chapter VI.

Assignment of the deformations is done mainly by comparison to these other modes in other C_{4v} molecules (see Table IX). $\nu_9(E)$ is readily assigned to the lowest frequency peak at 129 cm^{-1}, and the two remaining bands are assigned to $\nu_3(A_1)$ and $\nu_6(B_2)$.

Several combination bands are also observed in the infrared spectra of Cs_2TeOF_4 and K_2TeOF_4. The first overtone of ν_1 is assigned to the weak band at 1625 cm^{-1}. Combination bands $\nu_1 + \nu_7(E)$, $\nu_2 + \nu_7(E)$ and $\nu_4 + \nu_7(E)$ are observed at 1155, 790 and 700 cm^{-1} respectively , see Table VIII. All of these bands involve the strongest infrared band $\nu_7(E)$, and are also observed for $XeOF_4$, IF_5, BrF_5 and ClF_5 [73]. The assignment of these combination bands

TABLE IX

Comparison of the Spectra of C_{4v} Species (XZY_4) Isoelectronic with $TeOF_4^{2-}$

Class	Mode No.	SbF_5^{2-} [a]		$XeOF_4$ [b]		$TeOF_4^{2-}$ [c]		Approx Description of Mode (XZY_4)
		Raman	Ir	Raman	Ir	Raman	Ir	
A_1	ν_1	557 s	555 s	920 mw,p	926 s	837 vs	840 s	$\nu(XZ)$
	ν_2	427 m	-	567 s,p	576 m	461 m	480 m	$\nu_{sym}(XY_4)$-in phase
	ν_3	278 w	260 m	285 w,p	294 s	-	265 m	δ_{sym} XY_4) umbrella
B_1	ν_4	388w	-	527 m	-	390 m	-	ν sym(XY_4)-out of phase
	ν_5	-	-	-	-	-	-	$\delta_{asym}(XY_4)$-out of phase
B_2	ν_6	220 w	-	233 mw	-	190 w	-	$\delta_{sym}(XY_4)$-in phase
E	ν_7	347/375 w	359/377 vs	-	608 vs	335 m	330/360 vs	$\nu_{asym}(XY_4)$
	ν_8	307 m	288 m	365 mw	361 s	-	-	$\delta(ZY_4)$ wag
	ν_9	142	151	161 m	-	129 w	-	$\delta_{asym}(XY_4)$-in plane

a ref 58, b ref 56, c Cs_2TeOF_4 this work

substantiates the assignment of the stretching modes of the $TeOF_4^{2-}$ ion given in Tables VIII and IX.

$KTe(OH)F_4$:

The infrared spectrum of $KTe(OH)F_4$ is given in Figure 6, trace A, and the Raman spectrum below 800 cm^{-1} in Figure 7, trace A. The frequencies of the infrared and Raman bands are given in Table X along with those for $KTeF_5$, and are assigned according to the following considerations. The similarity of the spectra of the two salts and the absence of the apical Te-F stretch (611 cm^{-1}) and its replacement with a strong band at 697 cm^{-1}, suggests that the OH group is in the axial position. Thus the ($TeOF_4$) skeleton approximates to C_{4v} symmetry.

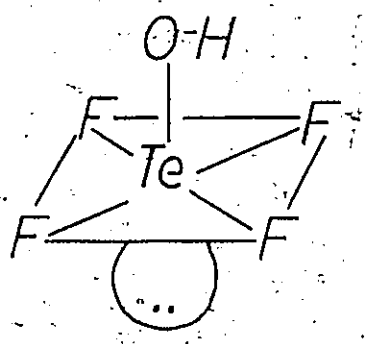

The close similarity of the spectra of the two ions is expected, with the exception of $\nu_1(A_1)$ and $\nu_8(E)$, both of which involve the apical ligand. In addition the non-linear Te-OH group might be expected to cause departures from the C_{4v} selection rules for vibrational spectra. The presence of the hydroxo group will, of course, introduce its own characteristic frequencies.

TABLE X

Raman and Infrared Spectra of TeF_5^- and $Te(OH)F_4^-$ Species (C_{4v})

Class	Mode No.	$KTeF_5$ [a]		$KTe(OH)F_4$ [b]		TeF_5^- [c]	$Te(OH)F_4^-$ [d]	Approx description
		Raman	Ir	Raman	Ir	(solution)	(solution)	of Mode (XZY_4)
A_1	ν_1	611 vs	618 ms	697 vs	689 m	636 vs,p	700 vs,p	$\nu(XZ)$
	ν_2	504 s	(466 vs)	502 vs	505 sh,w	528 s,p	505 s,p	$\nu_{sym}(XY_4)$ in phase
	ν_3	282 mw	283 m	266 w	250 sh	273 m,p	265 w, p	$\delta_{sym}(XY_4)$ umbrella
B_1	ν_4	(472 s)	-	465 m	(465 vs)	(508 s,sh)	460 m,sh	$\nu_{sym}(XY_4)$ out of phase
	ν_5	-	-	205 sh,vw	-	238 sh	-	$\delta_{asym}(XY_4)$ out of phase
B_2	ν_6	231 mw	-	223 w	-	225 m	225 w,sh	$\delta_{sym}(XY_4)$ in phase
E	ν_7	(472 s)	(466 vs)	427 w	(465 vs)	(508 s,sh)	425 w,sh	$\nu_{asym}(XY_4)$
					425 vs			
	ν_8	338 mw	336 m	378 w	375 s,br	333 m	340 w,br	$\delta(ZY_4)$ wag
				342 w	335 m			
	ν_9	-	164 mw	125 w,sh	-	168 sh	-	$\delta_{asym}(XY_4)$ in phase

a ref 66, b this work, c 2M TeO_2 in 26.0M HF, d $KTe(OH)F_4$ in water

Figure 7

Raman Spectra of $KTe(OH)F_4$ and some Solutions of TeO_2

A Solid $KTe(OH)F_4$

B 2M TeO_2 in 8M HF

C 2M TeO_2 in 10M HF

D 2M TeO_2 in 28M HF

S indicates slit width

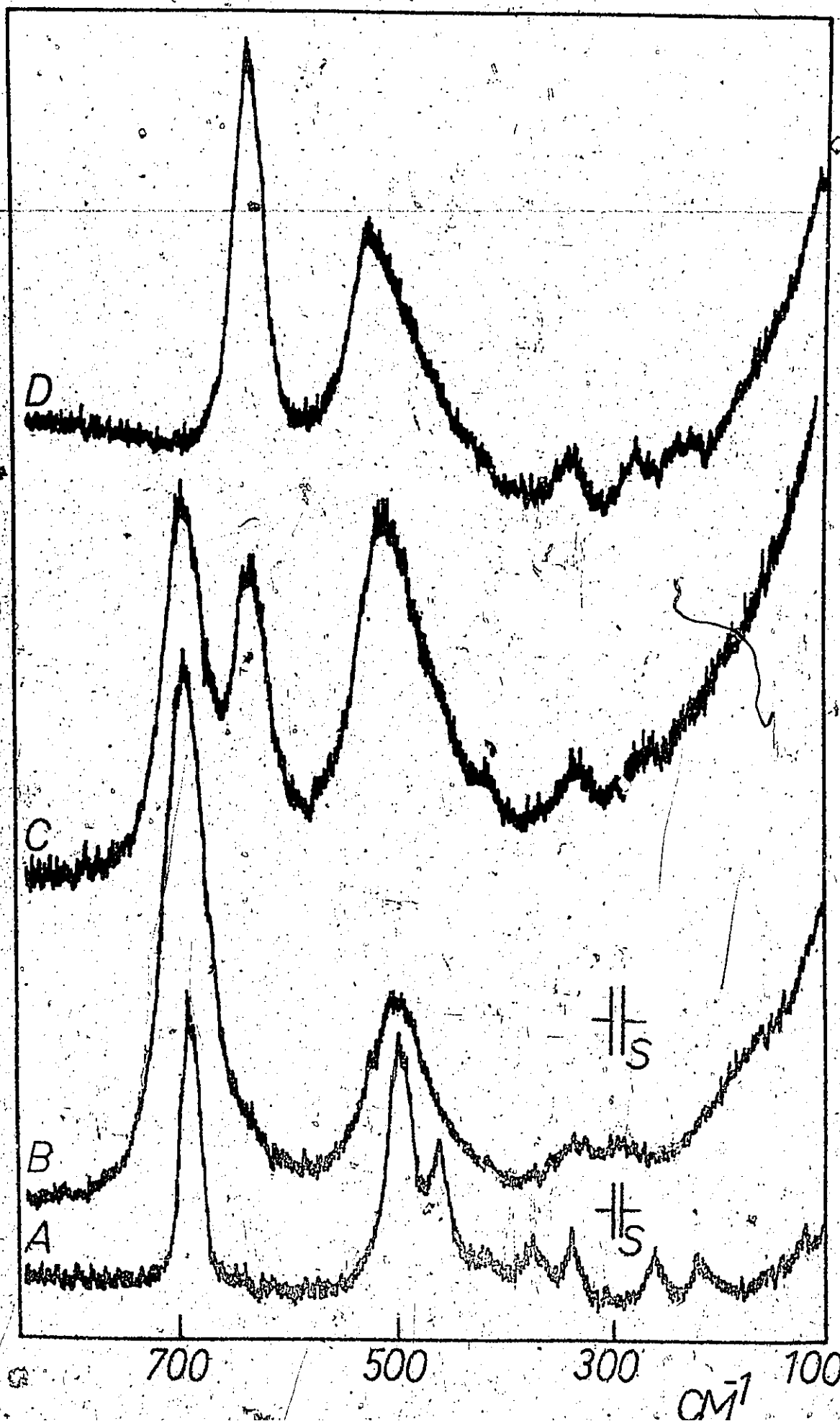
D
C
B
A
⊥
∥
⊥
∥
700
500
300
100
см⁻¹

Bearing the above reservations in mind, the assignment of the skeletal modes was made by analogy with $KTeF_5$, as given in Table X. As expected ν_1 and ν_6 are displaced by the substitution of the OH group. The shift in ν_1 is greater than that expected for a mass effect alone, and suggests that the Te-OH bond is stronger than the Te-F′ apical bond. Furthermore, ν_4 is split into 2 bands, 425 and 465 cm^{-1}, whereas only one band is observed in the infrared spectrum of $KTeF_5$, at 472 cm^{-1}. This extra band may be explained either by the removal of the degeneracy of $\nu_7(E)$ due to the reduced symmetry, or the occurrence of $\nu_4(B_1)$ as an infrared active band, again because of the breakdown of the selection rules for C_{4v} symmetry. The weak Raman band at 205 cm^{-1} has no analogue in the Raman spectra of known square pyramidal species and is assigned as $\nu_5(B_1)$ which has grown in intensity as a result of the reduced symmetry. The corresponding in-plane symmetric deformation in XeF_4 comes at 235 cm^{-1} (ref 136), and the calculated position for this mode, ν_5, in IF_5 is at 257 cm^{-1} (ref 75).

The characteristic hydroxo modes are observed in the infrared spectrum of $KTe(OH)F_4$: the OH stretching mode appears at 3285 cm^{-1}, and the bending mode at 1130 cm^{-1}. In addition the first overtone of this bending mode is observed as a weak absorption at 2240 cm^{-1}. This overtone is also observed in the infrared spectra of the tellurates and telluric acid[119]. The remaining weak band is assigned as the OH wag (630 cm^{-1}). This mode appears at 675 cm^{-1} in the infrared spectrum of HSO_4^- (ref 139), and at 744/812 cm^{-1} in $Sn(OH)_6^{2-}$ (ref 138) and is always weak and broad.

$Cs_2TeO_2F_2$ and $Rb_2TeO_2F_2$:

The infrared and Raman spectra of $Cs_2TeO_2F_2$ are given in Figures 8 and 9. In the liquid phase XeO_2F_2 exists as a discrete non-bridging species[93], whereas in $IO_2F_2^-$ the IO nearest neighbour distances of 2.82 and 2.85 Å (the sum of the van der Waals' radii = 3.5 Å) indicates considerable bridging over oxygen[94]. Both species have the C_{2v} symmetry predicted by VSEPR theory[3]: the oxygens sharing the equatorial plane with the lone electron pair. A similar shape is predicted for $TeO_2F_2^{2-}$ in the above salts, and so the assignment of the vibrational spectra is based upon the following molecular geometry.

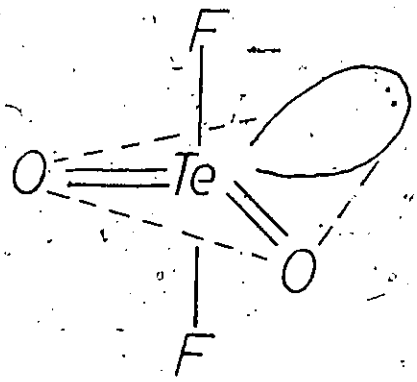

In C_{2v} symmetry the normal modes belong to the representation $\Gamma = 4A_1 + A_2 + 2B_1 + 2B_2$. The Raman spectrum should consist of 9 bands and the infrared spectrum 8. Considering 10 bands are observed in all, see Table XI, and $\nu_5(A_2)$ is not observed, there is some distortion evident from the predicted C_{2v} symmetry. However, in the case of KIO_2F_2 a similiar multiplicity of some bands is observed[96]. The C_{2v} model can still be used for an approximate assignment assuming that the doubled bands belong to one mode.

Figure 8

The Infrared Spectrum of $Cs_2TeO_2F_2$

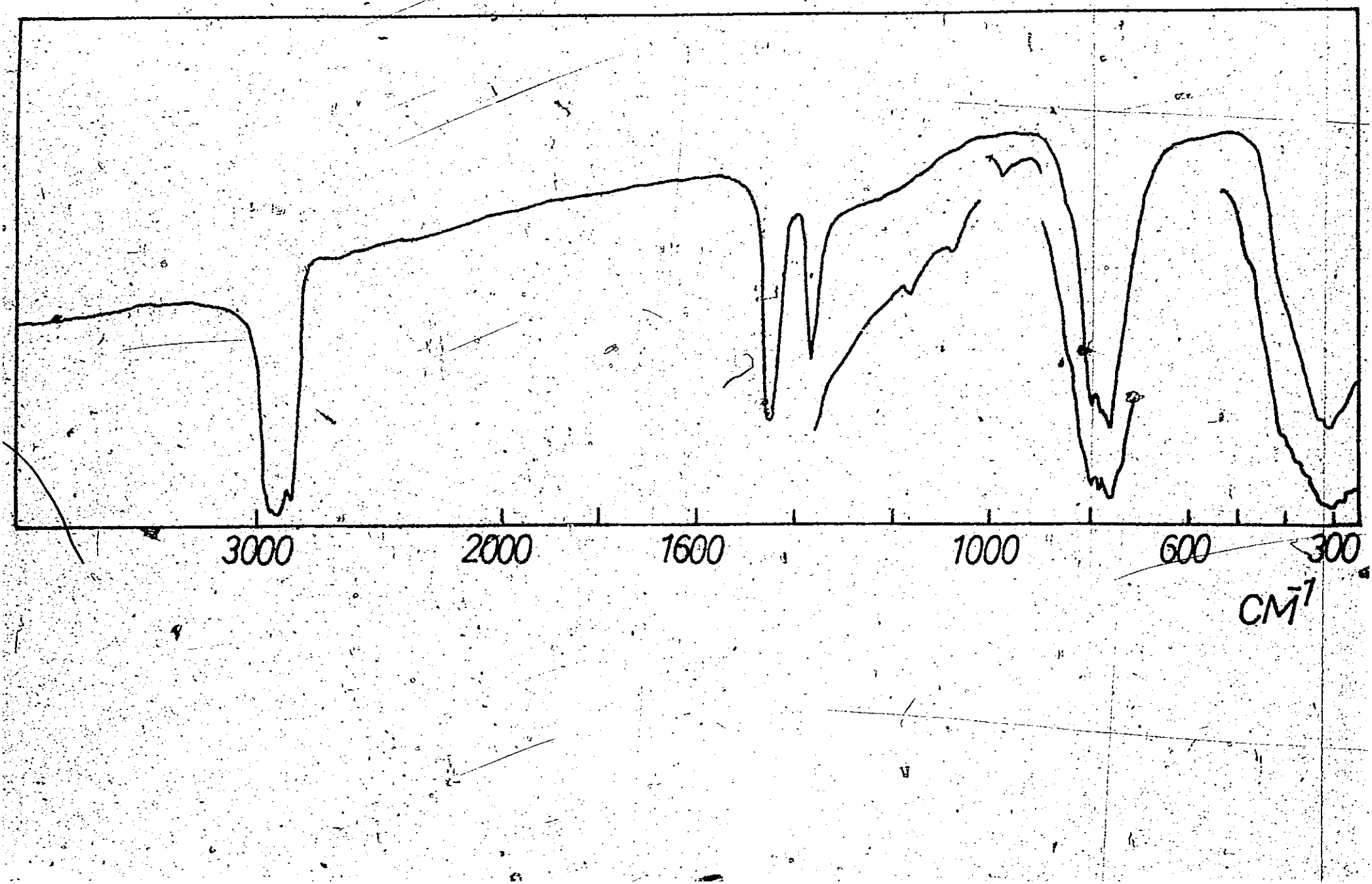
3000
2000
1600
1000
600
300
см⁻¹

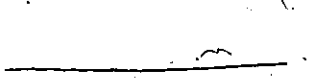

Figure 9

The Raman Spectrum of $Cs_2TeO_2F_2$

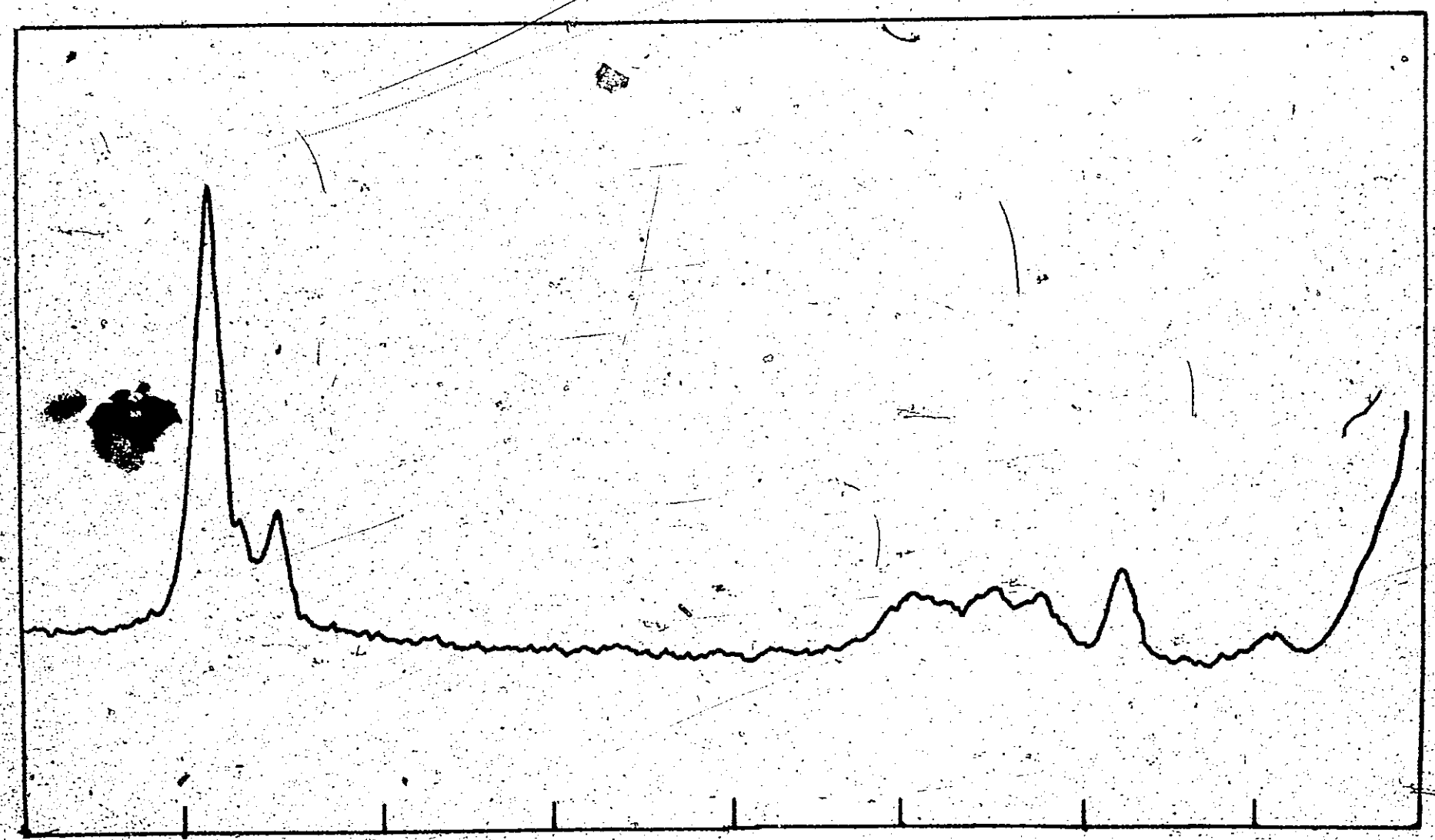
900
700
500
300
100
см⁻¹

TABLE XI

The Raman and Infrared Spectra of $Rb_2TeO_2F_2$ and $Cs_2TeO_2F_2$

$Rb_2TeO_2F_2$		$Cs_2TeO_2F_2$		Assignment (C_{2v})
Raman	Ir	Raman	Ir	
	1075 vw		1075 vw	$\nu_1 + \nu_3$
795 vs	805 vs	796 vs	795 s	$\nu_1(A_1)$
780 vs,sh		781 w	777 s	
788 m	765 vs	758 m	760 s	$\nu_6(B_1)$
767 m			755 vs	
	477 w,sh		480 w,sh	$\nu_5 + \nu_9$
411 w	400 ms,sh	404 mw	400 m,sh	$\nu_2(A_1)$
387 sh		385 w,sh		
358 w		353 mw		$\nu_3(A_1)$
330 w		326 w	330 sh	$\nu_7(B_1)$
311 w	320 vs,br	315 sh	305 vs,br	$\nu_8(B_2)$
282 w	ca270 m,sh	279 mw		$\nu_9(B_2)$
185 w		197 vw		$\nu_4(A_1)$

Two Te-O stretching modes, $\nu_1(A_1)$ and $\nu_6(B_1)$, are expected, and they will lie above 700 cm^{-1} by comparison with the Te-O stretching modes in TeO_2 and $TeOF_4^{2-}$. The two highest frequency bands are thus assigned to these modes, ν_1 being doubled in both the Raman and infrared spectra. The assignment of ν_1 the symmetric (TeO_2) stretching mode at a higher frequency than ν_6, the asymmetric stretch, is perhaps worthy of comment. Polarization studies on the isoelectronic $IO_2F_2^-$ (see Chapter IV) show a near coincidence of these two modes at 840 cm^{-1}, whereas in XeO_2F_2 the asymmetric stretch ν_6 lies higher than ν_1 [93]. Thus there seems to be a definite trend across the series XeO_2F_2, $IO_2F_2^-$, and $TeO_2F_2^{2-}$ with ν_6 falling below ν_1 in the tellurium species. This parallels the trend observed for the C_{3v} exo species XeO_3, IO_3^-, and TeO_3^{2-} where a similar inversion of the symmetric and asymmetric stretching vibration occurs[139].

The remaining 2 stretching modes are assigned as follows. Since the fluorines are axial in all these species, and the $\angle$(FTeF) is expected to be close to 180°, of the two (TeF_2) stretching modes expected one should be strong in the Raman and the other strong in the infrared spectrum. The symmetric (TeF_2) stretching mode $\nu_2(A_1)$, is thus assigned at 400 cm^{-1}, and the strong infrared band at 305 cm^{-1} to the asymmetric stretch, $\nu_8(B_2)$.

The deformations and the torsion $\nu_5(A_2)$, are assigned by comparison with isoelectronic species. It is tempting to argue for the assignment of the symmetric deformations $\nu_3(A_1)$ and $\nu_4(A_1)$, to the two most intense of the remaining Raman bands at 353 and 279 cm^{-1}. The measurement of the polarization of these modes in

$IO_2F_2^-$ allows for their definite assignment in this ion, and so the fall in frequency of these modes across the series XeO_2F_2, $IO_2F_2^-$ and $TeO_2F_2^{2-}$, is felt to be the more reliable method of assignment rather than intensity arguments alone. Furthur discussion on the trend in these modes across the series will be found in Chapter VI.

Three combination bands are observed in the infrared spectrum of $Cs_2TeO_2F_2$, see Figure 8 and Table XI. The weak shoulder at 480 cm^{-1} is attributed to $\nu_5 + \nu_9$, a combination also observed for XeO_2F_2 [93]. From this combination ν_5 is estimated to lie at 201 cm^{-1}.

Solutions

Raman Spectra

Solutions of TeO_2 up to 2.32 M in 26.0 M HF give the spectrum of the TeF_5^- ion shown in Figure 7, trace D. The observed frequencies are recorded in Table X. Confirmation of TeF_5^- as the only tellurium(IV) present is shown by the linearity of a plot of integrated peak intensity of $\nu_1(A_1)$ at 616 cm^{-1}, versus TeO_2 concentration in 26.0 M HF as shown in Figure 10. The data for this plot is given in Table XII, solutions 1-3. Moreover, there is excellent agreement with the Raman spectrum of TeF_5^- in CH_3CN [29] with the single exception of the peak at 590 cm^{-1}, assigned to $\nu_7(E)$, which has not been observed in this work. ν_7 is better assigned as coincident with $\nu_4(B_1)$. It was not possible, however, to resolve the strong band at 508 cm^{-1} into its constituent bands ν_4 and ν_7. The coincidence of these two modes agrees well with the

Figure 10

Plot of the Dependence of the Integrated Peak Intensity of ν_1 (616 cm^{-1}) on TeO_2 Concentration in 26.0 M Hydrofluoric Acid.

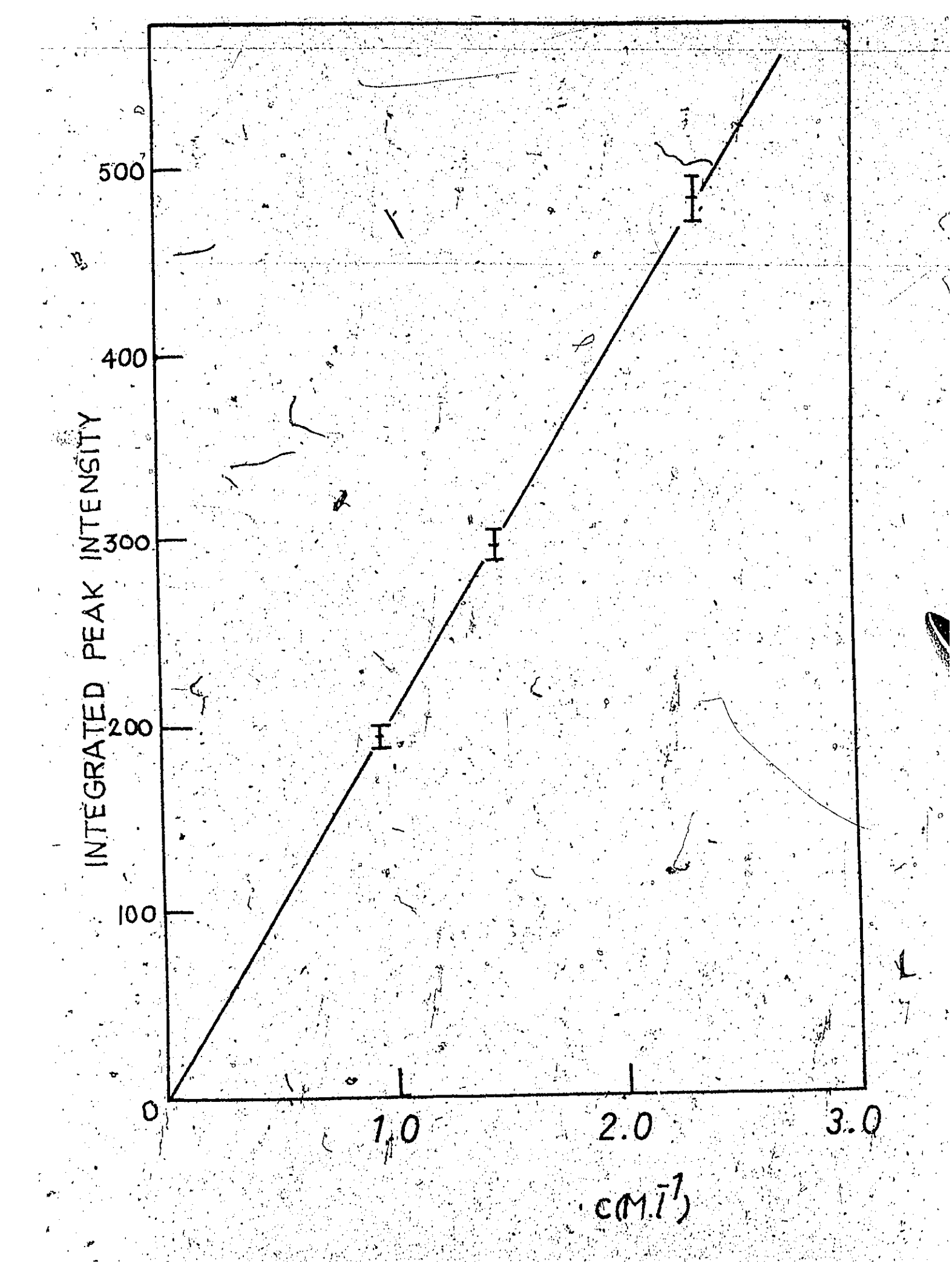
INTEGRATED PEAK INTENSITY
500
400
300
200
100
0
1.0
2.0
3.0
c(M.l⁻¹)

TABLE XII

Calculation of the Hydrolysis Constant K_h of the TeF_5^- Ion

Soln #	C_{HF} $M.l^{-1}$	Total Te(IV) $M.l^{-1}$	Int* TeF_5^-	$[TeF_5^-]$ $M.l^{-1}$	$[Te(OH)F_4^-]$ $M.l^{-1}$	M_{HF} $M.l^{-1}$	$[HF]$ $M.l^{-1}$	a_{H_2O} (N)	K_h $M.l^{-1}$
1	26.0	0.94	194	0.94	-	21.3	-	-	-
2	26.0	1.44	299	1.44	-	18.8	-	-	-
			292						
3	26.0	2.32	482	2.32	-	14.4	-	-	-
4	21.17	3.75	475	2.29	1.46	3.88	3.25	.947	2.19
5	18.82	3.75	330	1.60	2.15	2.22	1.94	.965	2.70
6	15.29	2.25	231	1.12	1.13	2.82	2.41	.957	2.54
7	12.94	2.31	226	1.09	1.22	2.61	2.24	.959	2.61
8	12.94	1.98	235	1.14	0.84	3.88	3.25	.947	2.52
9	8.83	1.91	88	0.43	1.48	0.76	0.75	.975	2.65

* Integrated Peak Intensity relative to ν_1 0.34M ClO_4^- (928 cm^{-1}) = 100

Mean $K_h = 2.5 \pm .1$ $M.l^{-1}$

change in position of ν_4 and ν_7 across the isoelectronic series SbF_5^{2-}, TeF_5^-, and IF_5. The observed polarization of the other three A_1 modes: ν_1(621 cm^{-1}), ν_2(520 cm^{-1}) and ν_3(273 cm^{-1}) confirms their assignment in $KTeF_5$.

As the mole ratio of HF to TeO_2 decreases the Raman spectrum of a new species appears and increases in intensity as the spectrum of TeF_5^- decreases, as shown in Figure 7. This new spectrum is the same as a solution of $KTe(OH)F_4$ in water, and on the basis of the close analogy with the solid, is attributed to the $Te(OH)F_4^-$ ion. The two highest frequency modes are both polarized as expected for $\nu_1(A_1)$ and $\nu_2(A_1)$ in this symmetry. In addition $\nu_3(A_1)$ is assigned to the polarized band at 265 cm^{-1}. The Raman spectrum of a solution of $KTeF_5$ run immediately after solution showed only the bands due to the $Te(OH)F_4^-$ ion, and indicates the rapid displacement of the apical fluorine in TeF_5^- by OH.

No evidence for the presence of lower fluoro tellurates such as may be derived from the $TeO_2F_2^{2-}$ ion was found in these solutions. A mixture which was made up with 3:1 mole ratio HF/TeO_2 yielded a clear solution on warming, but on cooling deposited TeO_2. The Raman spectrum of the clear solution showed only the spectrum of the $Te(OH)F_4^-$ ion. The absence of a band at 840 cm^{-1}, which is characteristic of the $TeOF_4^{2-}$ ion, indicates that the $Te(OH)F_4^-$ ion is not significantly dissociated to $TeOF_4^{2-}$. Furthurmore, the close agreement of the spectrum with that of $KTe(OH)F_4$ indicates the absence of the acid H_2TeOF_4 in solution, which must, therefore, be at least a moderately strong acid.

The changing intensities of the Raman spectra of the two ions with the changing HF/TeO_2 mole ratio, shown in Figure 7, indicates that the two tellurium(IV) ions are in equilibrium in these solutions.

$$TeF_5^- + H_2O \overset{K_h}{=} Te(OH)F_4^- + HF$$

The equilibrium constant, K_h, is given by:

$$K_h = \frac{a_{Te(OH)F_4^-} \cdot a_{HF}}{a_{TeF_5^-} \cdot a_{H_2O\,(N)}} = \frac{f_{Te(OH)F_4^-} \cdot [Te(OH)F_4^-] \cdot f_{HF}[HF]}{f_{TeF_5^-} \cdot [TeF_5^-] \cdot a_{H_2O\,(N)}}$$

Since the two complex ions are similar in both charge and structure, the factor of their activity coefficients may be set equal to unity as a good approximation. It is assumed that f_{HF} may also be set equal to unity. The equilibrium constant may then be evaluated by the quantitative determination of the Te(IV) anion concentrations once the molar absorptivity, J_i, is known for one of the species in solution[141]. This is obtained from the integrated peak intensity plot of ν_1 of TeF_5^- shown in Figure 10. Once $J_{TeF_5^-}$ is known, the stoichiometric concentration of TeF_5^- can be found for the solutions containing both this anion and $Te(OH)F_4^-$. The $Te(OH)F_4^-$ ion concentration and a partially corrected HF concentration M_{HF}, can then be determined from stoichiometry.

$$[Te(OH)F_4^-] = C_{TeO_2} - [TeF_5^-]$$

$$M_{HF} = C_{HF} - 5\left[TeF_5^-\right] - 4\left[Te(OH)F_4^-\right]$$

C_{TeO_2} and C_{HF} represent the total initial molarities of both species. Equilibrium molalities of molecular HF in aqueous solution have been measured up to a stoichiometric HF concentration of 4 m [142], and $\left[HF\right]$ has been evaluated from this data by interpolation. Concentrations were converted to the molar scale using density data from tables [143]. While water activities in aqueous HF have not been evaluated, values of a_{H_2O} were obtained from the vapour pressure measurements of Fredenhagen [144]. The validity of this approach has been shown for aqueous HCl solutions, where $a_{H_2O}(N)$ values from vapour pressure measurements agree within experimental limits with those determined by EMF methods [145].

The effect of a relatively small concentration of $HClO_4$ on $a_{H_2O}(N)$ and $\left[HF\right]$ has not been taken into consideration, but it must be small considering the agreement between K_h values given in Table XII. The hydrolysis constant was found to be $2.5 \pm .1$ $M.l^{-1}$.

<u>^{19}F NMR</u>

The ^{19}F NMR spectrum of a solution of TeO_2 in 26.0 M HF showed exchange of any fluoro or oxofluoro tellurium(IV) species present with the solvent down to the freezing point of the solution.

CHAPTER IV

Fluoro and Oxofluoro Anions of Iodine(V)

Iodine in its penultimate valence state provides an interesting bridge between the wide number of fluorides and oxyfluorides of xenon(VI) [2], and the little studied tellurium(IV) species. Furthur, iodine resembles xenon more than tellurium in much of its fluoride chemistry, both in the diversity of compounds isolated, and in the wide range of coordination observed. The formally lower coordinated species such as IO_2F are polymeric[95], and the $IO_2F_2^-$ ion has strong interanion bridging over oxygen in its salts[94].

The nature of the aqueous solution chemistry of iodine(V) has in particular been little studied, and provides a large amount of the material in this chapter.

X-Ray Powder Photography

$CsIOF_4$ and $KIOF_4$:

$CsIOF_4$ was not prepared pure. However, the infrared spectrum of a product prepared by the deliberate hydrolysis of CsF and IF_5 in CH_3CN showed $CsIOF_4$ to be the major constituent (see later). The x-ray powder photograph data for this material is given in Table XIII. It is evident from Chapter II that the possible impurities are $CsIF_6$ and $CsIO_2F_2$. Failure to isolate anhydrous $CsIO_2F_2$ (see later) precludes the identification of any reflexes due to this salt. However, Christe[23] reports the x-ray powder data for a number of hexafluoroiodate(V) salts including $CsIF_6$. Inspection of the data in Table XIII indicates the absence of any $CsIF_6$ in this product. Furthur of the 22 reflexes measured, 19 were fitted using the cell parameters reported by Ryan and Asprey[75]. It was therefore assumed that the product contained only $CsIO_2F_2$ as impurity.

It was also not possible to prepare $KIOF_4$ pure. However, the x-ray powder data for a product prepared according to the hypothetical reaction, in CH_3CN

$$2IF_5 + 2KF + KIO_3 = 3KIOF_4$$

is given in Table XIV. There is no evidence for the presence of any KIF_6 (d spacings, 4.53, 3.93), or KIO_3 (d spacings, 4.48, 3.16) The three major reflexes of KIO_2F_2 are present (d spacings, 3.34, 2.88 and 2.04).

TABLE XIII

X-Ray Powder Photography Data for $CsIOF_4$ + $CsIO_2F_2$ Product

d(Å)	Intensity	Exptl $\sin^2\theta$	Calcd $\sin^2\theta$	hkl
4.06	40			
3.77	10	.0417	.0418	121
3.56	40			
3.25	40	.0561	.0560	140
3.09	10	.0623	.0619	050
2.56	10			
2.39	10	.1033	.1032	231
2.20	100	.1224	.1235	052
2.14	10	.1293	.1295	212
1.88	70	.1680	.1671	162
			.1667	242
1.81	50	.1819	.1830	072
1.71	30	.2025	.2005	053
			.2024	341
1.68	10	.2095	.2090	302
			.2093	350
1.57	50	.2415	.2437	243
			.2395	281
1.50	10	.2649	.2626	104
			.2651	114
			.2660	253
1.48	20	.2703	.2685	034
			.2725	124
			.2709	352
			.2688	370
			.2719	420
1.44	20	.2881	.2858	044
			.2859	303
			.2884	313
			.2873	421

TABLE XIII (Continued)

d(Å)	Intensity	Exptl $\sin^2\theta$	Calcd $\sin^2\theta$	hkl
1.41	30	.3001	.3023	144
			.2981	362
			.2997	431
			.3017	340
1.37	20	.3164	.3134	183
			.3142	214
			.3171	441
1.34	20		.3303	372
1.08	20	.5075	.5062	075
			.5122	255
			.5108	414
			.5106	542
1.03	10	.5594	.5541	006
			.5565	016
			.5640	026
			.5545	335
			.5578	523

a = 6.024 Å
b = 15.448
c = 6.214

TABLE XIV

X-Ray Powder Photography Data for $KIOF_4$ + KIO_2F_2 Product

$KIOF_4$ + KIO_2F_2 Cu-Kα Irradiation

d	Intensity
5.52	70
4.41	20
3.84	50
3.60	50
3.34	100
3.08	20
2.88	50
2.50	20
2.12	20
2.04	20
1.88	10
1.86	10
1.81	10
1.68	10
1.63	10

The $CsIOF_4$ and $KIOF_4$ salts appear to be isomorphous. Thus the x-ray powder photography indicates that the $CsIOF_4$ and $KIOF_4$ products contain only $CsIO_2F_2$ and KIO_2F_2 impurities respectively, with the absence of the hexafluoroiodate(V) salts and the corresponding alkali metal fluorides

$CsIO_2F_2.1/3H_2O$, $Co(NH_3)_6(IO_2F_2)_3.H_2O$ and $CsIO_2F_2.HIO_2F_2.2H_2O$:

The x-ray powder photographs for these three salts show them to be crystalline, and the data is given in Table XV.

TABLE XV

X-Ray Powder Photography Data for $IO_2F_2^-$ Species

$CsIO_2F_2.1/3H_2O$ Cu-Kα Irradiation

d	Intensity
3.553	100
3.132	50
3.104	50
2.787	10
2.406	10
2.207	80
1.998	10
1.903	20
1.870	50
1.807	30
1.685	10
1.437	30
1.278	30

$Co(NH_3)_6(IO_2F_2)_3.H_2O$

3.432	100
3.303	100
3.098	50
3.042	20
2.856	10
2.031	50
2.003	10
1.975	20
1.954	20

TABLE XV (Continued)

d	Intensity
1.541	20
1.463	10
1.443	10
1.392	30
1.382	30
1.302	10
1.260	10
1.146	20
0.995	20

$CsIO_2F_2.HOIOF_2.2H_2O$

3.542	50
3.480	50
3.349	50
3.117	100
2.545	100
2.208	30
1.970	40
1.816	100
1.568	40
1.476	30
1.404	40
1.344	10
1.189	100
1.079	20
1.050	20
0.996	20
0.973	30
0.875	50

Vibrational Spectra

$CsIOF_4$ and $KIOF_4$:

The observed Raman spectrum of a mixture of $CsIOF_4$ and $CsIO_2F_2$ is given in Figure 11, trace A, along with the Raman spectrum of KIO_2F_2, trace B. The observed vibrational frequencies for $CsIOF_4$ were determined and are given in Table XVI. The infrared spectrum of the same product is given in Figure 12, trace A, and the fundamental frequencies in Table XVI. These have again been obtained by removal of the characteristic $IO_2F_2^-$ frequencies. The absence of any $CsIF_6$ in this product can be seen by comparison with the infrared spectrum of a product known to contain IF_6^-. Figure 12, trace C, shows the infrared spectrum of $KIOF_4$ contaminated with both KIO_2F_2 and KIF_6. This product was obtained by reaction in excess IF_5 (see Chapter II). Figure 12, trace B, shows the infrared spectrum of a product contaminated with a substantial amount of $CsIO_2F_2$, but again $CsIF_6$ is absent. This product was obtained using CH_3CN as solvent.

The definitive assignment of the vibrational spectrum of the IOF_4^- ion is difficult in the absence of a pure salt. However, the following assignment is based upon the Raman spectrum in Figure 11, trace A, and the infrared spectra of Figure 12, traces A and B. The assignment is given in Table XVII.

The IOF_4^- ion in $CsIOF_4$ has been shown to be square pyramidal, with the oxygen occupying the apical position[75]. For idealized C_{4v} symmetry 9 modes are expected; all are Raman active while only six ($3A_1 + 3E$) are infrared active. 8 modes are observed

Figure 11

Raman Spectra of $CsIOF_4$ and KIO_2F_2

A $CsIOF_4$ + $CsIO_2F_2$

B KIO_2F_2

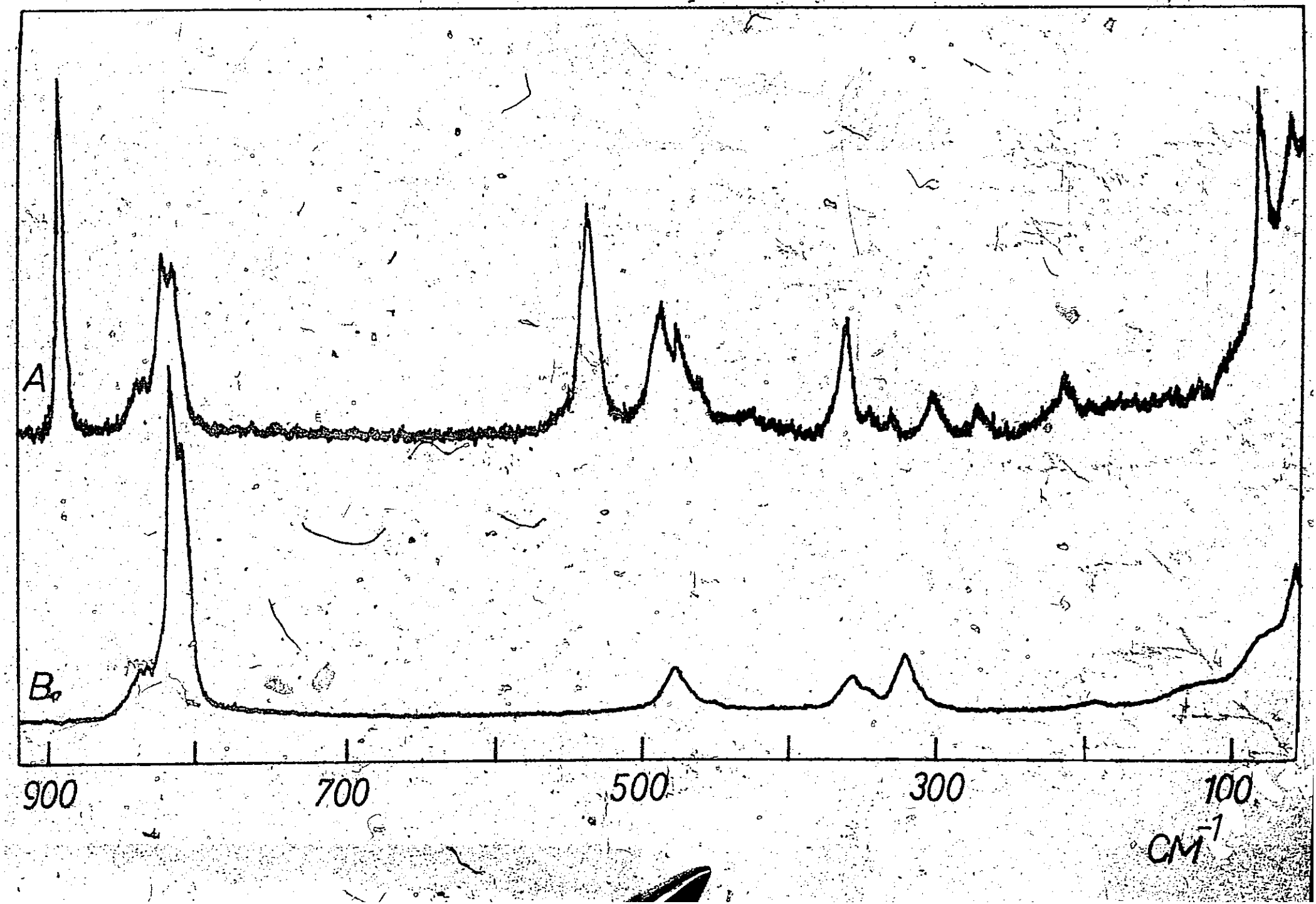
A
B
900
700
500
300
100
см⁻¹

Figure 12

Infrared Spectra of IOF_4^- Products

A $CsIOF_4$ + $CsIO_2F_2$

B " "

C $KIOF_4$ + KIO_2F_2 + KIF_6

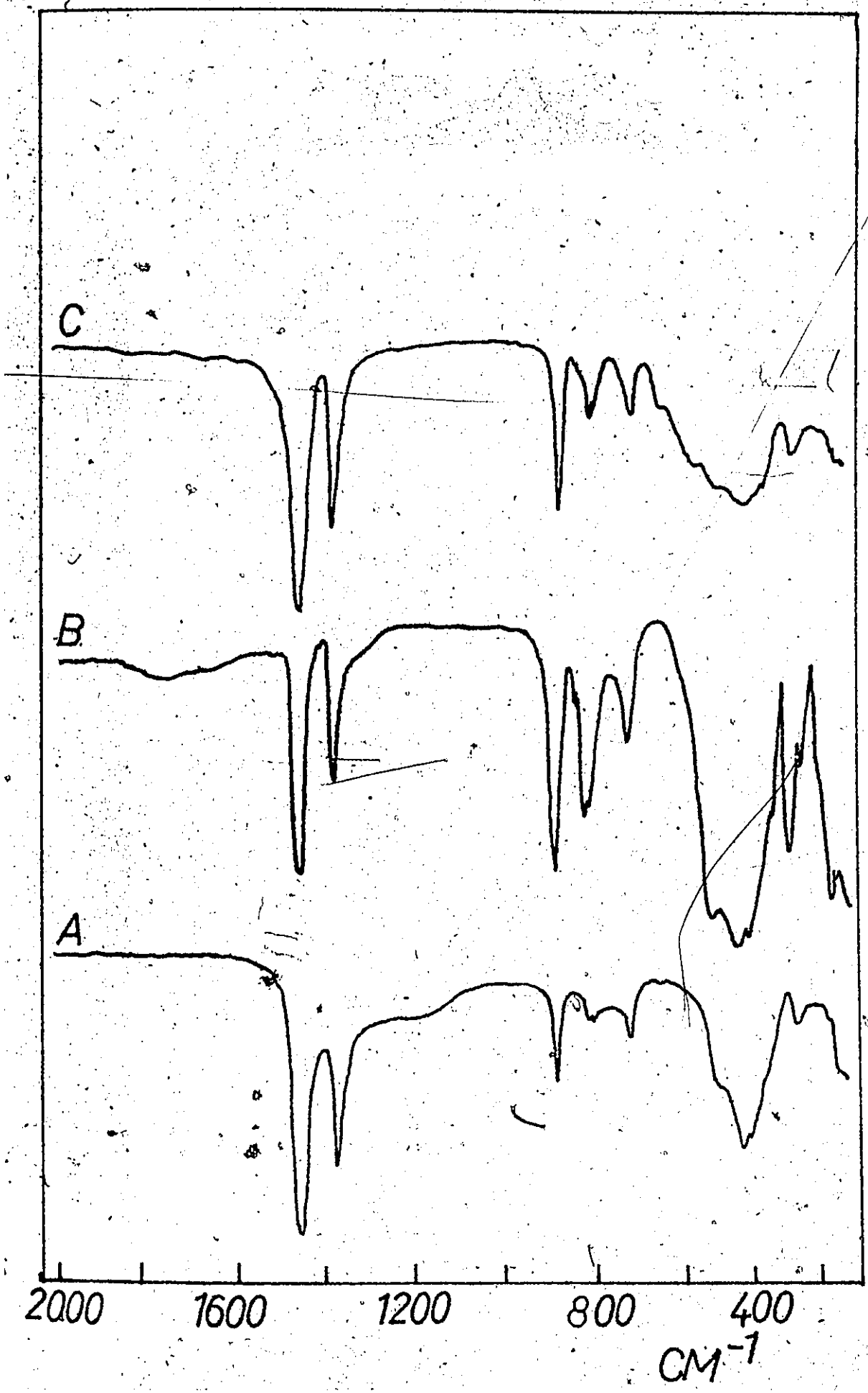
C
B
A
2000
1600
1200
800
400
CM-1

TABLE XVI

Raman and Infrared Spectra of $CsIOF_4$ + $CsIO_2F_2$ Product

$CsIOF_4/CsIO_2F_2$ [a]		KIO_2F_2 [b]		$CsIOF_4$	
Raman	Ir	Raman	Ir	Raman	Ir
888 vs	885 m			888 vs	885 m
835 mw,sh	845 w	838 w	851 m		
			845 m		
817 ms	825 w	817 vs	819 m		
810 ms		814 w,sh	805 w,sh		
533 s	535 m,sh			533 s	535 m,sh
485 m	482 vs,br	479 s	485 vs	485 m	[482 vs, br]
475 w,sh				475 w,sh	
440 vw,sh		456 vw	440 m		
			407 m		
365 m	385 mw,br	360 m	360 s	365 m	385 mw,br
			351 w,sh		
345 vw		346 w	345 s		
332 w		323 s			
303 w	305 sh,br				
273 w				273 w	
214 mw			220 m,sh	214 mw	
190-160 w,vbr		194 vw	197 s	160 w,vbr	
90 m					
75 w					

a Ir bands below 300 cm-1 not assigned. b ref 145

TABLE XVII

Raman and Infrared Spectra of $CsIOF_4$ (C_{4v})

Class	Mode No.	Raman	Ir	Approx description of mode (C_{4v})
A_1	ν_1	888 vs	885 m	ν(IO)
	ν_2	533 s	535 m,sh	$\nu_{sym}(IF_4)$-in phase
	ν_3	273 w		$\delta_{sym}(IF_4)$ umbrella
B_1	ν_4	485 m	[482 vs,br]	$\nu_{sym}(IF_4)$-out of phase
	ν_5			$\delta_{asym}(IF_4)$ -out of plane
B_2	ν_6	214 mw		$\delta_{sym}(IF_4)$ - in plane
E	ν_7	475 w,sh	[482 vs,br]	$\nu_{asym}(IF_4)$
	ν_8	365 m	385 mw,br	$\delta(OF_4)$ wag
	ν_9	160 mw,br		$\delta_{asym}(IF_4)$-in plane

in all, the one absence being accounted for by $\nu_5(B_1)$, which is rarely observed for this symmetry[66]. Four stretching modes are expected($2A_1 + B_1 + E$), and judging from the spectra of IF_5 [58], IF_4^- (ref 152))and $XeOF_4$ [73], all four stretching modes should lie above 400 cm^{-1}. Four fundamental stretching bands appear in the Raman spectrum of $CsIOF_4$, and the highest frequency peak at 888 cm^{-1} must be $\nu_1(A_1)$ the IO stretching mode, since this is the only peak in the characteristic IO stretching region. The corresponding mode in $XeOF_4$ occurs at 929 cm^{-1} (ref 73). The next most intense peak in the Raman spectrum lies at 533 cm^{-1} and is assigned to $\nu_2(A_1)$. IF_4^-, which has idealized D_{4h} symmetry, has a corresponding in-phase symmetric stretching (IF_4) mode at 522 cm^{-1} (ref 152). Of the remaining two stretching modes $\nu_7(E)$, the asymmetric (IF_4) stretch, is expected to be the most intense in the infrared, and is thus assigned to the band at 482 cm^{-1}. The intensity of the coincident $IO_2F_2^-$ band at 485 cm^{-1} can be estimated from the intensity of the IO stretches, and is too weak to account for the observed intensity of the band in this region in Figure 11, trace A. This assignment results in $\nu_4(B_1)$ being at 485 cm^{-1}, and thus ν_4 and ν_7 are almost coincident. This coincidence is also found in the isoelectronic TeF_5^- ion (see Chapter III). The corresponding modes in the IF_4^- ion occur at 455 and 448 cm^{-1} (ref 152).

The deformations are assigned by comparison with other C_{4v} molecules, especially $XeOF_4$ [73] and $TeOF_4^{2-}$ (see Table XXXIV, Chapter VI). The two lowest frequency peaks are assigned to $\nu_9(E)$ and $\nu_6(B_2)$ at 160 and 214 cm^{-1} respectively. The umbrella deformation $\nu_3(A_1)$ is assigned to the peak at 273 cm^{-1}; this mode is

seemingly little altered across the isoelectronic series $XeOF_4$, IOF_4^- and $TeOF_4^{2-}$. The corresponding umbrella deformation in IF_4^- occurs at 271 cm^{-1} (ref 152). Finally, the other little-altered mode, the wagging deformation $\nu_8(E)$, which does not involve motion of the central atom, is attributed to the peak at 365 cm^{-1}.

KIO_2F_2:

The Raman spectrum of KIO_2F_2 is given in Figure 11, trace B, and the infrared spectrum in Figure 14, trace A. The spectra recorded for KIO_2F_2 are in excellent agreement with those reported by Finch et al[145] and are included in Table XVIII. The given assignment is confirmed by the solution Raman spectrum obtained for $IO_2F_2^-$ (see later).

$CsIO_2F_2.1/3H_2O$:

The Raman spectrum of this salt is given in Figure 13, trace A, and the infrared spectrum in Figure 14, trace B. The observed frequencies are recorded in Table XVIII. Crystallization from 15% HF did not yield anhydrous $CsIO_2F_2$, as reported by Weinland and Koppen[126], but the hydrate $CsIO_2F_2.1/3H_2O$. The infrared spectrum of $CsIO_2F_2.1/3H_2O$ confirms that the product is a hydrate and does not contain a hydroxo group, since it has a band at 1655 cm^{-1}, the characteristic (HOH) deformation of the H_2O molecule. The other characteristic water bands, the OH stretching modes (3425 cm^{-1}) and the torsional mode (595/615 cm^{-1}) are also observed.

Comparison of the spectra of the $IO_2F_2^-$ ion in

Figure 13

Raman Spectra of $IO_2F_2^-$ Species

A $CsIO_2F_2.1/3H_2O$

B $CsIO_2F_2.HIO_2F_2.2H_2O$

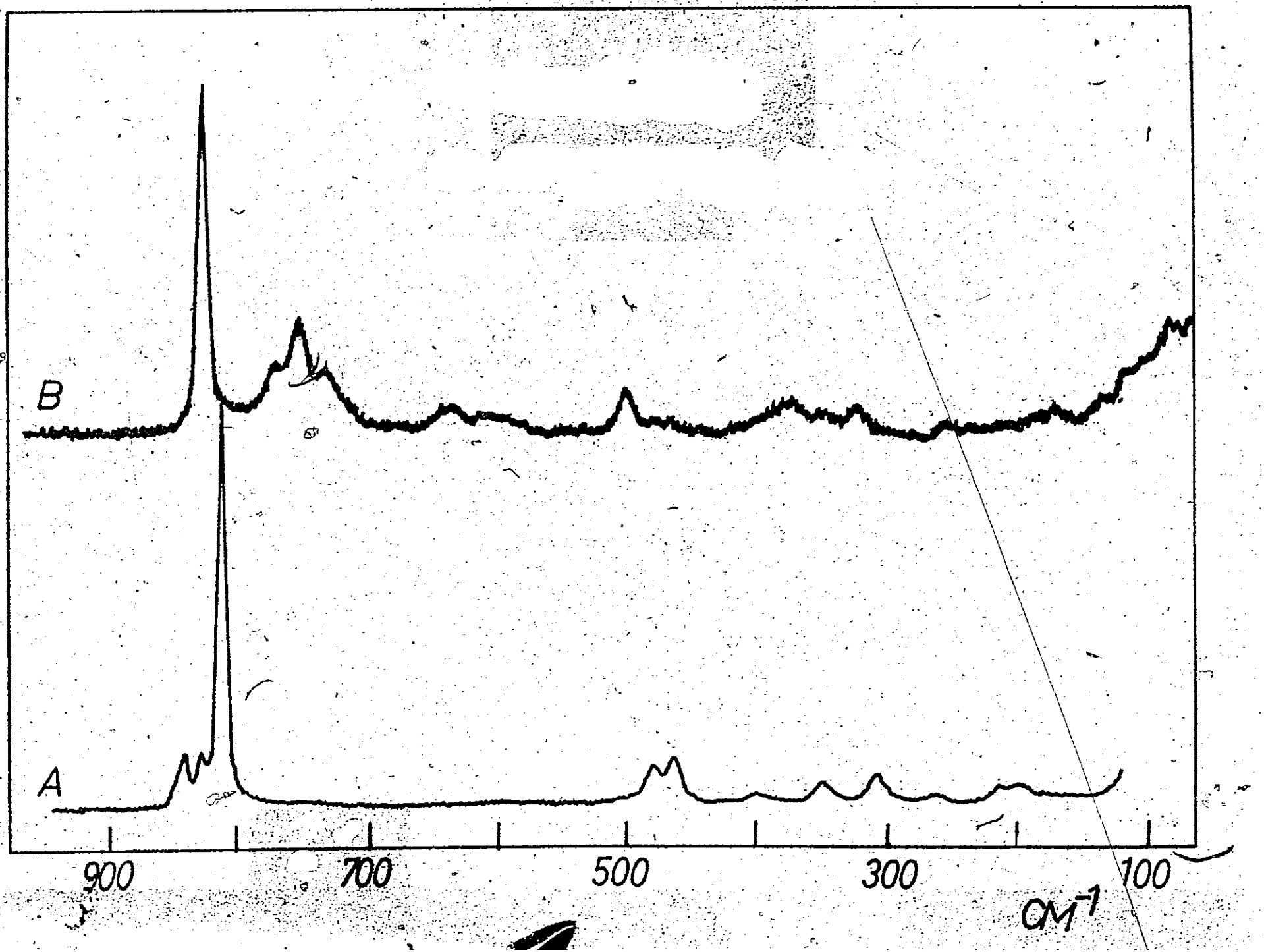
B
A
900
700
500
300
100
см⁻¹

Figure 14

Infrared Spectra of $IO_2F_2^-$ Species

A KIO_2F_2

B $CsIO_2F_2 \cdot 1/3H_2O$

C $Co(NH_3)_6(IO_2F_2)_3H_2O$

D $CsIO_2F_2 \cdot HIO_2F_2 \cdot 2H_2O$

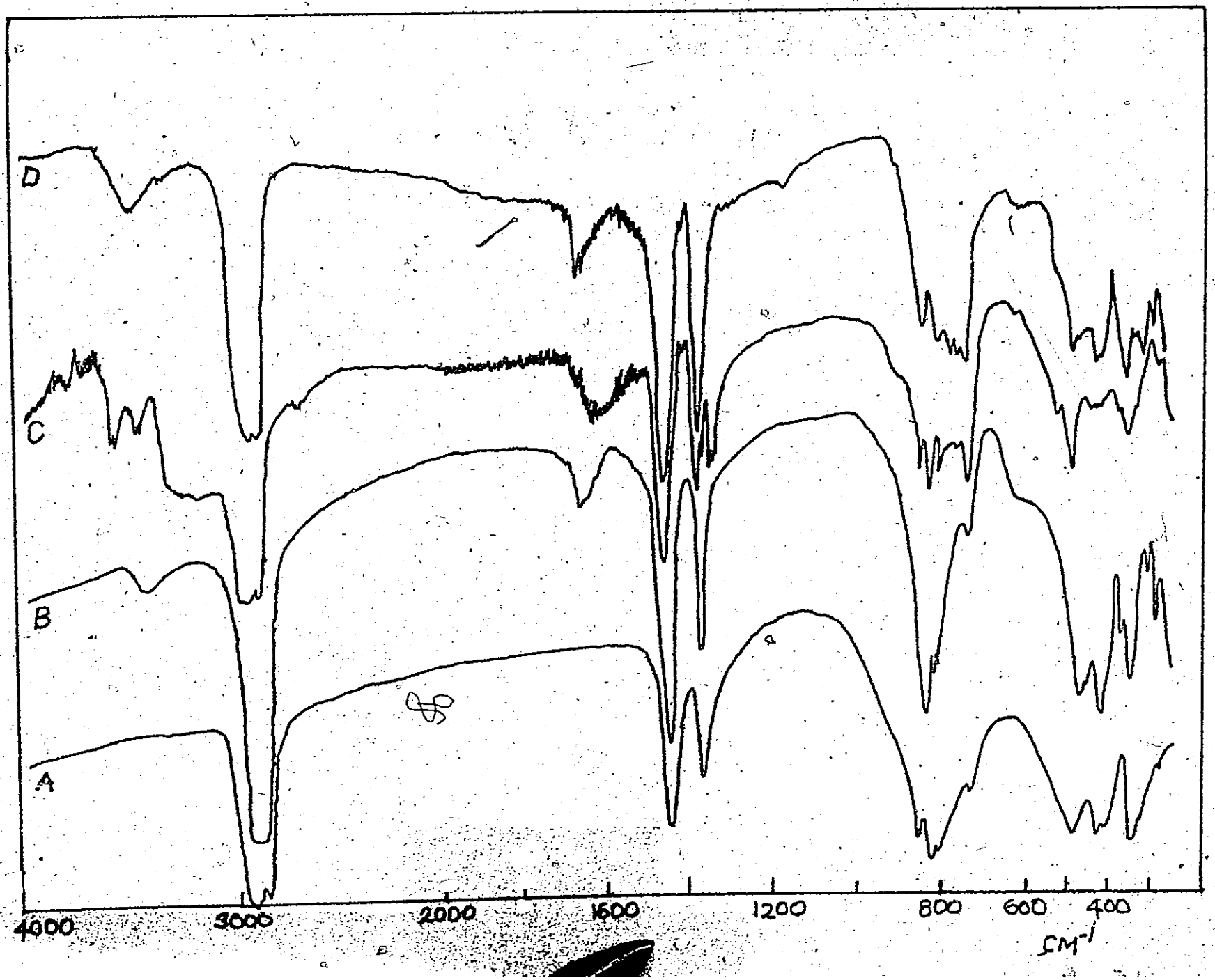
D
C
B
A
4000
3000
2000
1600
1200
800
600
400
CM⁻¹

this salt and in KIO_2F_2 reveals a considerable difference in the nature of the anion bridging in the two compounds.

$Co(NH_3)_6(IO_2F_2)_3.H_2O$:

The Raman spectrum of this salt is given in Figure 15, and the infrared spectrum in Figure 14, trace C. The observed frequencies are included in Table XVIII. Once again the infrared spectrum confirms the formulation of the compound as a hydrate, three OH stretching modes being observed at 3800, 3570 and 3450 cm^{-1}. This multiplicity of these OH stretching modes has been observed for other hydrates[146]. Five bands appear in the IO stretching region, indicating a more complex structure for this compound compared to KIO_2F_2 or $CsIO_2F_2.1/3H_2O$. The doubling up of many of the bands suggests that there are two types of $IO_2F_2^-$ ion in the substance, differing perhaps in the nature of their oxygen bridging or hydrogen bonding.

$CsIO_2F_2.HIO_2F_2.2H_2O$:

Crystallization of 2:1 cesium fluoride/iodic acid mixtures from 40% HF yields $CsIO_2F_2.HIO_2F_2.2H_2O$. The Raman spectrum of this compound is given in Figure 13, trace B, and the infrared spectrum in Figure 14, trace D. These spectra support the formulation of the compound as a hydrate and not a salt containing $H_5O_2^+$ or H_3O^+ ions. The bands at 3425 and 1670 cm^{-1} in the infrared spectrum are characteristic of a hydrate[139] and the band at 610 cm^{-1} may also be due to H_2O. The characteristic bands for $H_5O_2^+$ (ref 147) are

Figure 15

Raman Spectrum of $Co(NH_3)_6(IO_2F_2)_3 \cdot H_2O$

1000
800
600
400
200
CM-1

not present in the spectrum of this compound. The observation of a weak band at 1170 cm^{-1} shows the presence of a hydroxo group, and the broad band at 2900 cm^{-1} is indicative of a strong hydrogen bond, supporting the anion formulation as $H(IO_2F_2)_2^-$. In this regard the spectra are similar to those reported for the $H(IO_3)_2^-$ ion[148]. A complete assignment of the spectra for this compound is not possible due to the complexity of the spectra. A partial assignment is given in Table XVIII based upon the assumption that the $IO_2F_2^-$ and HIO_2F_2 parts of the spectrum can be separated.

Solutions

The section on solutions of HIO_3 in hydrofluoric acid is divided into two parts: the first deals with solutions in up to 48% HF, where the fluoro species present is $IO_2F_2^-$, and the second in the region 48 - 100% HF where the situation is more complex. A third section deals with the IF_5/H_2O system in acetonitrile.

1. HIO_3 in dilute HF solutions (up to 48% HF)

Raman Spectra

The Raman spectrum of a 3.0 M solution of HIO_3 in 48% HF shows no peaks that can be attributed to either HIO_3 or IO_3^-. The absence of a peak in the I-OH stretching region[139] furthermore eliminates the possibility of HIO_2F_2 being present. The Raman spectrum of this solution is given in Figure 16, trace B, and the similarity of this spectrum to that of KIO_2F_2 confirms that $IO_2F_2^-$ is the only species present, see Table XVIII. Polarization measurements confirm the assignment for KIO_2F_2. It was not possible to observe the

TABLE XVIII

Raman and Infrared Spectra of $IO_2F_2^-$ Species

Class	Mode No.	KIO_2F_2[a]		$CsIO_2F_2 \cdot 1/3H_2O$[b]		$CsIO_2F_2 \cdot HIO_2F_2 \cdot 2H_2O$[c]		$Co(NH_3)_6(IO_2F_2)_3H_2O$[d]		$IO_2F_2^-$[e]	Approx Description
		Raman	Ir	Raman	Ir	Raman	Ir	Raman	Ir	Raman	of Mode
A_1	ν_1	817 vs 814 w,sh	819 m 805 w,sh	814 vs	815 s 805 sh	833 vs	830 s	810 vs 788 s	790 s 760 m,br	840 vs,p(.16)	$\nu_{sym}(IO_2)$
	ν_2	479 s	485 vs	484 m	475 s	492 m	500 sh	484[f]	500 mw 470 s	483 m,p(.34)	$\nu_{sym}(IF_2)$
	ν_3	360 m	360 s 351 w,sh	372 w	380 sh	370 ms,br		371 w 359 mw	365 sh 378 sh	(335) mw,p	$\delta_{sym}(IO_2)$
	ν_4	194 vw	197 s	190 w,br				190[f] 184 m		170 w,p(.52)	$\delta_{sym}(IF_2)$
A_2	ν_5		220 m,sh	256 vw 213 w,br	283 m	230, vw,br	250 m		255 w 250 w		τ
B_1	ν_6	838 w	851 m 845 m	836 m 822 m	825 vs		830 ms	839 w 833 w 817 sh	810 vs		$\nu_{asym}(IO_2)$
	ν_7	346 w	345 s	352 w	345 s		340 sh	352 w 340 m	350 sh	(335) mw	$\delta_{asym}(IO_2)$
B_2	ν_8	456 vw	440 m 407 m	464 m	460 ms 422 s		445 sh	451 m 435 sh	425 m	420[f]	$\nu_{asym}(IF_2)$
	ν_9	323 s	345 s	314 m	320 sh 305 w	310 w	315 ms	330 mw 311 mw	340 ms	(335) mw	$\delta_{asym}(IF_2)$

a ref 145

b Ir bands due to H_2O: 3425 m,br, 1655 mw,br, 595/615 w,vbr

c Ir bands due to H_2O: 3425 m,vbr, 1670 m,br, 610 vw,vbr
Ir bands due to HIO_2F_2: 2900 w, 1170 vw, 780 m, 742s, 685 s,405/395 vs, 332 vs, 292 vs, 270 ms. Raman: 737ms, 775s, 755 ms, 635 w, 600 w,br, 450/460 vw, 335 vw, 150 w,br.

d Ir bands due to H_2O: 3800 vw, 3750 m,3450 m, 1655 sh.
Ir bands due to cation: 3270 s, 3150 s 1355 m, 1348 m, 975 vw, 640 s, 330 s, 270 s.
Raman bands due to cation: 496 s, 447 m,sh, 321 w.

e .2M HIO_3 in 24M HF

f band superimposed on glass or sapphire

Figure 16

Raman Spectra of KIO_2F_2 and $IO_2F_2^-$ in Solution

A KIO_2F_2

B 3.0 M HIO_3 in 48% HF

C " " (Gain x5)

D " " (Gain x2)

S indicates slit width

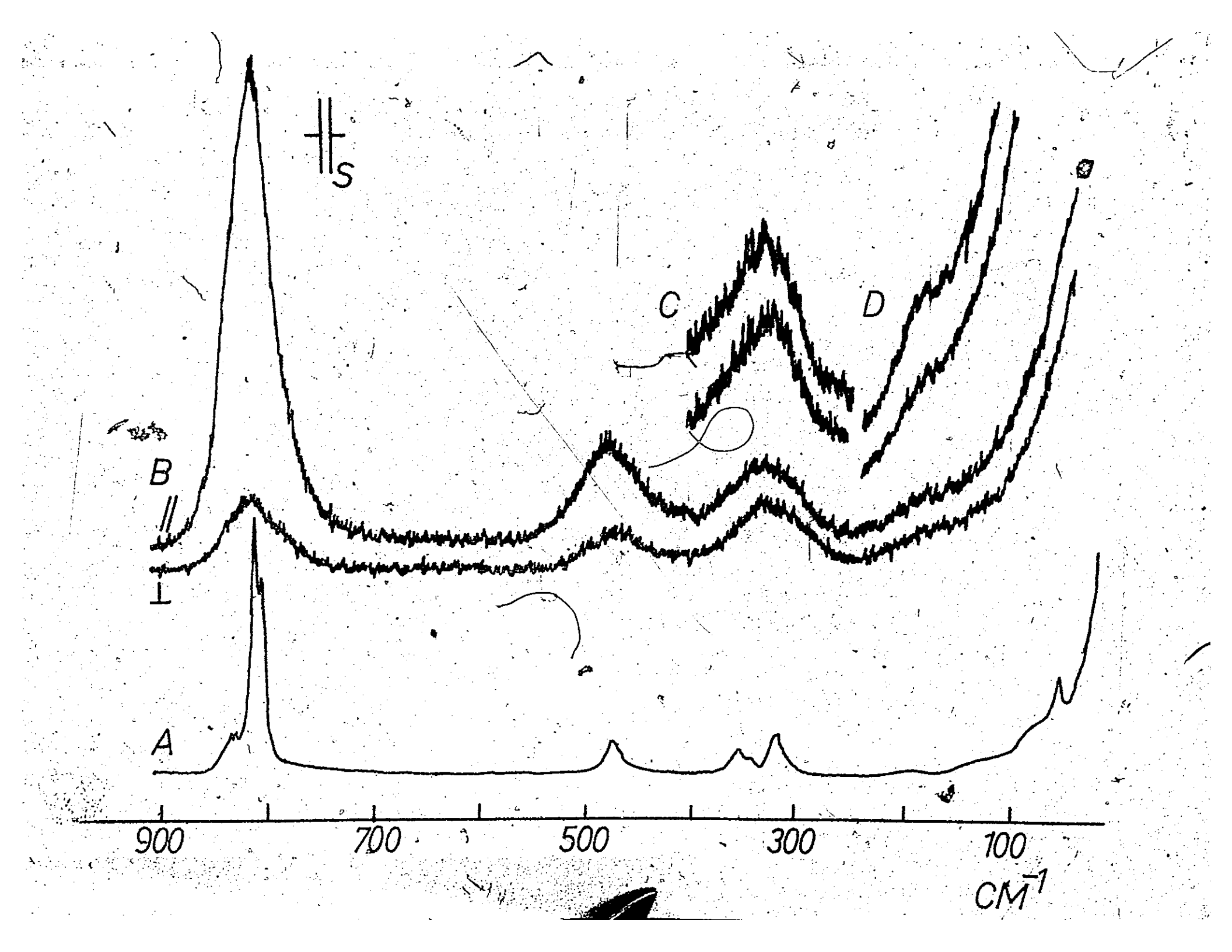
S
C
D
B
A
900
700
500
300
100
CM⁻¹

symmetric (IO_2) deformation, $\nu_3(A_1)$, since the envelope centered at 335 cm^{-1} also includes $\nu_7(B_1)$ and $\nu_9(B_2)$. This band shows a degree of polarization little different from the 0.75 expected for a depolarized band, and no certain conclusion can be drawn from the relative ordering of these three bands.

Furthur evidence that $IO_2F_2^-$ is the only species present in solutions of HIO_3 in 48% HF comes from a linear plot of the integrated peak intensity of ν_2 of $IO_2F_2^-$ (483 cm^{-1}) versus initial iodic acid concentration, c_{HIO_3}, shown in Figure 17, plot A. The data for this plot is given in Table XIX, solutions 4-6. As HF concentration is reduced, holding c_{HIO_3} constant, the Raman spectrum of the solution changes as shown in Figure 18, the new species being identified as HIO_3 from its characteristic I-OH stretching mode, $\nu_1(A_1)$, at 644 cm^{-1} (ref 139). These changes are governed by the equilibria:

$$IO_2F_2^- + H_2O \overset{K_h}{\rightleftharpoons} IO_3^- + 2HF$$

$$HIO_3 \overset{K_d}{\rightleftharpoons} H^+ + IO_3^-$$

The hydrolysis constant K_h, is given by

$$K_h = \frac{a_{IO_3^-} \cdot a_{HF}^2}{a_{IO_2F_2^-} \cdot a_{H_2O(N)}} = \frac{f_{IO_3^-} \cdot [IO_3^-] \cdot f_{HF}^2 \cdot [HF]^2}{f_{IO_2F_2^-} \cdot [IO_2F_2^-] \cdot a_{H_2O(N)}}$$

Figure 17

Dependence of Integrated Peak Intensity on Concentration for:

A ν_2 (483 cm^{-1}) of $IO_2F_2^-$

B ν_4 (690 cm^{-1}) of HIO_3

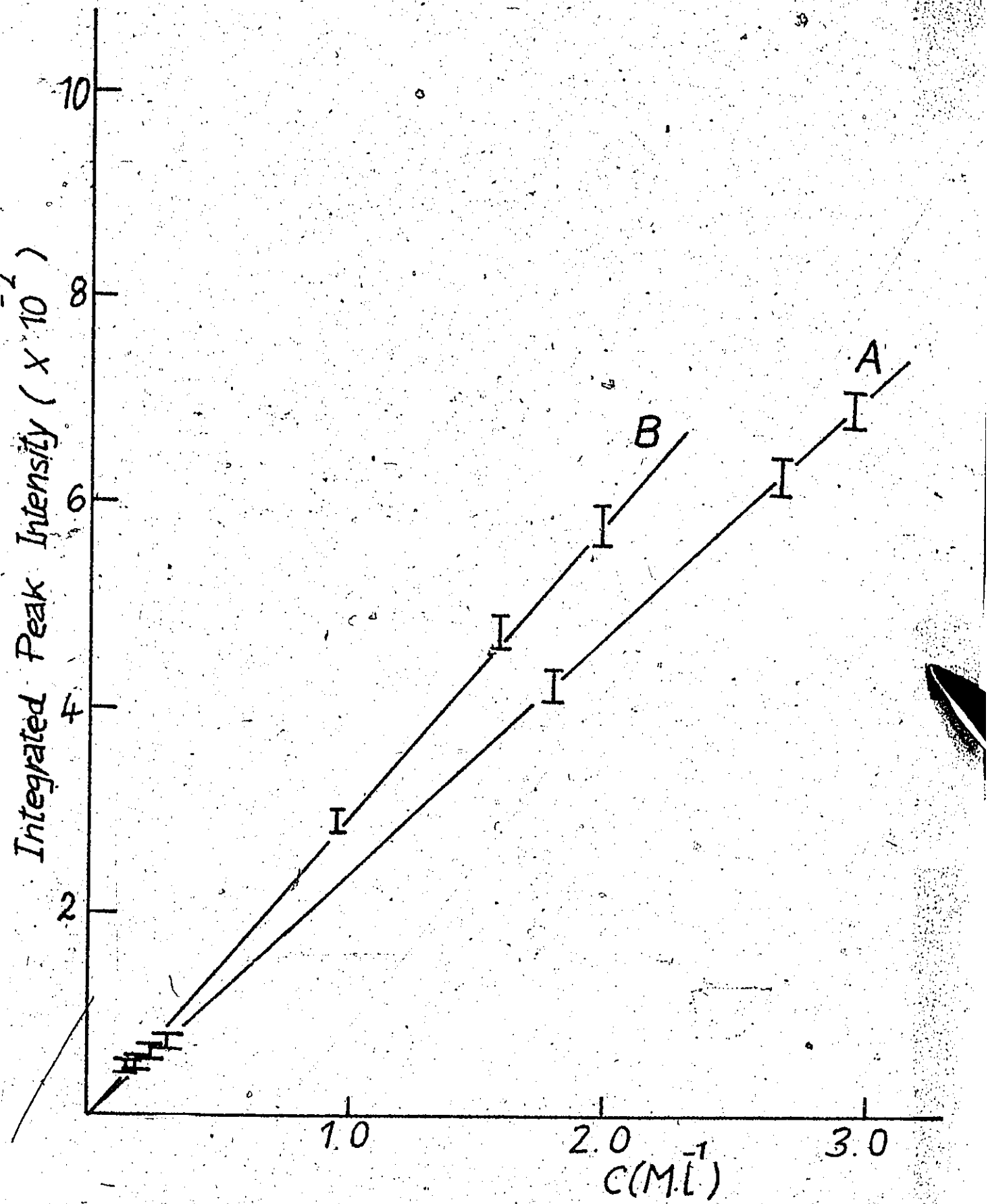
Integrated Peak Intensity (X 10^{-2})
10
8
6
4
2
A
B
1.0
2.0
3.0
C(M.l^{-1})

Figure 18

Raman Spectra of HIO_3 Solutions

A 2.83 M HIO_3 in H_2O

B 2.91 M HIO_3 in 24.2 M HF

C 3.01 M HIO_3 in 4.15 M HF

S indicates slit width

* sapphire (417 cm^{-1})

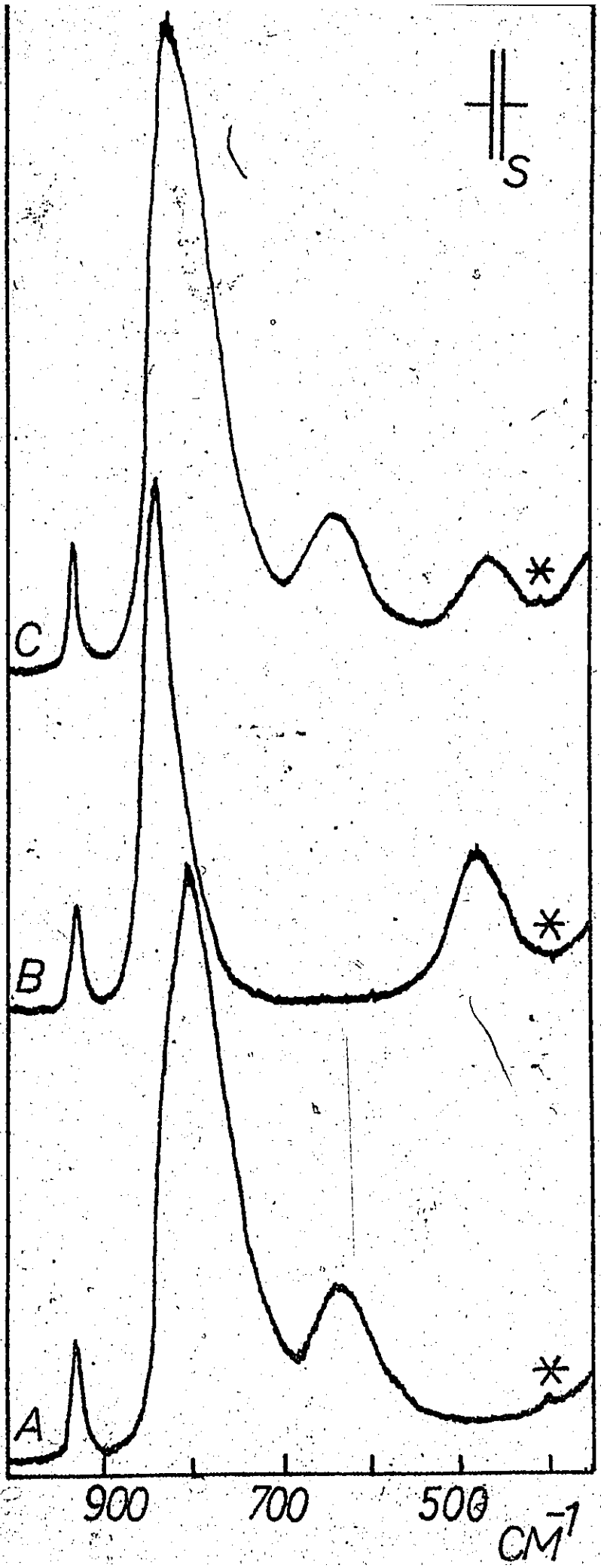
S
C
B
A
*
*
*
900
700
500
см⁻¹

The term $a_{H_2O}(N)$ denotes the activity of water on the mole fraction scale, referred to pure water where by definition $a_{H_2O}(N) = 1$. Since the two I(V) anions have the same charge, their activity coefficients may be assumed to cancel to a good approximation. The concentrations of the various I(V) species may be determined from the integrated peak intensities of ν_2 of $IO_2F_2^-$ (483 cm^{-1}) and ν_4 of HIO_3 (644 cm^{-1})

The concentration of $IO_2F_2^-$ may be determined in a given HIO_3 - HF solution from the plot of integrated peak intensity of ν_2 against $IO_2F_2^-$ concentration given in Figure 17, trace A. However, the concentration of IO_3^- cannot be determined in this manner due to the overlap of the IO stretching modes of HIO_3, IO_3^- and $IO_2F_2^-$ ions. Instead, HIO_3 concentration may be determined from the integrated peak intensity of ν_4 of HIO_3 at 644 cm^{-1} and $[IO_3^-]$ found from the stoichiometry.

$$c_{HIO_3} = [HIO_3] + [IO_3^-] + [IO_2F_2^-]$$

The molar intensity of ν_4 for HIO_3, J_{HIO_3}, may be evaluated from the data in Table XX and the HIO_3 concentration, calculated from the dissociation constant for HIO_3 [112]. The molar activity coefficients for the hypothetical completely dissociated iodic acid, f_{HIO_3}, listed in Table XX, have been calculated using the data and method of Durig et al[112] and the densities listed in ref.143. An initial calculation of iodic acid concentration is made, using the dissociation constant for iodic acid, $K_d = 0.18\ M.l^{-1}$ and,

assuming all activity coefficients, $f_{\pm HIO_3}$, are unity. Hydronium ion concentration was taken as the sum of that arising from iodic acid and the 0.34 M $HClO_4$ present in all solutions. The results of this calculation are given in Table XX and a plot of integrated peak intensity against HIO_3 calculated in this way gives a value of $J_{HIO_3} = 238$. The calculation was now improved by introducing ionic activity coefficients, $f_{\pm HIO_3}$ as calculated according to Durig et al[112] for the iodate ion concentration. The molecular iodic acid activity coefficient was still assumed to be unity. The results of this calculation are given in Table XX and Figure 17, trace B. The highest iodate concentration could not be used since the activity coefficient data do not extend to high enough concentrations. This plot gives a value of $J_{HIO_3} = 295$. This calculation takes no account of the effect of 0.34 M $HClO_4$ on $f_{\pm HIO_3}$. For the solution of lowest iodic acid concentration an estimate of $f_{\pm HIO_3}$ could be made, assuming $HClO_4$ to affect the activity coefficient exactly as hypothetical completely as ionized HIO_3 does. Thus, $f_{\pm HIO_3}$ was taken from ref.112 for an iodate concentration of .110 + .34 (= .45, $f_{\pm HIO_3}$ = .620). Calculation using this value gives $J_{HIO_3} = 340$. The greatest error in the determination of K_h arises from the uncertainty in J_{HIO_3}. A value of $J_{HIO_3} = 300 \pm 50$ was chosen for subsequent calculation.

The other parameters in the expression for K_h were evaluated as in Chapter III. The initial concentration of HF, c_{HF}, was corrected for reaction with iodate to give a partially corrected HF concentration, M_{HF}:

TABLE XIX

Calculation of the Hydrolysis Constant of the $IO_2F_2^-$ Ion

Solution #	Total Iodate(V) $M.l^{-1}$	Integrated Peak Intensity $\nu(IOH)_{HIO_3}$ [a]	$[HIO_3]$ $M.l^{-1}$	$[IO_3^-]$ $M.l^{-1}$	Integrated Peak Intensity $\nu(IF_2)_{IO_2F_2^-}$ [a]	$[IO_2F_2^-]$ $M.l^{-1}$	C_{HF} $M.l^{-1}$	M_{HF} $M.l^{-1}$	HF $M.l^{-1}$	$a_{H_2O}(N)$	K_h $M^2.l^{-2}$
1	1.80	-	-	-	428	1.80	24.20	-	-	-	-
2	2.69	-	-	-	637	2.69	24.20	-	-	-	-
3	2.91	-	-	-	677	2.91	24.20	-	-	-	-
4	1.99	265	.88	.92	45	0.19	2.35	1.97	1.74	0.968	15
5	1.99	179	.60	.83	132	0.56	4.70	3.58	3.12	0.942	15
6	3.01	310	1.03	1.12	203	0.86	5.87	4.15	3.59	0.936	18
7	3.06	230	.77	.96	315	1.34	8.22	5.54	4.75	0.913	18
8	3.59	168	.56	.88	508	2.16	11.75	7.43	6.33	0.886	18

a All Integrated Peak Intensities relative to ν_1 of 0.34M ClO_4^- = 100

Mean K_h = 17 ± 2 $M^2.l^{-2}$

TABLE XX

Calculation of the Molar Intensity for Iodic Acid, J_{HIO_3}

c_{HIO_3} $M.l^{-1}$	Integrated Peak Intensity $\nu(I\text{-}OH)_{HIO_3}$ (ν_4)	$[IO_3^-]^a$	$f_{\pm HIO_3}$	$[IO_3^-]^b$	$[HIO_3]$
.272	47	.080	.770	.110	.162
.327	51	.096	.756	.131	.196
.429	62	.120	.739	.169	.260
.524	73	.142	.725	.203	.321
1.46	291	.310	.656	.490	.97
2.29	478	.430	.628	.690	1.60
2.83	580	.500	.615	.822	2.01
4.40	890	.670	-	-	-

a calculated assuming $f_{\pm HIO_3} = 1$

b calculated using $f_{\pm HIO_3}$ in column 4 (see text)

$$M_{HF} = c_{HF} - 2[IO_2F_2^-]$$

Equilibrium molalities of HF, in aqueous solutions nave been measured up to an initial HF concentration of 4 m[142], and [HF] listed in Table XIX has been evaluated from these data by interpolation and using density data in ref.143. It was assumed that $f_{HF} = 1$. The [HF] at higher concentrations than 4 m (3.82 M) have been arrived at by a linear extension of Hamer and Wu's data[142]. The justification for this procedure comes from Fredenhagen's work[144] where it was shown that the partial pressure of HF over aqueous solutions shows a linear dependence on HF concentration up to above 7.0 M HF. Hydrogen fluoride vapour is known to be monomeric up to vapour pressures greater than those measured over 7.0 M HF[146]. Water activities have been calculated from H_2O vapour pressure measurements over aqueous HF solutions[144] as was done in Chapter III. The effect of $HClO_4$, present for normalization purposes, and the I(V) anions on [HF] and $a_{H_2O}(N)$ in these solutions has not been taken into consideration. In spite of this, there is satisfactory agreement in K_h over a wide range of c_{HIO_3} and c_{HF} as shown in Table XIX, solutions 4 - 8 . The hydrolysis constant, K_h, was found to be $17 \pm 2\ M^2.1^{-2}$.

^{19}F NMR in aqueous HF solutions (up to 48% HF)

The ^{19}F NMR spectrum of a HIO_3 solution in 48% HF at -45° showed only one peak in addition to that due to the solvent. This peak was identified as being due to $IO_2F_2^-$ as follows. The ratio of the integration of the high field peak, due to HF, to the low field peak was equal to the ratio $HF:IO_2F_2^-$ calculated from the stoichiometry of the solution.

The observed shifts and peak areas are given in Table XXI.

2. HIO_3 in Concentrated HF Solutions (48-100% HF)

Raman Spectra

In solutions of HIO_3 in 48% HF the only iodine(V) species present is $IO_2F_2^-$. However, as the HF concentration is increased the Raman spectrum of a new species becomes apparent, increasing in intensity as the Raman Spectrum of $IO_2F_2^-$ diminishes. For a solution of HIO_3 in 78% HF this new species is a major constituent, see Figure 19, trace A. The similarity of the Raman spectrum of this new species to that of $IO_2F_2^-$, and the appearance of a band at 700 cm^{-1}, characteristic of an I-OH stretching mode[139], indicates this new species is HIO_2F_2.

$$IO_2F_2^- + 2HF \rightleftharpoons HIO_2F_2 + HF_2^-$$

Thus as the acid strength of HF increases the reaction moves to the right. In 78% HF there still remains a small amount of $IO_2F_2^-$,

Figure 19

Raman Spectra of HIO_3 solutions in HF

A 3.0 M HIO_3 in 78% HF

B 3.0 M HIO_3 in 65% HF

C 3.0 M HIO_3 in 48% HF

S indicates slit width

* sapphire (417 cm^{-1})

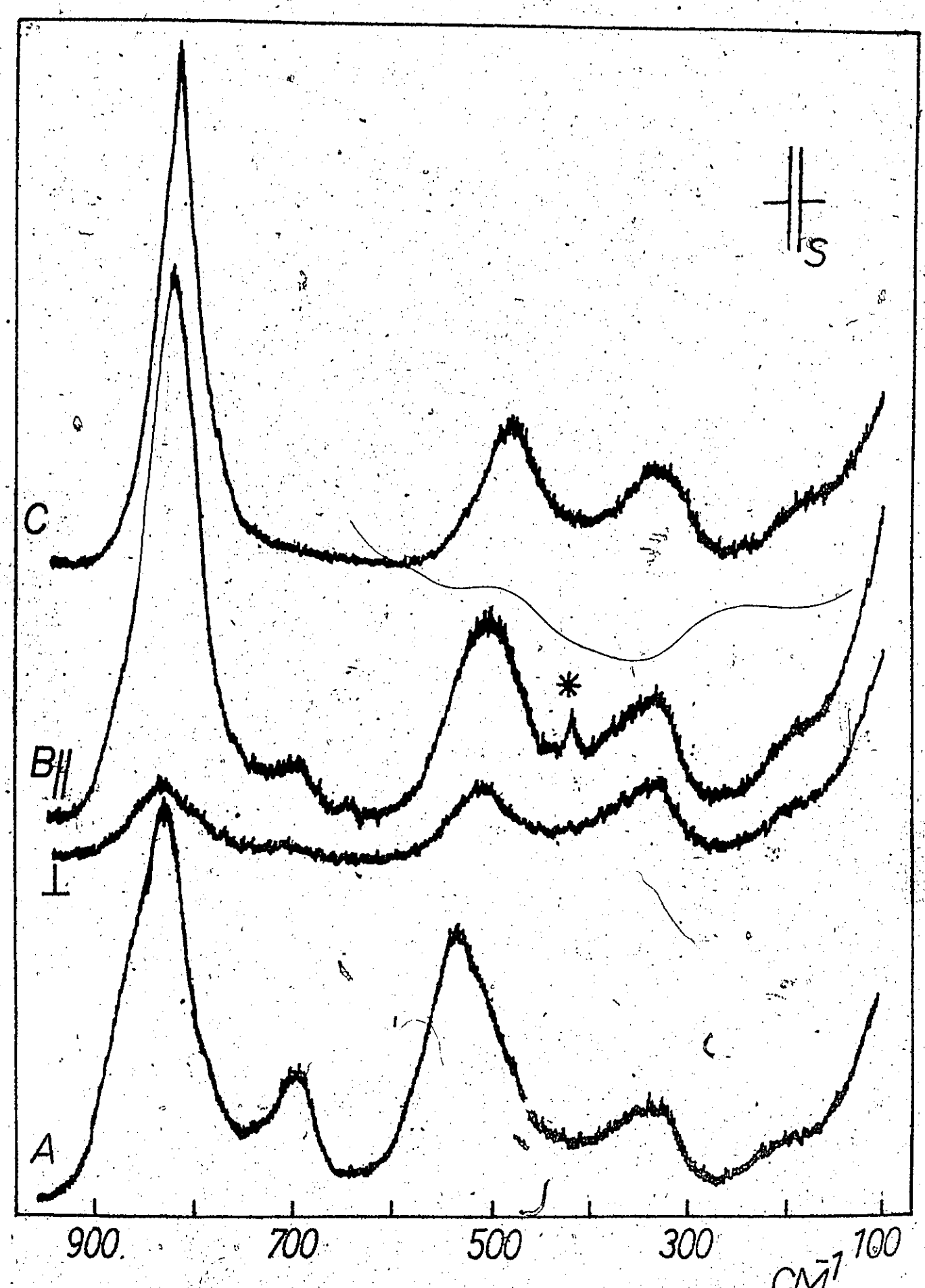
C
B||
⊥
A
*
S
900
700
500
300
100
см⁻¹

TABLE XXI

^{19}F NMR Spectra of I(V) Solutions in HF & MeCN

Solution	Temp °C	Chemical Shifts [a] ppm	Integration	Comments
2.20M HIO_3 in 48% HF	-58	$IO_2F_2^-$: -.7 (+2.3)[b] HF: +152	IO_2F_2:HF = 1:4.89 (Theor = 1:4.95	$IO_2F_2^-$ is the only I(V) species in soln.
	-68	$IO_2F_2^-$: -0.8 HF: -		
5.80 M HIO_3 in 71% HF	-20	exchange of all species.		Solution freezes before exchange stopped
5.65 M HIO_3 in 83% HF	-20	exchange of all species.		Soln freezes before exchange is stopped.
8.6 M HIO_3 in 96.5% HF	-70	IF_5: 0, - HIO_2F_2: ~ -7 HF: + 86		

a shifts relative to $CFCl_3$ or high field doublet of IF_5

b shift relative to high field doublet of IF_5

TABLE XXI (Continued)

Solution	Temp °C	Chemical Shift[a] ppm	Integration	Comments
3.3M IF_5 in 100% HF	20	IF_5: -7.7, -47.2 HF: -		Some solid phase separated at 15°C
5.2 M HIO_3 in 100% HF	-60	IF_5: -3.1, - IF_5: 0, - HF: - HIO_2F_2: +2.7		$J_{FF'}$ = 78 cps Solution supercooled.
	-84	IF_5: 0, - HF: - HIO_2F_2: -1.6		Weak IF_5 signals indicating IF_5 froze out of solution.
6.4 M HIO_3 in 100% HF	-70	IF_5: 0, -49.8 HF: +97.9 HIO_2F_2: +3.4	Peak ratio in IF_5 = 1:3.8 (Theor. = 1:4)	

[a] chemical shift relative to $CFCl_3$ as external standard, or high field doublet of IF_5.

TABLE XXI (Continued)

Solution	Temp °C	Chemical Shifts [a] ppm	Integration	Comments
5.24 M IF_5 2.37 M H_2O in CH_3CN	10	IF_5: -4.9, -47.3 Exchanging: +40.2	Area IF_5: Exchanging band=1:0.72 (theor = 1:0.83)	$J_{FF'}$ = 80 cps
	-45	Broadening of doublet (see p. 122)		

a shifts relative to $CFCl_3$ as external standard

see Figure 19, trace A, it is assumed that its spectrum can be identified, and the Raman spectrum of HIO_2F_2 can be tentatively assigned.

The replacement of one of the oxygen atoms in $IO_2F_2^-$ with an OH group will lower the symmetry of HIO_2F_2 to C_s or even C_1. Ignoring the characteristic OH modes, which will be weak in the Raman spectrum, HIO_2F_2 in either symmetry will have 9 Raman active modes, 4 of these being stretching vibrations. If the OH group lies in the (IO_2) plane, or if the OH is freely rotating, the molecule will have C_s symmetry, the two IF bonds being equivalent. As a result the stretching modes $\nu(IF)$ and $\nu(IF')$ will be replaced by $\nu_{sym}(IF_2)$ and $\nu_{asym}(IF_2)$, and the symmetric stretch will be stronger in the Raman spectrum of HIO_2F_2. The observed frequencies for HIO_2F_2 are given in Table XXII, and the existence of a single strong band at 540 cm^{-1}, the characteristic IF stretching region, suggests the molecule can be considered as having C_s symmetry since there is some exclusion of $\nu_{asym}(IF_2)$ in the Raman spectrum. This asymmetric stretching mode is assigned to the band at 330 cm^{-1}. In $IO_2F_2^-$ the symmetric (IF_2) stretching vibration occurs at 485 cm^{-1}, and the asymmetric as a weaker band at 335 cm^{-1}, see Table XVIII.

In the solution spectrum of HIO_2F_2 the three strongest bands are expected to be ν_1(I-OH), ν_2(IO) and $\nu_3(IF_2)_{sym}$. In going from the anion $IO_2F_2^-$ to the acid HIO_2F_2, ν_3 is expected to increase in frequency. For example, an increase is observed on going from $TeOF_4^{2-}$ to $Te(OH)F_4^-$, see Chapter III. Thus ν_2 is assigned to the strong band at 540 cm^{-1}, an increase in 55 cm^{-1} from the corresponding mode in $IO_2F_2^-$. The IO stretching mode ν_2, is also expected

TABLE XXII

The Raman Spectrum of HIO_2F_2 (C_s)

Class	Mode No.	Frequency cm^{-1}	Approx description of Mode (C_s)
A′	ν_1	700 m, p	ν(I-OH)
	ν_2	850 m,br,p	ν(IO)
	ν_3	540 s,p	$\nu_{sym}(IF_2)$
	ν_4	350 sh, p?	δ_{sym}(OIOH)-in plane
	ν_5		$\delta(IF_2)$wagging
	ν_6	210 w,p?	$\delta_{sym}(IF_2)$
A″	ν_7	(330 m,br)	$\nu_{asym}(IF_2)$
	ν_8	(330 m,br)	δ_{asym}(OIOH)-out of plane
	ν_9	(330 m,br)	$\delta_{asym}(IF_2)$

to increase in frequency compared to the (IO_2) stretching modes in $IO_2F_2^-$, and so ν_2 is assigned to the shoulder at 850 cm^{-1} in Figure 19, trace A. An increase of 20 cm^{-1} is observed in moving from $HSeO_3^-$ to H_2SeO_3, where a single SeO replaces a pair of (SeO_2) stretching vibrations[121]. The band at 700 cm^{-1} is characteristic of an I-OH stretching mode and so this is assigned to ν_1. All of these three bands are polarized, actual polarization ratios being difficult to access due to the presence of the $IO_2F_2^-$ modes.

The deformations prove a more difficult problem in assignment. The symmetric (IF_2) deformation ν_6, has also moved to higher frequency; 205 cm^{-1}, compared to 170 cm^{-1} in $IO_2F_2^-$. Of the remaining 4 deformations and the asymmetric (IF_2) stretching mode, ν_7, ν_8 and ν_9 most likely lie under the broad envelope centered at 330 cm^{-1}, and ν_5 is not observed. ν_4 is tentatively assigned to the shoulder at 350 cm^{-1} which appears to be polarized as is expected for this A′ mode. Definite assignment of these modes is impossible due to the presence of $IO_2F_2^-$ in the solution.

A comparison of the spectrum of HIO_2F_2 observed in this solution with that of the salt $CsIO_2F_2.HIO_2F_2.2H_2O$ reveals little similarity. This is perhaps not suprising since there is considerable hydrogen bonding in the salt, see Table XVIII

Dissolution of HIO_3 in 90% HF, Figure 20, trace C, confirms the assignment for HIO_2F_2 as the new species in the lower HF concentration solutions, the bands due to HIO_2F_2 increasing in intensity as those due to $IO_2F_2^-$ are furthur reduced in relative

Figure 20

Raman Spectra of HIO_3 in More Concentrated HF Solutions

A IF_5 in CH_3CN

B 3.0 M HIO_3 in 100% HF

C 3.0 M HIO_3 in 90% HF

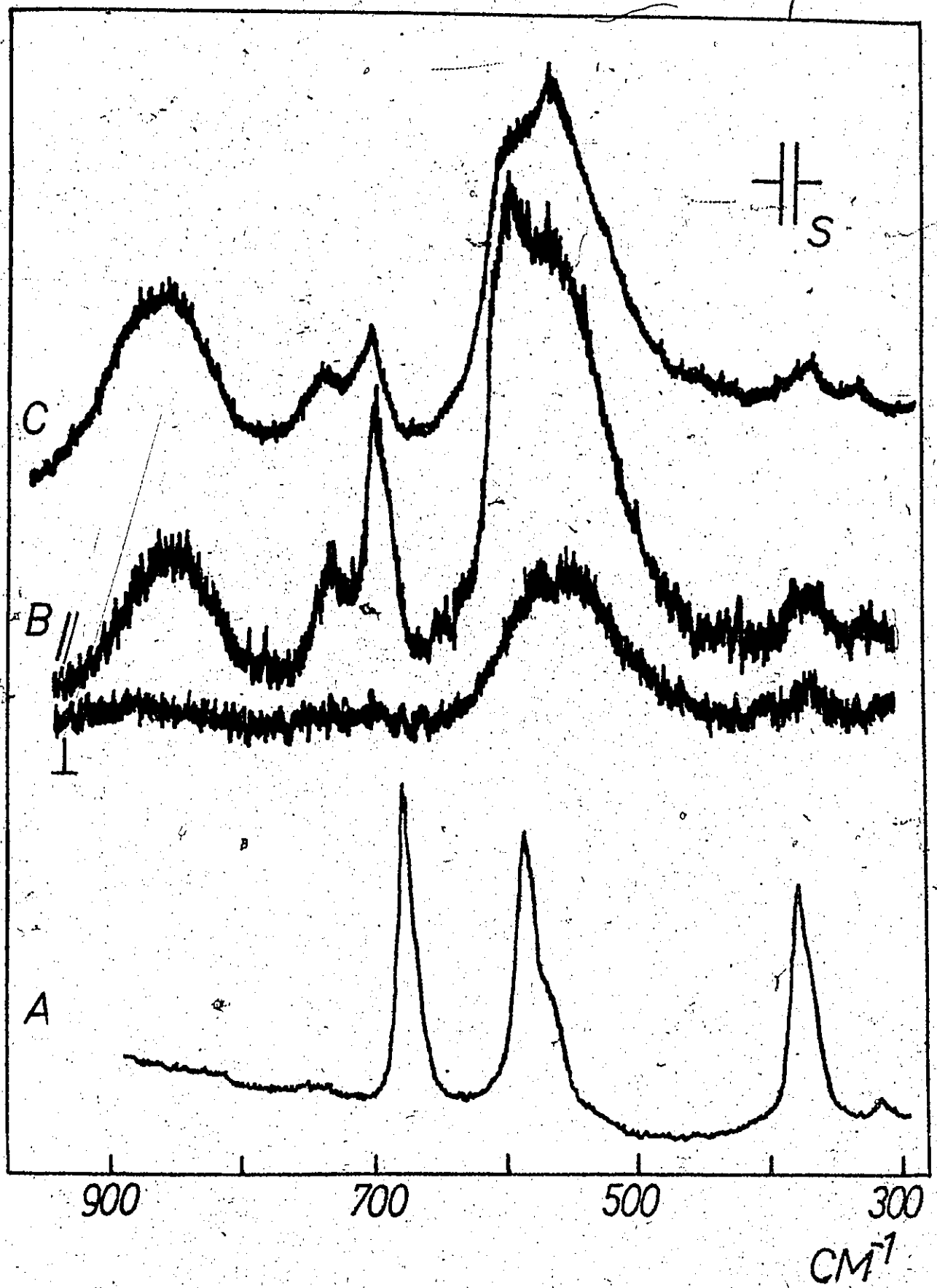
S
C
B
A
900
700
500
300
см⁻¹

intensity in the more acidic solution.

In these more acidic solutions, 90 and 100% HF, see Figure 20 traces B and C, the appearance of the Raman spectrum of a second new species is apparent. In these solutions the band in the (IF_2) stretching region at ca 540 cm^{-1} has a shoulder at 590 cm^{-1} which increases in intensity with increasing HF concentration, becoming a sharp peak in the 100% HF solution. A second band appears at 690 cm^{-1} and this too increases in intensity becoming a sharp peak in the 100% HF solution, see Figure 20, trace B. Both of these bands are polarized, and their similarity to the IF' (apical) and (IF_4) stretching modes of IF_5 in hexafluorobenzene[58] indicates that IF_5 is indeed the new species. The little or no change in the profile of the IO stretching region, 800 - 900 cm^{-1}, of the spectrum and the absence of a band at 530 cm^{-1} indicates the absence of IOF_4^- in these solutions.

The change in the profile of the band assigned to ν_1 of HIO_2F_2 at 700 cm^{-1} however, requires some explanation. In the highly acidic HF solutions this band has sharpened considerably and centered at 730 cm^{-1}, see Figure 20, trace B. The absence of a band at 624 cm^{-1}, the characteristic (IF_4) symmetric stretching mode of $HOIF_4$ (see below) eliminates the possibility of this protonated species. The sharpening of the I-OH stretch can be accounted for by the following scheme.

In the 78% HF solution some $IO_2F_2^-$ is present, and therefore a bridged species such as $H(IO_2F_2)_2^-$ can be formed.

$$HIO_2F_2 + IO_2F_2^- = H(IO_2F_2)_2^-$$

The broad peak in this 78% HF solution at 700 cm^{-1}, see Figure 19, trace A, is characteristic of such a species. As the HF concentration is increased, the increased acidity of the solution results in the complete protonation of $IO_2F_2^-$, and thus, the sharp peak at 730 cm^{-1} in the 100% HF solution is due to the I-OH stretching vibration in HIO_2F_2

$$H(IO_2F_2)_2^- + 2HF \rightleftharpoons 2HIO_2F_2 + HF_2^-$$

An alternate explanation also involves the existence of a bridged species in the lower concentration HF solutions, with protonation occuring in 100% HF.

$$H(IO_2F_2)_2^- + 2HF \rightleftharpoons H_2(IO_2F_2)_2 + HF_2^-$$

Such a bridging species does not account for the sharpness of the peak at 730 cm^{-1} in the 100% HF solution, however.

^{19}F NMR Spectroscopy

The ^{19}F NMR spectrum of a solution of IF_5 in 100% HF at 20°C gives the characteristic IF_5 signals[156] in addition to a broad solvent band. On cooling to ~15° a second phase separates in the tube, and this does not redissolve immediately on warming. The observed shifts are given in Table XXI.

Dissolution of HIO_3 in 100% HF gives the IF_5 signals at -60°, and on cooling to -77°, an additional peak at +2.7 ppm from the high field doublet of IF_5. The observed shifts and coupling constant are given in Table XXI. Some of the shifts were measured from $CFCl_3$ as an external standard, and due to difficulties with this reference in the inter-annular space, others were referenced to the high field doublet of IF_5. This single extra peak at +2.7 ppm from the doublet of IF_5 is most likely not due to $IO_2F_2^-$, which has a shift of +2.3 ppm from IF_5 at -68°. The Raman spectrum of a solution of HIO_3 in 100% HF shows the spectrum of IF_5 and a second species identified as HIO_2F_2. Thus the additional signal on cooling the HIO_3/HF solution is identified as being the ^{19}F NMR signal of HIO_2F_2, and is not due to IOF_4^- or $HIOF_4$ since these are not observed in the Raman spectrum.

On reducing the concentration of HF to 96.5%, the signals due to IF_5 and HIO_2F_2 are again observed on cooling below -60°. The observed shifts are given in Table XXI.

Furthur reduction in the HF concentration to 83 and 71% HF, gave solutions a part of which froze at ~-20°. Thus, in these solutions only a broad exchanging band was observed.

Finally, reduction of the HF concentration to 48% gave the signal due to $IO_2F_2^-$ on cooling to -45°.

3. IF_5/H_2O in Acetonitrile

Raman Spectra

While this work is mainly concerned with the examination of fluoro and oxofluoro anions of iodine(V) in HF solutions, it was felt that an examination of the IF_5/H_2O system in CH_3CN might furnish the Raman spectrum of IOF_4^- in solution, of particular interest in the elucidation of the spectra of the HIO_3 solutions in HF.

IF_5 readily dissolves in CH_3CN and its Raman spectrum in this solvent is given in Figure 21, trace A. The characteristic Raman frequencies of IF_5 in the gas, liquid and solid[58] in addition to the spectrum in CH_3CN are given in Table XXIII. It can be immediately seen that the spectrum of IF_5 in CH_3CN differs from that of the liquid or gas phase spectrum in two respects. Firstly, the highest frequency bands ν_1, ν_2 and ν_4 are shifted 20 - 30 cm^{-1} from their position in the gas phase spectrum. Secondly, there is a noticeable change in the ordering of the intensities of ν_1 and ν_2, the former becoming the stronger in the CH_3CN solution. The observed half-width of ν_1 is 14 cm^{-1}, and is indicative of a non-bridging IF_5 molecule. The half-width reported by Alexander and Beattie[58] for the gas phase is 10 cm^{-1}, and 40 cm^{-1} for liquid IF_5.

The shift in frequency of ν_1, ν_2 and ν_4 can perhaps be rationalized in terms of an $IF_5.CH_3CN$ adduct. Solid adducts of IF_5 with donor solvents such as pyridine have been isolated[150], and a $BrF_5.CH_3CN$ adduct is reported[151]. The increased electron density at the nucleus as a result of the adduct formation would cause a weakening of both the IF′ (apical) and IF (basal) bonds,

Figure 21

Raman Spectra of IF_5 and IF_5/H_2O in Acetonitrile

A 1.50 M IF_5 in CH_3CN

B 1.66 M IF_5 and 0.8 M H_2O in CH_3CN

C 1.66 M IF_5 and 1.20 M H_2O in CH_3CN

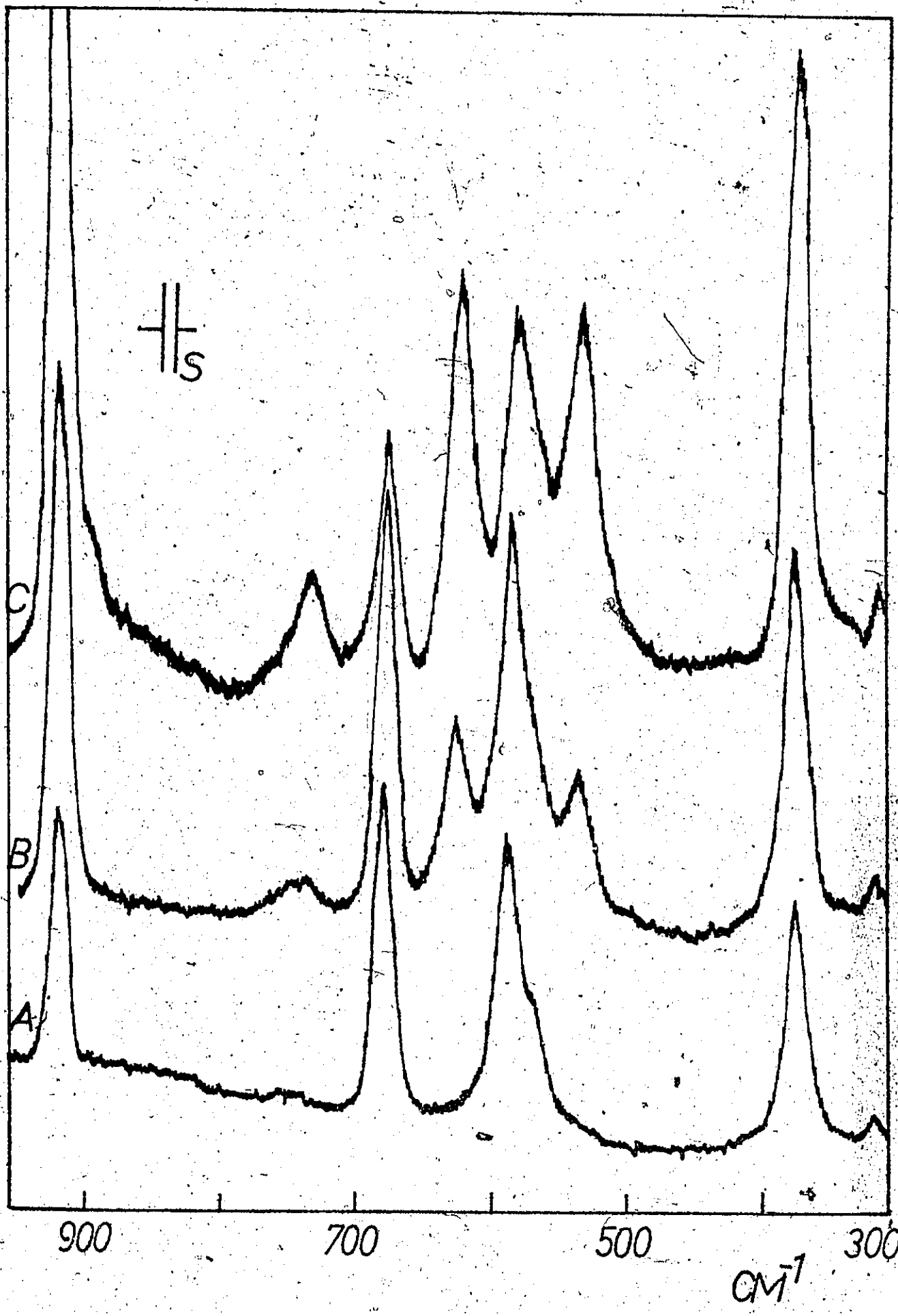
C
B
A
900
700
500
300
cm⁻¹

TABLE XXIII

Raman Spectra of IF_5

Solid (0°)[a]	Liquid (20°)[a]	Gas (120°)[a]	CH_3CN Soln.[b]	Mode No.[c]
718 m	705 s,pol	710 s,pol	678 vs,pol	$\nu_1(A_1)$
705 m	697 s,pol			
607 w	ca 630 vw,sh	631 sh		$\nu_7(E)$
599 m	598 s,pol	614 vs,pol	588 s,pol	$\nu_2(A_1)$
584 m		602 sh	568 sh	$\nu_4(B_1)$
568 s	575 s			
378 m	375 m	370 w	(377)[d]	$\nu_8(E)$
330 w	316 m,pol	318 m,pol	319 m,pol	$\nu_3(A_1)$
277 m	274 m	274 w		$\nu_6(B_2)$
202 w	191 w	ca 200 w		$\nu_9(E)$

a Alexander and Beattie, ref 58

b 1.50 M IF_5 in CH_3CN, this work.

c C_{4v} symmetry assumed for all phases.

d Feature obscured by solvent band.

and a resultant fall in frequency of the stretching modes involving these bonds.

On addition of H_2O to the solution four new bands appear in the Raman spectrum, see Figure 21, trace B, and all four increase in intensity on furthur addition of H_2O, see Figure 21, trace C. One of these bands, that at 880/900 cm^{-1} lies under a solvent band, but its intensity can be estimated by comparison with the solvent bands in the solution of IF_5 in CH_3CN. This band is characteristic of an IO stretch, whereas the band at 735 cm^{-1} is characteristic of an I-OH stretching vibration. The remaining two new bands are in the IF stretching region. All four bands are polarized; the observed frequencies and their assignment are given in Table XXIV, and are based upon the following considerations.

The existence of IOF_4^- is expected in these solutions: Klamm and Meinert[24] observing it on addition of H_2O to a solution of IF_6^- in CH_3CN.

$$2IF_6^- + 3H_2O = IOF_4^- + IO_2F_2^- + 6HF$$

Ryan and Asprey[75] isolated the cesium salt, $CsIOF_4$, from a solution of CsF and IF_5 in CH_3CN. The the band at 880/900 cm^{-1} is assigned to $\nu_1(A_1)$ of the IOF_4^- ion. This mode occurs at 888 cm^{-1} in the cesium salt.

The remaining bands at 735 and 624 cm^{-1} present a more complex problem of assignment since no known oxo species of iodine (V) has Raman bands in this region of the spectrum. The facile replacement of the apical F in TeF_5^- to give $Te(OH)F_4^-$ (see

TABLE XXIV

Raman Spectra of IF_5- H_2O Solutions in Acetonitrile

IF_5 [a]	IF_5- H_2O [b]			Mode No.
	IF_5	$HOIF_4$	IOF_4^-	
678 s,pol	678 s,pol	735 m,pol	890 vbr,pol	$\nu_1(A_1)$
588 vs,pol	582 vs,pol	624 vs,pol	534 vs,pol	$\nu_2(A_1)$
319 m,pol	(318) pol	(318) pol		$\nu_3(A_1)$
568 sh	568 sh			$\nu_4(B_1)$

a 1.50 M IF_5 in CH_3CN

b 1.66 M IF_5, 1.2 M H_2O

Chapter III), and also in IF_5 to give IF_4OMe [154], suggests the observed bands are part of the Raman spectrum of $HOIF_4$. The band at 735 cm^{-1} is characteristic of an I-OH stretch, and so it is assigned to $\nu_1(A_1)$ of $HOIF_4$, the I-OH stretching mode. This species will have a strong Raman band $\nu_2(A_1)$, the in phase symmetric (IF_4) stretching mode. Thus the band at 624 cm^{-1} is assigned to this mode. None of these bands belongs to HIO_2F_2. The absence of both $IO_2F_2^-$ and HIO_2F_2 in these solutions can furthur be seen from the low strength of a band in the 830 - 850 cm^{-1} region of the spectrum.

Thus the three bands in the IF stretching region in the Raman spectrum of IF_5/H_2O in CH_3CN, see Figure 21, trace C, are assigned to the symmetric in phase (IF_4) stretching vibrations in IF_5 (582 cm^{-1}), $HOIF_4$ (624 cm^{-1}) and IOF_4^- (534 cm^{-1}). This assignment is shown in Table XXIV.

The existence of this mode for IOF_4^- some 50 cm^{-1} below that for IF_5 is to be expected due to the weakened (IF_4) basal bonds as a result of the increased steric crowding by the IO bond compared to the IF_a (apical) bond. However, this mode in $HOIF_4$ occurs 40 cm^{-1} above ν_2 in IF_5, and this is surprising, since in the isoelectronic pair TeF_5^- and $Te(OH)F_4^-$ these symmetric in phase (TeF_4) stretches lie within 10 cm^{-1} of each other. The observed value for ν_2 of $HOIF_4$ at 624 cm^{-1} agrees well with the value for this mode in gaseous IF_5, 614 cm^{-1}. The observed large difference in these modes in CH_3CN is due to the lower value of ν_2 in the adduct $IF_5.CH_3CN$.

^{19}F NMR

The observed chemical shifts and peak areas in the ^{19}F

NMR spectrum of an IF_5/H_2O solution in MeCN are given in Table XXI. The IF_5 doublet and quintet were observed on cooling to 10°, as was an additional broad band. The shift of this band is +40.2 ppm from $CFCl_3$, and since this shift is intermediate between the observed shifts of F-on-I and HF, this band must be the result of exchange between HF and one or more fluoroiodate(V) species in solution. IF_5 is hydrolysed as follows:

(1) $IF_5 + H_2O = HOIF_4 + HF$

(2) $IF_5 + 2H_2O = IOF_4^- + H_3O^+ + HF$

and the Raman spectrum of a solution of IF_5 and H_2O in MeCN in the same mole ratios, shows the presence of both IOF^- and $HOIF_4$ at 25°. Proof that reactions (1) and (2) are occuring in the solution at 10° comes from the integration of the IF_5 peaks and the exchanging band. The theoretical ratio of these signals, IF_5 : exchanging peak ($HIOF_4$ + HF) can be obtained from the stoichiometry of the solution, assuming only reaction (1) is occurring, and this ratio should be 1:0.82. The observed ratio is 1:0.72, and this indicates some of the water is being protonated as in reaction (2) above.

Furthur cooling of the solution to -35° results in the doubling of the IF_5 high field doublet. This situation persists down to the freezing point of the solution at -50°. The doubled IF_5 signal is shown below, and H represents the direction of field increase.

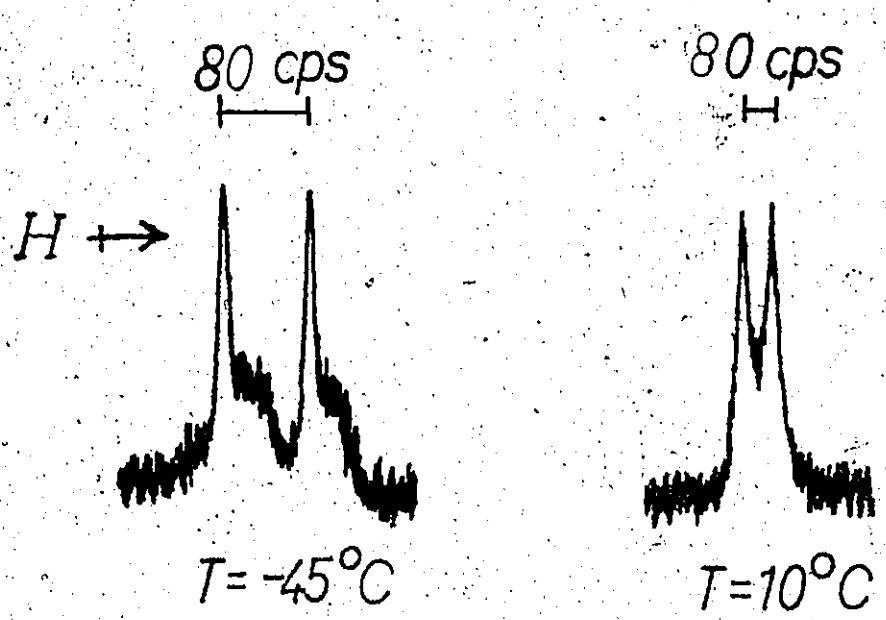

These doublets may be explained in two ways. Firstly, Raman spectroscopy has shown an adduct with acetonitrile, $IF_5.CH_3CN$, exists in these solutions at 25°. It is thus tempting to argue that the second signals may be due to this adduct which has frozen out of the solution. Secondly, at these lower temperatures some IF_5 may have been frozen out of the solution, and the broader doublet is due to this solid phase IF_5.

CHAPTER V

An Introductory Study of Fluoro and Oxofluoro Species of Antimony(III) and Selenium(IV)

1. Antimony(III) Species

X-Ray Powder Photography

K_2SbF_5 and Cs_2SbF_5:

The x-ray powder photograph data for these two salts is given in Table XXV. The calculated values for the cell parameters agree well with those reported by Bystrom and Wilhelmi[43].

Vibrational Spectroscopy

Cs_2SbF_5:

The observed Raman spectrum of Cs_2SbF_5 is given in Figure 22, trace A, and the frequencies of both the Raman and infrared spectra are given in Table XXVI. These spectra agree well with those reported by Downs and Adams[29] for Cs_2SbF_5 with the single exception of the weak peak at 484 cm^{-1} which is not observed in this work. The assignment made in Table XXVI follows that of Alexander and Beattie[58] for the single crystal Raman spectrum of K_2SbF_5. The assignment of $\nu_4(B_1)$ at 371 cm^{-1} agrees well with the observed trend in this mode across the isoelectronic series IF_5, TeF_5^-, and SbF_5^{2-} (ref 140 and see also Chapter VI)

TABLE XXV

X-Ray Powder Photograph Data for the $M^{I}_{2}SbF_{5}$ Salts

Cs_2SbF_5 Cu-K Irradiation

d	Intensity
4.193	10
3.799	10
3.492	10
3.358	100
3.278	10
2.399	50
2.381	30
2.244	10
2.009	10
1.997	20
1.931	20
1.921	30
1.696	30
1.651	10
1.556	20
1.551	20
1.513	10
1.494	10
1.418	20
1.357	10
1.329	10
1.308	10
1.289	10
1.271	20
1.254	20

TABLE XXV (Continued)

K_2SbF_5

d	Intensity
5.673	40
4.690	40
4.270	40
3.411	10
3.231	10
3.210	100
3.123	10
2.810	10
2.665	10
2.600	10
2.516	20
2.281	10
2.248	50
1.869	40
1.821	20
1.722	10
1.657	10
1.623	10
1.603	20
1.564	10
1.441	10
1.427	10
1.238	20

Figure 22

Raman Spectra of Cs_2SbF_5 and solutions of SbF_3

A Cs_2SbF_5

B 3.0 M SbF_3 in 48% HF

C 3.0 M SbF_3 in water

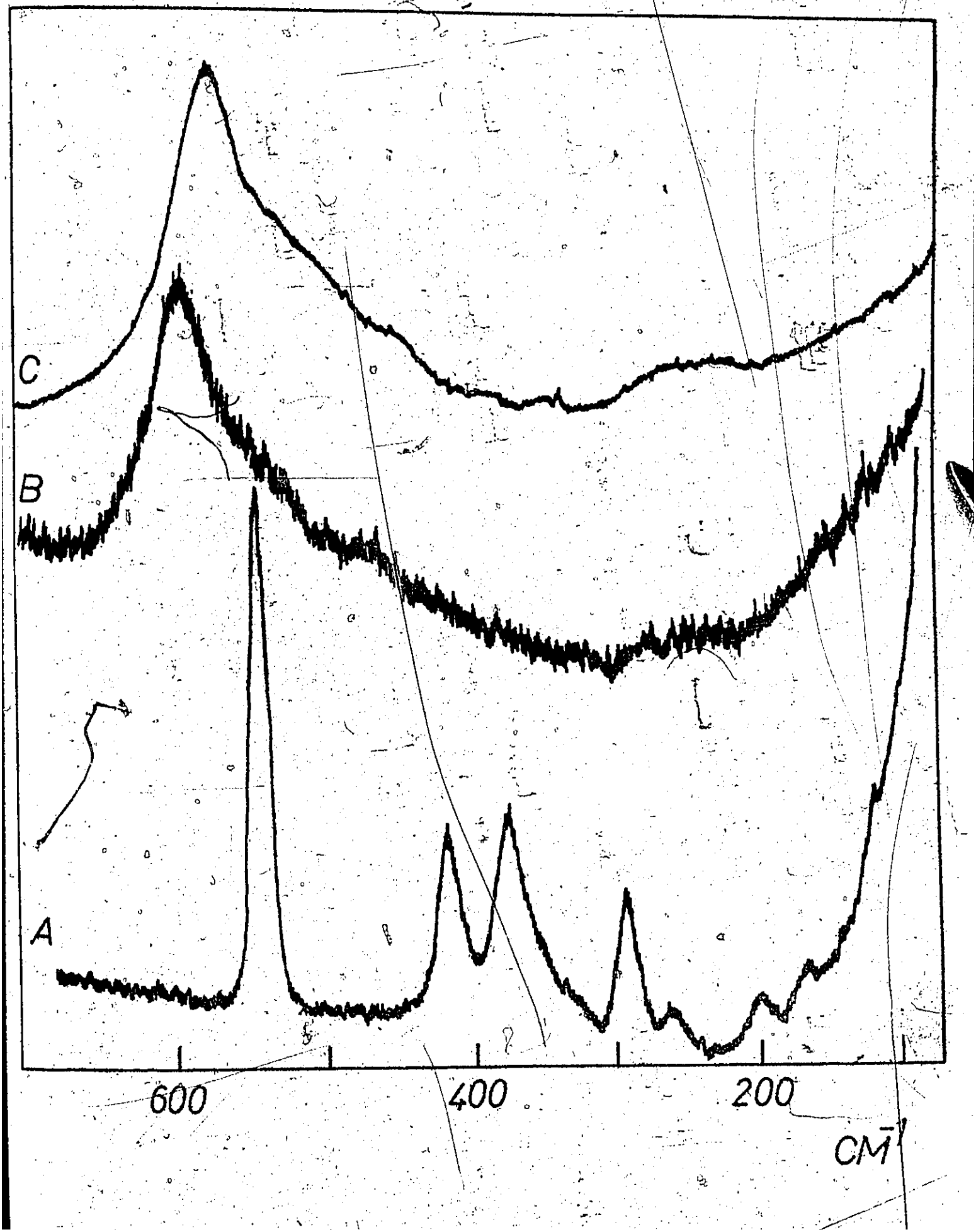
C
B
A
600
400
200
см⁻¹

TABLE XXVI

The Raman and Infrared Spectrum of Cs_2SbF_5

Class	Mode No.	Raman	Ir	Approx Description of mode C_{4v}
A_1	ν_1	542 s	540 m	$\nu(SbF')$
	ν_2	416 m		$\nu_{sym}(SbF_4)$-in phase
	ν_3	265 w	ca 250 m	$\delta_{sym}(SbF_4)$ umbrella
B_1	ν_4	371 m		$\nu_{sym}(SbF_4)$-out of phase
	ν_5			$\delta_{asym}(SbF_4)$-out of plane
B_2	ν_6	207 w		$\delta_{sym}(SbF_4)$-in plane
E	ν_7	354 sh	380/345 vs	$\nu_{asym}(SbF_4)$
	ν_8	297 mw	280 m	$\delta(F'F_4)$ wag
	ν_9	172 vw		$\delta_{asym}(SbF_4)$-in plane

$Co(NH_3)_6Sb_2F_9$:

The observed frequencies in the vibrational spectrum of this salt are given in Table XXVII. The Raman spectrum is given in Figure 23, and the infrared spectrum in Figure 24. The assignment in Table XXVII is based upon the following considerations. A single crystal x-ray structure has shown the $Sb_2F_9^{3-}$ ion in this salt to consist of two square pyramids sharing a corner[41].

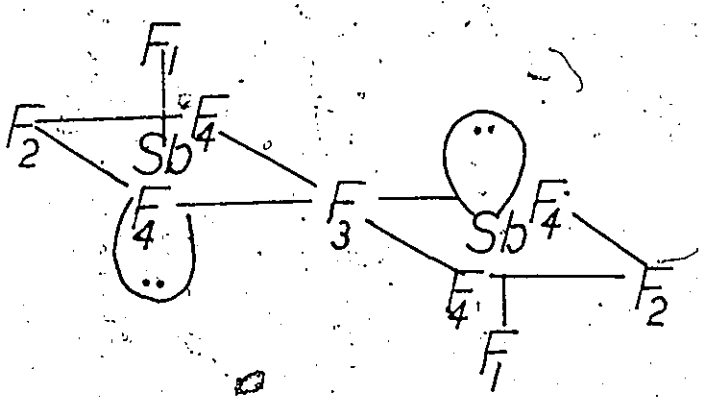

The vibrational spectrum of the $Sb_2F_9^{3-}$ ion may be expected to show some similarity to the spectrum of the square pyramidal SbF_5^{2-}, since the immediate environment about each antimony is similar. Thus the apical Sb-F_1 stretching mode is expected to be the highest frequency mode since the Sb-F_1 bond distances (1.948 Å) are shorter, and the bonds are stronger, than the other Sb-F bond distances in the ion. The peak at 529 cm^{-1} is thus assigned to this mode. The corresponding mode, $\nu_1(A_1)$, in SbF_5^{2-} occurs at 541 cm^{-1}.

The crystal structure reveals the Sb-F_2 bond distances, where F_2 are the fluorines trans to the bridge, to be 2.015 Å. This is shorter than the non-bridging basal bonds Sb-F_4 (2.08 Å), and

TABLE XXVII

Raman and Infrared Spectra of $Co(NH_3)_6Sb_2F_9$

Ir	Raman	Approx Assignment
3275/ 3150 vs,vbr		Cation
1625 m,vbr		"
1350 s		"
1340 s		"
840 m,br		"
523 ms	529 s	$\nu(Sb\text{-}F_1)$
490 sh	491 vs	$\nu(Sb\text{-}F_2)$
	447 s, 439 s	$\nu(Sb\text{-}F_4)$
322/ 313 vs	(333) m,vbr[a]	$\nu(Sb\text{-}F_3)$
	195 sh[b], 185 sh[b], 141 w, 114 w	deformations

a feature obscured by cation band

b feature obscured by glass band

Figure 23

The Raman Spectrum of $Co(NH_3)_6Sb_2F_9$

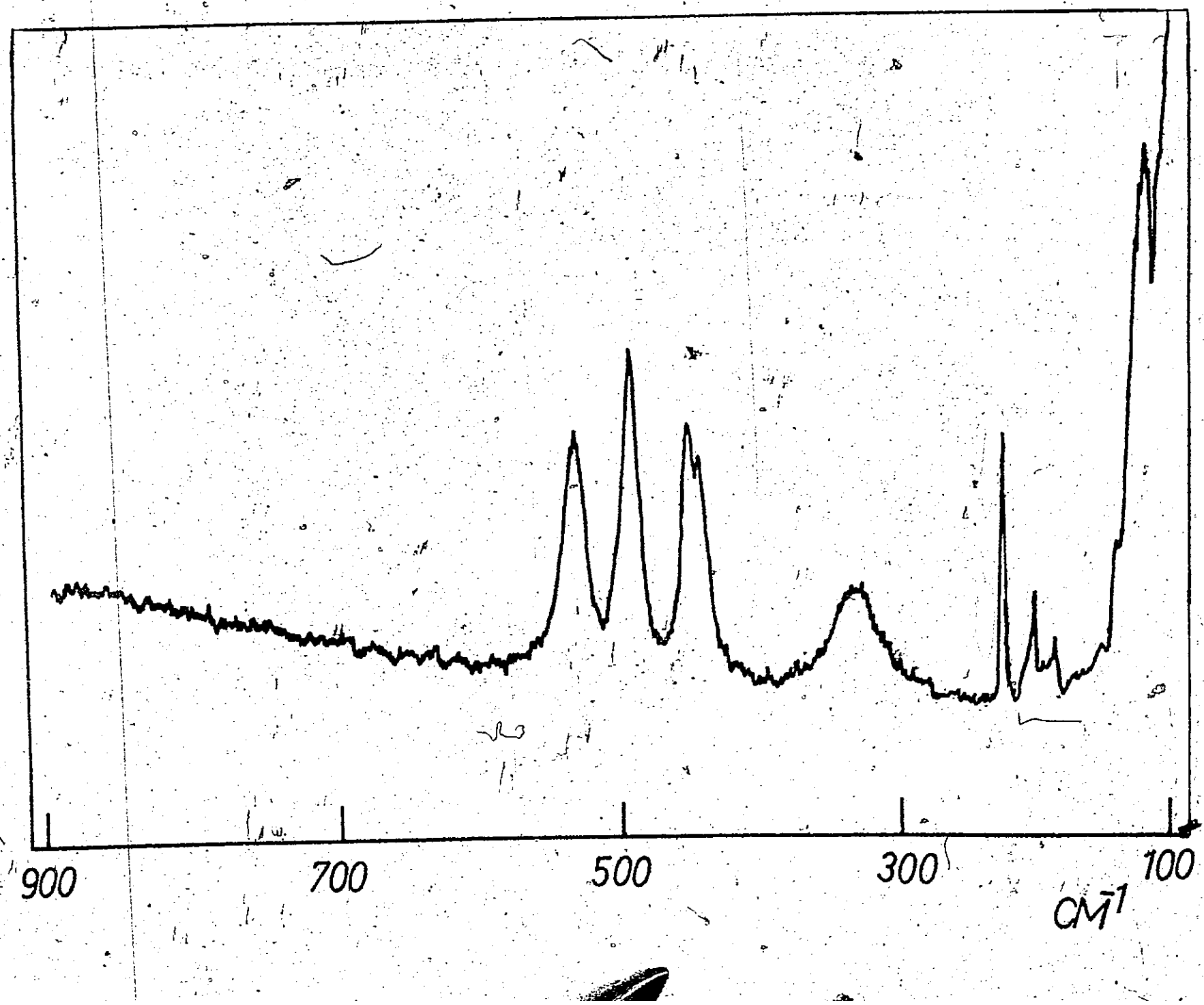
900
700
500
300
100
CM⁻¹

Figure 24

The Infrared Spectrum of $Co(NH_3)_6Sb_2F_9$

* slower scan speed

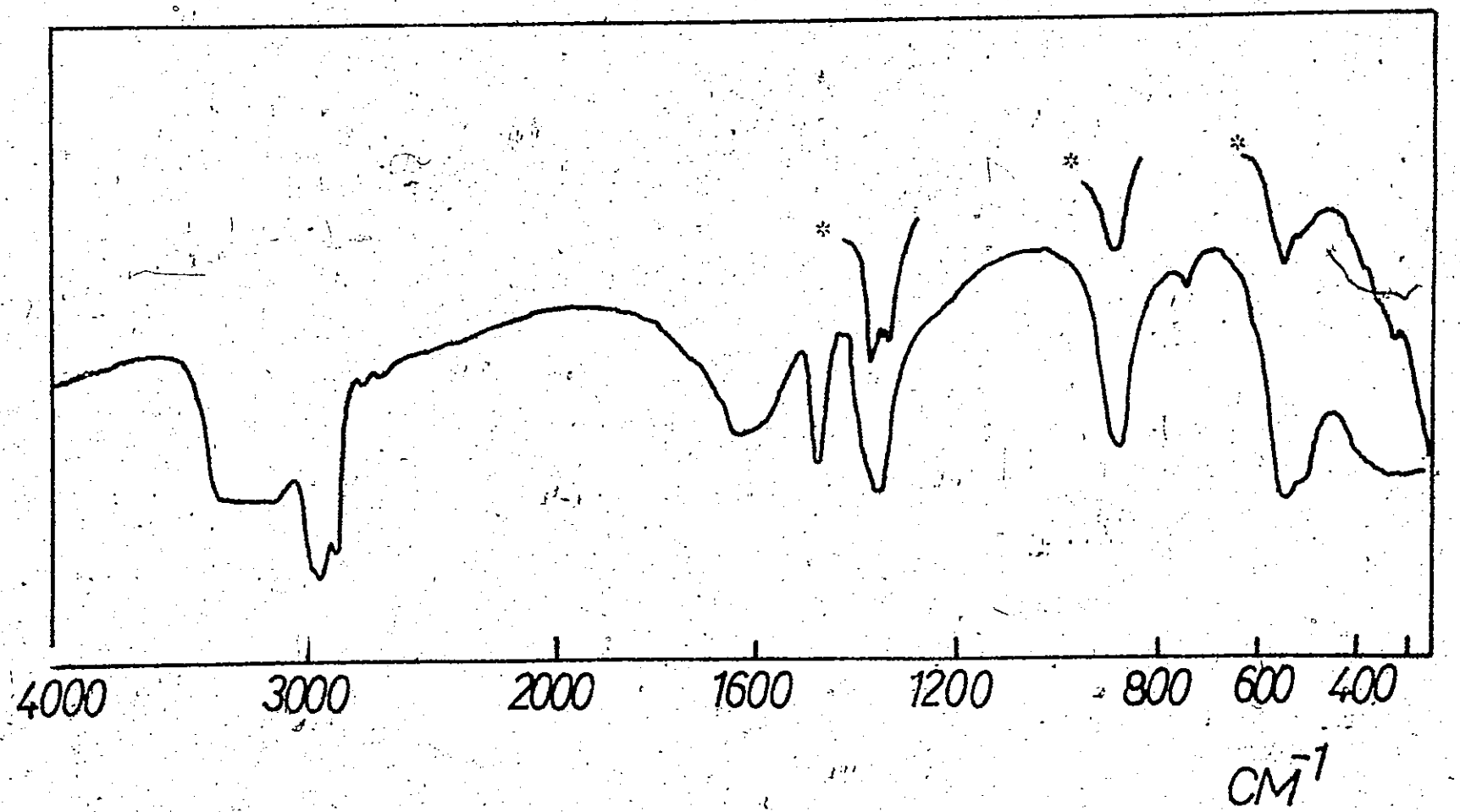
4000
3000
2000
1600
1200
800
600
400
CM⁻¹

so the stretching mode for $Sb-F_2$ is expected to be unique, and will be higher than either the remaining basal stretches or the bridging stretch. The peak at 491 cm^{-1} is thus assigned to $\nu(Sb-F_2)$, and is considerably higher than the (SbF_4) basal stretches in SbF_5^{2-}, 416 cm^{-1}. The remaining peaks in the Sb-F stretching region of the spectrum, 300 - 600 cm^{-1}, are tentatively assigned to the $Sb-F_4$ basal stretches at 447 and 439 cm^{-1}, and the bridging $Sb-F_3$ stretch at 333 cm^{-1}. Once again a bridging stretching mode can be identified from its uniquely low frequency.

No attempt is made to assign the deformations.

Solutions

Raman Spectra

The observed Raman spectrum of a 3.0 M solution of SbF_3 in water is given in Figure 22, trace C, and the observed frequencies are recorded in Table XXVIII.

As the ratio of F:Sb is increased in the solution by the addition of HF, there is little change in the profile of the spectrum. Dissolution of SbF_3 in 48% HF gives the Raman spectrum shown in Figure 22, trace B. The observed frequencies are given in Table XXVIII. Salts of the SbF_5^{2-} ion readily crystallize out of these solutions[70], and it is surprising that the Raman spectrum of SbF_3 in 48% HF does not show the spectrum of the SbF_5^{2-} ion. The observed spectrum is quite different from that of Cs_2SbF_5, given in Figure 22, trace A, or the reported Raman spectrum of the SbF_5^{2-} ion in acetonitrile or nitromethane[29]. The frequencies of the

TABLE XXVIII

Raman Spectra of SbF_3 in Solution

SbF_3 [a]		SbF_3 in H_2O [b]	SbF_4^- [c]	SbF_3 in 48% HF [d]
Gas	Soln.			
666 s,p	593 s,p	579 s,p	596 s,p	597 s,p
634 m	530 m	550 sh	566 m	545 sh
		450 sh	449 m,p	460 sh
			425 vw	420 vw
	270 w		285 w,p	275 w
250 m.p	235 w	250 w,vbr	256 w	240 w

a ref 153, solution in MeOH. b 3.0 M SbF_3 in H_2O. c ref 29, $Bu^n_4NSbF_4$ in MeCN. d 3.0M SbF_3 in 48% HF.

observed bands suggest that SbF_4^- is a major constituent of the solution, see Table XXVIII, but the width of the bands observed is indicative of a number of fluoroantimonate(III) species in solution. In addition to the difficulty in assigning the SbF stretching frequencies (300-600 cm^{-1}), the low intensity of the remaining bands, characteristic of SbF deformations, makes this region of the spectrum of little use in the identification of the species present. Increasing the concentration of Sb(III) to ca. 12M resulted in difficulty in obtaining a good spectrum due to fluorescence.

There is, however, no evidence for either oxofluoro species of antimony(III), characteristic frequencies 850-750 cm^{-1}, or hydroxo species, 700-600 cm^{-1}, judging from the observed spectra of oxofluoro and hydroxo species of tellurium(IV) and iodine(V).

Returning to the spectrum of SbF_3 in water, Figure 22, trace C, it is perhaps surprising that the Raman spectrum of this solution should bear such a close resembence to that of SbF_4^- which seems to be the major species in the 48% HF solution. The Raman spectra of SbF_3 in the gas phase and in solution in methanol are given in TableXXVIII along with the observed frequencies of the aqueous solution. The marked difference between the spectra of SbF_3 in the gas phase and in solution is evident; the highest frequency peak being 666 cm^{-1} in the former[153] and 593 (ref 153) and 579 cm^{-1} in the solutions. The similarity of the solution spectra of SbF_3 to that of SbF_4^- is evident from Table XXVIII & Figure 22. Perhaps in these solutions there is dissociation of SbF_3 to other fluoro species of antimony(III), for example:

$$2SbF_3 = SbF_4^- + SbF_2(OH)_n^+$$

The existence of species other than SbF_4^- should be evident in the Raman spectrum of SbF_3 in water if such a dissociation is in fact taking place. The width of the band in the SbF stretching region, see Figure 22, trace C, is perhaps indicative of such species.

The solution spectrum of SbF_3 in methanol is also much different from that of SbF_3 in the gas phase. Perhaps also in this case there is some dissociation of SbF_3 to either hydroxy or methoxy species of antimony(III).

2. Selenium(IV) Species

Vibrational Spectra

$KSeO_2F$:

This salt, and the cesium salt $CsSeO_2F$, could be prepared from aqueous solutions of 48% HF and DMSO (see Chapter II), in addition to the methods reported by Paetzold and Aurich[106].

The Raman spectrum of $KSeO_2F$ is given in Figure 25, trace D, and the observed frequencies for this and the infrared spectrum are given in Table XXIX. The observed spectra agree well with those reported by Paetzold and Aurich[106], with the single exception of the weak shoulder at 480 cm^{-1}, which was observed in this work.

The approximate assignment given in Table XXIX is based upon the following considerations, and closely follows that given in reference 106. Two bands are observed in the SeO characteristic stretching region[139], and these are assigned as the symmetric and asymmetric (SeO_2) stretching modes. The observation of just these two modes in the SeO stretching region shows the absence of bridging over oxygen in the ion. There is no evidence of a Se-O-Se bond; such a bridge bond occurs in SeO_2, and this has an infrared band at ca. 650 cm^{-1} (ref 104).

The strong band in the infrared spectrum at 440 cm^{-1} is assigned to the SeF stretching mode, and the observed frequency indicates the SeO_2F^- to be polymeric with fluorine bridges, since this stretch is characteristic of a long Se-F bond such as a bridging bond. Non bridging SeF vibrations occur at 500-700 cm^{-1} (refs 66, 153). The peak at 415 cm^{-1} is assigned to the (SeO_2) deformation

TABLE XXIX

Raman and Infrared Spectra of $KSeO_2F$

Raman	Infrared	Approx Assignment
920 vs	912 vs	$\nu_{sym}(SeO_2)$
885 sh	884 vs	$\nu_{asym}(SeO_2)$
450 w,sh	440 s	$\nu_{(SeF)}$
418 m	403 vs	$\delta_{(SeO_2)}$
322 mw	320 ms	deformations
283 mw	280 sh	deformations
256 w	ca. 250	deformations

since the corresponding mode in $HSeO_3^-$ occurs at 410 cm^{-1} (ref 121). No attempt is made to assign the other deformations.

Solutions

SeO_2 in aqueous HF (0-48% HF)

The Raman spectrum of a 3.0 M solution of SeO_2 is given in Figure 25, trace A, and the observed frequencies are recorded in Table XXX. The only two species present in this solution are H_2SeO_3 and $HSeO_3^-$, and the spectra of these species are included in Table XXX. The reactions occuring in solution are[121]:

$$SeO_2 + H_2O = H_2SeO_3$$

$$H_2SeO_3 + H_2O = H_3O^+ + HSeO_3^-$$

A solution of a similar concentration of SeO_2 in 10% HF has the Raman spectrum shown in Figure 25, trace B. In this solution the Raman spectrum has changed little from that of the aqueous solution. However, the band at 690 cm^{-1} has increased in relative intensity compared to the band at 890 cm^{-1}. Since the higher frequency band is characteristic of a SeO, or SeO_2, stretching mode, and the band at 690 cm^{-1} is in the Se-OH stretching region, this change in the Raman spectrum can be explained as follows. In the acidic solution, 10% HF, protonation of $HSeO_3^-$ has taken place, and a pair of SeO_2 stretching modes is replaced by one SeO stretch and one Se-OH stretch.

Figure 25

Raman Spectra of $KSeO_2F$ and Solutions of SeO_2

A 3.0 M SeO_2 in water

B 3.0 M SeO_2 in 10% HF

C 3.0 M SeO_2 in 48% HF

D $KSeO_2F$

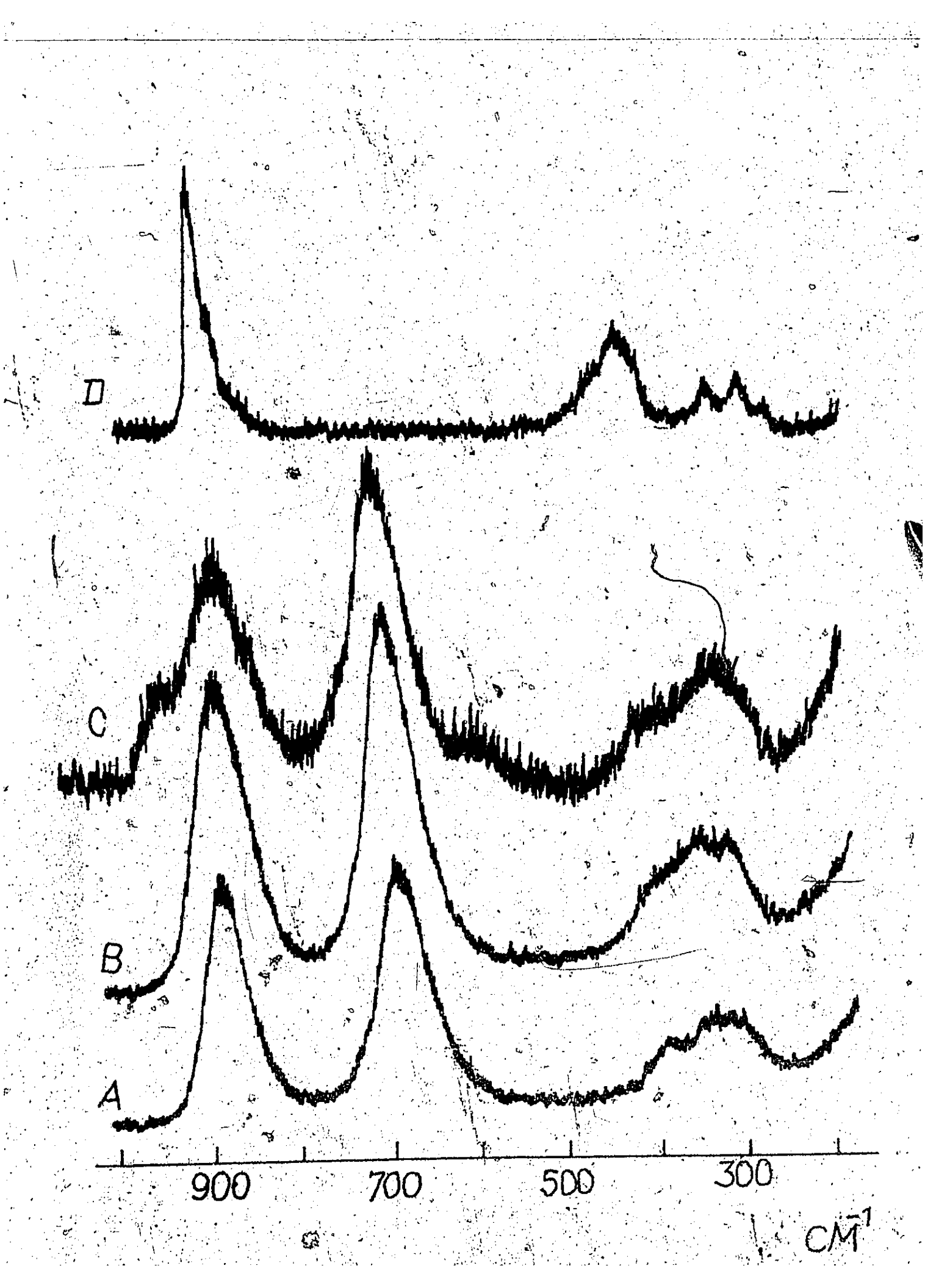
D
C
B
A
900
700
500
300
см⁻¹

$$HOSeO_2^- + H_3O^+ = (HO)_2SeO + H_2O$$

The bulk of the solution is thus H_2SeO_3. This acid has a low dissociation constant $K_1 = 2.4 \times 10^{-3}$ at 25°C (ref 155).

There is no evidence for any fluoro or oxofluoro selenium(IV) species in this solution; all the bands can be accounted for by the spectrum of H_2SeO_3, see Table XXX.

Dissolution of SeO_2 in 48% HF, however, shows bands in the Raman spectrum which cannot be accounted for by H_2SeO_3 or the other oxo species $HSeO_3^-$ and SeO_3^{2-} (ref 121, see also Table XXX). This spectrum is shown in Figure 25, trace C, and the observed frequencies are given in Table XXX. The new species is an oxofluoro species of selenium(IV) since its Raman spectrum has bands characteristic of both SeO and SeF stretching modes (SeO, 1050-850 cm^{-1}, refs 121, 139, and SeF, 500-700 cm^{-1}, refs 66, 153).

There are two known oxofluoro selenium(IV) anions: SeO_2F^- (ref 106) and $SeOF_3^-$ (ref 85). The Raman spectrum of $KSeO_2F$ is given in Figure 25, trace D, and inspection of this figure shows the spectrum of SeO_2F^- in this salt to bear little resemblance to the Raman spectrum of the oxofluoro selenium(IV) species in the 48% HF solution. $KSeO_2F$ is known to be polymeric, with bridging fluorines, and so the spectrum of this salt is of little assistance in the elucidation of the solution spectrum. ($KSeO_2F$ can be crystallized out of a solution of SeO_2 and KF in 48% HF).

<u>^{19}F NMR</u>

The ^{19}F NMR spectrum of a solution of SeO_2 in 48% HF showed a broad exchanging band which collapsed at -60°.

TABLE XXX

Raman Spectra of H_2SeO_3, $HSeO_3^-$ and SeO_2 Solutions

$HSeO_3^-$ [a]	H_2SeO_3 [a]	3.0M SeO_2 in H_2O	3.0 M SeO_2 in 10% HF	3.0M SeO_2 in 48% HF
				945 sh
	900 w			
	875 s	890 s	890 s	890 s
855 s				
790 w				
	690 s	690 s	690 vs	690 vs
615 m				
				595 w,vbr
410 w				
	394 m	395 sh	395 sh	395 sh
345 w				
	342 m	340 m,br	340 m,br	335 m,vbr
320 w				
	314 m	315 m	315 m	310 sh

a ref 121

SeO_2 in More Concentrated HF Solutions (85-100 % HF)

A 3.0 M SeO_2 solution in 100% HF has the Raman spectrum shown in Figure 26, trace A. The spectrum of $SeOF_2$ is readily observed in this solution, and the polarized spectrum confirms the assignment of the $SeOF_2$ bands. The observed frequencies for this solution are given in Table XXXI along with the reported spectrum of $SeOF_2$ [153].

In addition to the spectrum of $SeOF_2$, three other bands are apparent in the Raman spectrum of SeO_2 in 100% HF: at 950 cm^{-1}, 708 cm^{-1} and 290 cm^{-1}.

Dissolution of SeO_2 in 85% HF gives the Raman spectrum shown in Figure 26, trace B. In this solution the bands due to $SeOF_2$ are still present although they have decreased in intensity relative to the bands at 950, 708 and 290 cm^{-1}. In addition, the shoulder at 603 cm^{-1} has also increased in intensity, and so it must be due to a coincident band in $SeOF_2$ and the other species in solution.

Of these four new bands, two of them correspond to the bands of the oxofluoro species which is apparent in the 48% HF solution. The remaining two bands are accounted for as follows. The band at 290 cm^{-1} could also be present in the 48% HF solution, lying under the broad band centred at 325 cm^{-1} in the spectrum of H_2SeO_3 (see Table XXX1 and Figure 25, trace C). Thus little information can be obtained from this band as to the nature of the species in solution. The band at 708 cm^{-1}, however, lies in the Se-OH stretching region of the spectrum. The (Se-OH) stretches in H_2SeO_3 occur at 690 and 615 cm^{-1} (ref 121). Thus two explanations are possible for

Figure 26

Raman Spectra of SeO_2 in Concentrated HF

A 3.0 M SeO_2 in 100% HF

B 3.0 M SeO_2 in 85% HF

1300
1100
900
700
500
300
100
A
//
⊥
B

TABLE XXXI

Raman Spectra of SeO_2 solutions in Concentrated HF, and $SeOF_2$

SeO_2 in 48% HF[a]	SeO_2 in 85% HF[a]	SeO_2 in 100% HF[a]	$SeOF_2$[b]
	1005 ms	1008 vs,p	1007 vs,p
945 sh	942 s	950 m,p	
890 s			
690 vs	705 s	708 m,p	
	662 vs	662 vs,p	658 vs,p
595 w,vbr	605 s	603 sh	603 s
395 w,sh			
	385 w	385 mw	375 m
335 m,vbr			
310 sh		310 m	309 ms
	300 br		
		290 sh	283 m

a 3.0 M SeO_2 solution. b $SeOF_{2(g)}$ data from ref 153

the assignment of the band at 708 cm^{-1}. Firstly this band may be assigned as the Se-$(OH)_2$ stretching modes in H_2SeO_3. The width of the band in the SeO region can also be accounted for by the existence of this acid in these solutions, in addition to the oxofluoro species. Secondly, this band could be due to the protonated species, $HSeO_2F$.

$$SeO_2F^- + 2HF = HSeO_2F + HF_2^-$$

This is exactly analogous to the protonation of $IO_2F_2^-$ in concentrated HF solutions. This protonated species is expected to have a SeO stretching mode at 900-1000 cm^{-1}, and can also explain the observed width of the band in these solutions. However, the nature of the oxofluoro species must remain in doubt.

^{19}F NMR

The ^{19}F NMR spectrum of a solution of SeO_2 in 100% HF showed one peak in addition to that of the solvent on cooling to -85°. The observed shift of this peak was -26.6 ppm, and that of the solvent +178 ppm from $CFCl_3$. It was not possible to identify the peak as being due to $SeOF_2$ in the absence of the reported shift, and the ^{77}Se satelites (expected signal intensity 3% of F-on-Se peak) were not observed due to a poor signal to noise ratio. However, integration of the observed peaks revealed that 92% of the selenium in solution could be accounted for assuming that the peak at -26.6 ppm was due to $SeOF_2$.

CHAPTER VI

Some Observations on the Vibrational Spectra of Fluoro and Oxofluoro Species of Iodine(V), Tellurium(IV), Selenium(IV) and Antimony(III)

The known square pyramidal, C_{4v} symmetry, species of xenon, iodine, tellurium, selenium and antimony in their penultimate valance state are given in Table XXXII. The species enclosed in the heavy lines have been investigated in this work.

TABLE XXXII

Xenon	Iodine	Tellurium	Selenium	Antimony
XeF_5^+	IF_5	TeF_5^-	SeF_5^-	SbF_5^{2-}
—	$HOIF_4$ *	$Te(OH)F_4^-$ *	—	—
$XeOF_4$	IOF_4^-	$TeOF_4^{2-}$ *	—	—
XeO_2F_2	$IO_2F_2^-$	$TeO_2F_2^{2-}$ *	—	—

* indicates new species prepared in this thesis

Inspection of this table shows a number of trends in isoelectronic species which can be investigated in these compounds. In this chapter the vibrational spectra of the various species are correlated, and the observed trends discussed. The C_{2v} species XeO_2F_2, $IO_2F_2^-$, and $TeO_2F_2^{2-}$ are also included in the table since

they provide an interesting isoelectronic series for investigation.

Four series are investigated: (i) the pentafluoro species AF_5E, (ii) the AOF_4E species, (iii) the AXF_4E series, (X = F, OH or O) and (iv) the AO_2F_2E species.

(i) AF_5E Species (A = I, Te and Sb)

The vibrational spectra of these compounds are well known[29,58,66,140], and all modes fall in frequency with the decreasing oxidation state of the central atom A. As we move to the left in the periodic chart there is a decrease in the electronegativity difference between A and fluorine. The weakening of the AF bond is evident from the fall in the stretching vibrations involving these bonds. Inspection of Table XXXIII reveals, for example, the smooth decrease in the frequency of $\nu_1(A_1)$ as we move from IF_5 (710 cm^{-1}) through TeF_5^- (611 cm^{-1}) to SbF_5^{2-} (522 cm^{-1}). This trend is shown in Figure 27 along with the trends in the other three stretching modes, $\nu_2(A_1)$, $\nu_4(B_1)$ and $\nu_7(E)$. A smooth transition is observed for all 4 modes, with ν_4 approaching ν_7 in TeF_5^- (there is some uncertainty in both of these modes in TeF_5^- due to their near coincidence) and finally falling well below ν_7 in SbF_5^{2-}.

This figure also shows the A-F' (apical) bond to be stronger than the basal bonds, since ν_1 lies almost 100 cm^{-1} above ν_2 in all three species.

TABLE XXXIII

Comparison of the Spectra of the Pentafluoro Species

Class	Mode No.	IF_5 [a]	TeF_5^- [b]	SbF_5^{2-} [c]
A_1	ν_1 *	710	611	542
	ν_2 *	616	504	416
	ν_3	318	282	265
B_1	ν_4 *	604	472	371
	ν_5			
B_2	ν_6	276	231	207
E	ν_7 *	631	466	380/345
	ν_8	372	336	297
	ν_9	200	164	172

a ref 58 gaseous IF_5. b ref 58 $KTeF_5$. c this work Cs_2SbF_5

* modes plotted in Figure 27

Figure 27

Plot of Stretching Frequencies in AF_5E Species

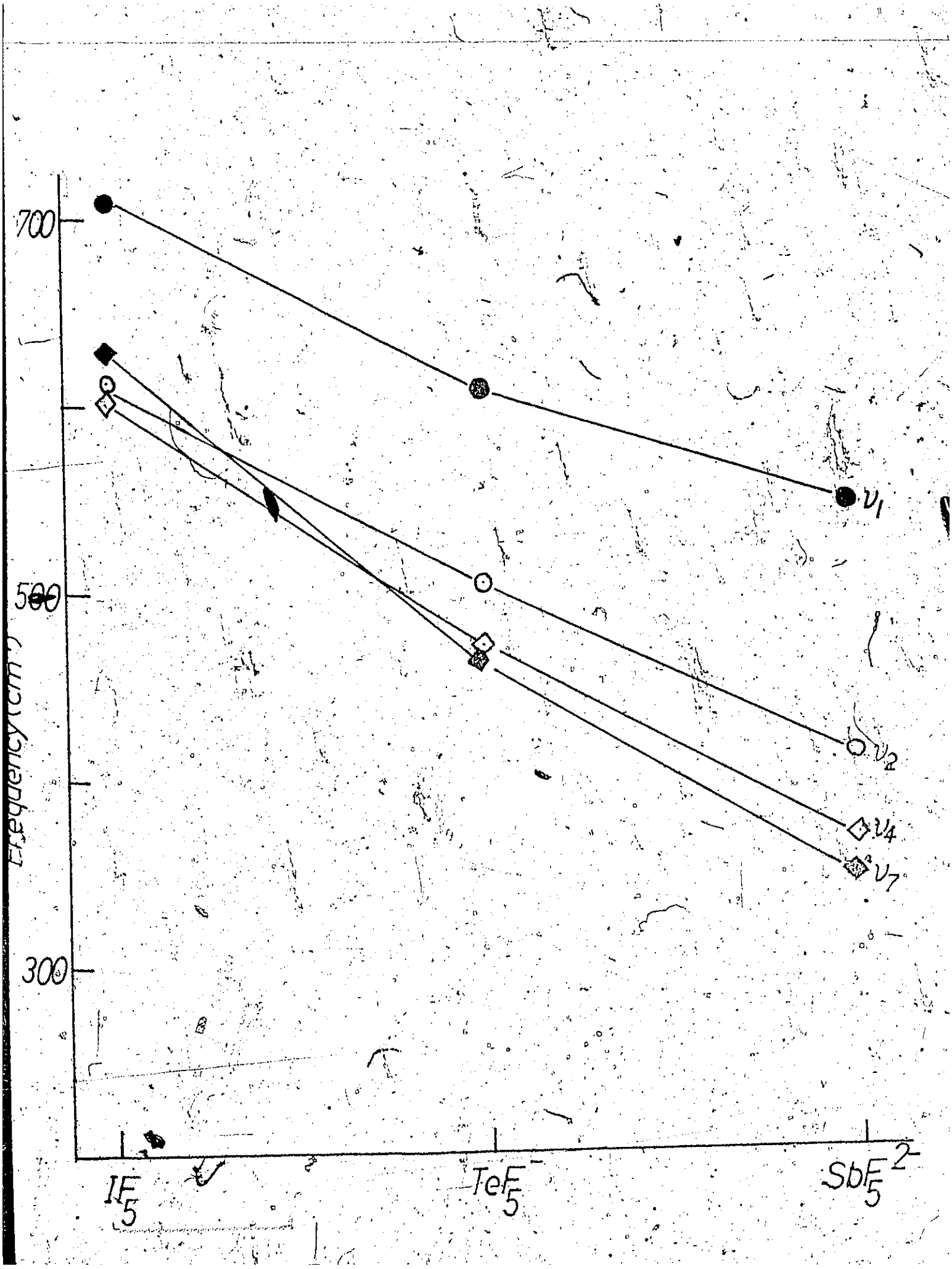
700
500
300
Frequency (cm⁻¹)
ν_1
ν_2
ν_4
ν_7
IF_5
TeF_5^-
SbF_5^{2-}

(ii) AOF_4E Species (A = Xe, I and Te)

The three species considered are $XeOF_4$, IOF_4^- and $TeOF_4^{2-}$, and the observed frequencies of their vibrational spectra are given in Table XXXIV. Inspection of this table reveals all modes fall in frequency as the oxidation state and electronegativity of the central atom decreases, and substantiates the assignment of the deformations in $TeOF_4^{2-}$ ($\nu_s > 320$ cm^{-1} and $\delta_s < 320$ cm^{-1}) and IOF_4^- ($\nu_s > 450$ and δ_s 450 cm^{-1}). With the decreasing oxidation state of A, there is a fall in frequency in $\nu_1(A_1)$ as a result of the lengthening of the AO bond. A similar trend is observed for the other three stretching modes ν_2, ν_4 and ν_7. However, Table XXXIV shows ν_7 falls off more rapidly than ν_4, coming below ν_4 in $TeOF_4^{2-}$. This trend in these two modes is shown in Figure 28, and exactly parallels the behaviour of these two modes in the isoelectronic pentafluoro species, where the coincidence of ν_4 and ν_7 occurs in TeF_5^-. IOF_4^- is isoelectronic with TeF_5^-.

Table XXXIV shows the deformations are much less sensitive to changes in the central atom A, than are the stretching vibrations.

The similarity of the (IF_4) stretching modes in IOF_4^- and IF_4^- was mentioned in Chapter IV. A comparison of the vibrational spectra of these two species provides some insight into the stereochemical role of the lone valence electron pair in the AOF_4E species.

IOF_4^- has a C_{4v} structure with the oxygen in the apical position, trans to the lone pair[75].

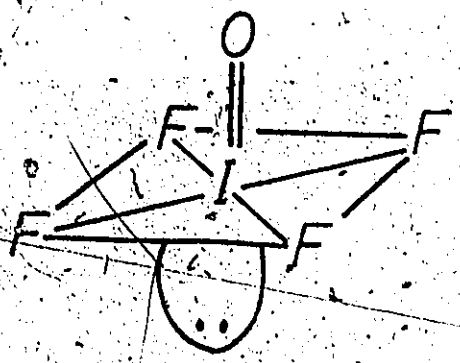

The vibrational spectrum of IF_4^- is consistent with D_{4h} symmetry[152], the structure predicted by VSEPR theory[3].

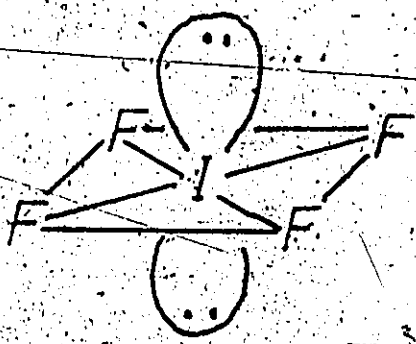

Table XXXV shows the (IF_4^-) modes which may be compared in both of these iodine ions, and the similarity observed indicates that the stereochemical influence of a lone pair in IF_4^- is very similar to that of the oxygen in IOF_4^-. The doubly bonded IO bond evidently has a similar repulsive effect upon the basal IF bonds. For example, $\nu_2(A_1)$ in IOF_4^- occurs at 533 cm^{-1} while the corresponding $\nu_1(A_1)$ in IF_4^- occurs at 522 cm^{-1}.

The $\angle$(OIF) in IOF_4^- is very close to 90°, being 88° (ref 75), and so clearly the geometry of the two ions is very closely related.

TABLE XXXIV

Comparison of the Fundamental Frequencies of C_{4v} Species (AOF_4E)

Class	Mode No.	$XeOF_4$ [a]	IOF_4^- [b]	$TeOF_4^{2-}$ [c]
A_1	ν_1	920	888	837
	ν_2	567	533	461
	ν_3	285	273	265
B_1	ν_4 *	527	485	390
	ν_5			
B_2	ν_6	233	214	190
E	ν_7 *	608	482	330/360
	ν_8	365	365	
	ν_9	161	160	129

a ref 73

b $CsIOF_4$ this work

c Cs_2TeOF_4 this work

* these modes plotted in Figure 28

TABLE XXXV

Comparison of the Fundamental Frequencies of IOF_4^- and IF_4^-

IOF_4^- [a]	Mode(C_{4v})	IF_4^- [b]	Mode(D_{4h})	Approx description of mode
533	$\nu_2(A_1)$	522	$\nu_1(A_1)$	$\nu_{sym}(IF_4)$ in phase
475	$\nu_7(E)$	448	$\nu_6(E)$	$\nu_{asym}(IF_4)$
273	$\nu_3(A_1)$	271	$\nu_2(A_1)$	$\delta_{sym}(IF_4)$ umbrella
485	$\nu_4(B_1)$	455	$\nu_4(B_2)$	$\delta_{sym}(IF_4)$ out of phase

a $CsIOF_4$ this work

b $CsIF_4$ ref 152

Figure 28

Plot of Stretching Frequencies ν_4 & ν_7 in AOF_4 E Species

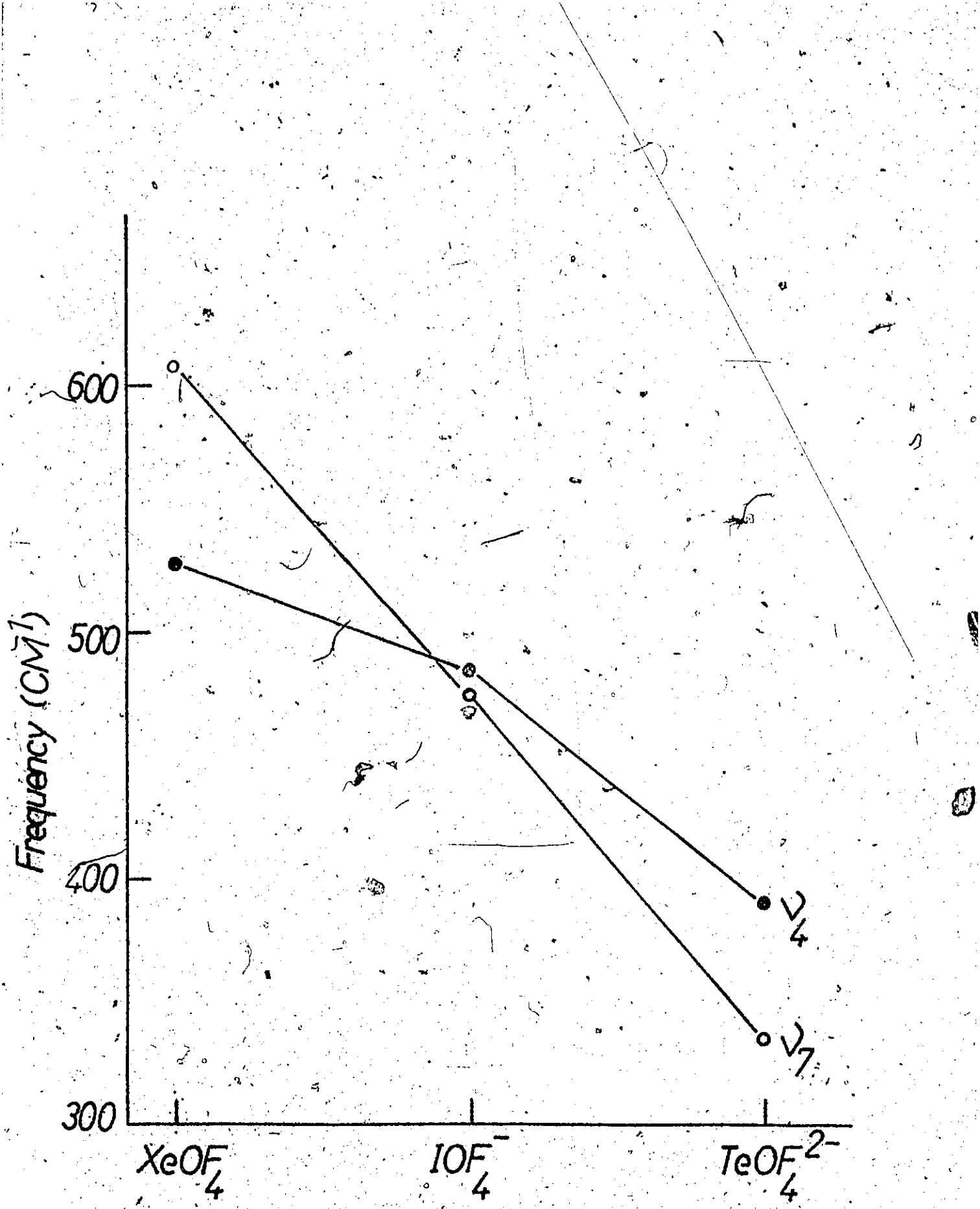
600
500
400
300
Frequency (CM⁻¹)
XeOF4
IOF4⁻
TeOF4²⁻
ν4
ν7

(iii) AXF_4E Species (X= F′, OH or O)

Comparison of the tellurium(IV) ions TeF_5^-, $Te(OH)F_4^-$ and $TeOF_4^{2-}$ illustrates the effect of replacing the apical fluorine in a square pyramidal species with OH and O. The observed frequencies of the vibrational spectra of these three anions are given in Table XXXVI. The trends in the 4 stretching modes $\nu_1(A_1)$, $\nu_2(A_1)$, $\nu_4(B_1)$ and $\nu_7(E)$ are shown in Figure 29. As F′ (apical) is replaced with OH and O, ν_1 increases in frequency. An increase in frequency is expected on replacing F (at. wt. 19) with OH (mol. wt. 17). Using a simple diatomic model, and the force constant for the Te-F′ (apical) bond from reference 66, the expected increase was calculated, and it was found to be less than 5%. However, on going from TeF_5^- to $Te(OH)F_4^-$ the observed increase in the frequency of ν_1 is 14%. Thus, this increase from 611 to 697 cm^{-1} must in part be due to the multiple bond nature of the Te-OH bond.

The other stretching modes, ν_2, ν_4 and ν_7 all involve the basal (TeF_4) bonds, and these bonds are expected to be sensitive to the nature of the Te-OH and Te=O bond. In view of the multiple bonding in the Te-OH bond indicated by the increase in frequency in ν_1, the observed fall in ν_2 is less than might be predicted. However, the decrease of 39 cm^{-1} in ν_7 clearly reflects the increased repulsive effect of the Te-OH bond on the basal bonds compared to the Te-F′ bond.

As the Te-OH bond is replaced with a Te=O bond the sharp increase in ν_1 is evident. Again, the stretching modes involving the basal bonds fall off in frequency as a result of the increased repulsion of the doubly bonded oxygen. This decline is greatest in the asymmetric stretching mode, ν_7.

TABLE XXXVI

Comparison of the Frequencies of C_{4v} Species $TeXF_4E$

Class	Mode No.		TeF_5^- [a]	$Te(OH)F_4^-$ [b]	$TeOF_4^{2-}$ [c]
A_1	ν_1	*	611	697	837
	ν_2	*	504	502	461
	ν_3		282	266	265
B_1	ν_4	*	472	465	390
	ν_5			205	
B_2	ν_6		231	223	190
E	ν_7	*	466	427	330/360
	ν_8		338	378/342	
	ν_9		164	125	129

a $KTeF_5$ ref 58

b $KTe(OH)F_4$ this work

c Cs_2TeOF_4 this work

* these modes plotted in Figure 29

Figure 29

Plot of the Stretching Frequencies in $TeXF_4$ E Species

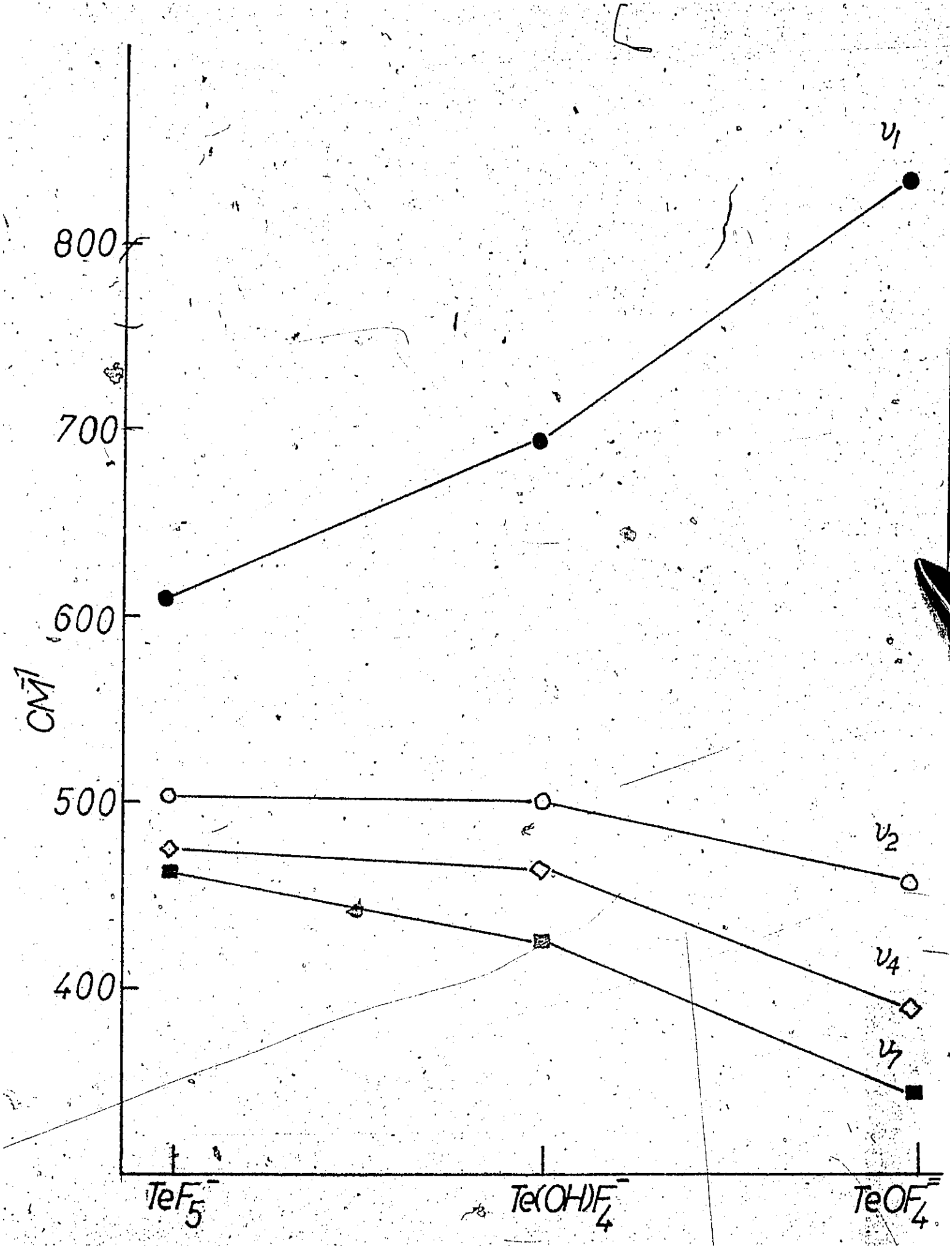
800
700
600
500
400
cm⁻¹
ν1
ν2
ν4
ν5
TeF5⁻
Te(OH)F4⁻
TeOF4⁼

Thus, because of the doubly bonded TeO bond, the oxygen plays a more dominant role in the stereochemistry of $TeOF_4^{2-}$ than do the other apical ligands, F in TeF_5^-, and OH in $Te(OH)F_4^-$. In these two latter ions the effect of the lone valence electron pair predominates. It is likely, therefore, that the (OTeF) angle is opened up considerably from the value of 78.8° observed for the (F TeF) angle in TeF_5^- (ref 26). This effect has been observed for the pairs $XeF_5^+/XeOF_4$ and IF_5/IOF_4^- (see Tables I & II). The crystal structure of $KTe(OH)F_4$ should be of particular interest since the (HOTeF) angle will give a definite idea of the degree of multiple bonding in the Te-OH bond.

An exactly analogous effect is observed in the frequencies of the stretching modes in IF_5, $HIOF_4$ and IOF_4^-. However, since only a partial Raman spectrum of $HIOF_4$ was observed, the trends can only be examined in the two modes ν_1 and ν_2. The observed frequencies for these modes are given in Table XXXVII, and the trends are plotted in Figure 30.

Again, as a result of the multiple bonding in the IO bond, the weakening in the basal bonds is reflected in the fall in frequency in the (IF_4) symmetric in phase stretching mode, ν_2. The small increase in the frequency of ν_1 can be mostly accounted for by a mass effect alone, and this indicates that there is little multiple bond character in the I-OH bond.

TABLE XXXVII

Comparison of the Vibrational Modes in IXF_4E Species

Class	Mode No.	IF_5 [a]	$HIOF_4$ [b]	IOF_4^- [c]
A_1	ν_1 *	710	735	888
	ν_2 *	614	624	534

a gaseous IF_5, ref 58

b CH_3CN solution, this work

c $CsIOF_4$, this work

* these modes plotted in Figure 30

Figure 30

Plot of the Stretching Frequencies ν_1 & ν_2 in IXF_4E Species

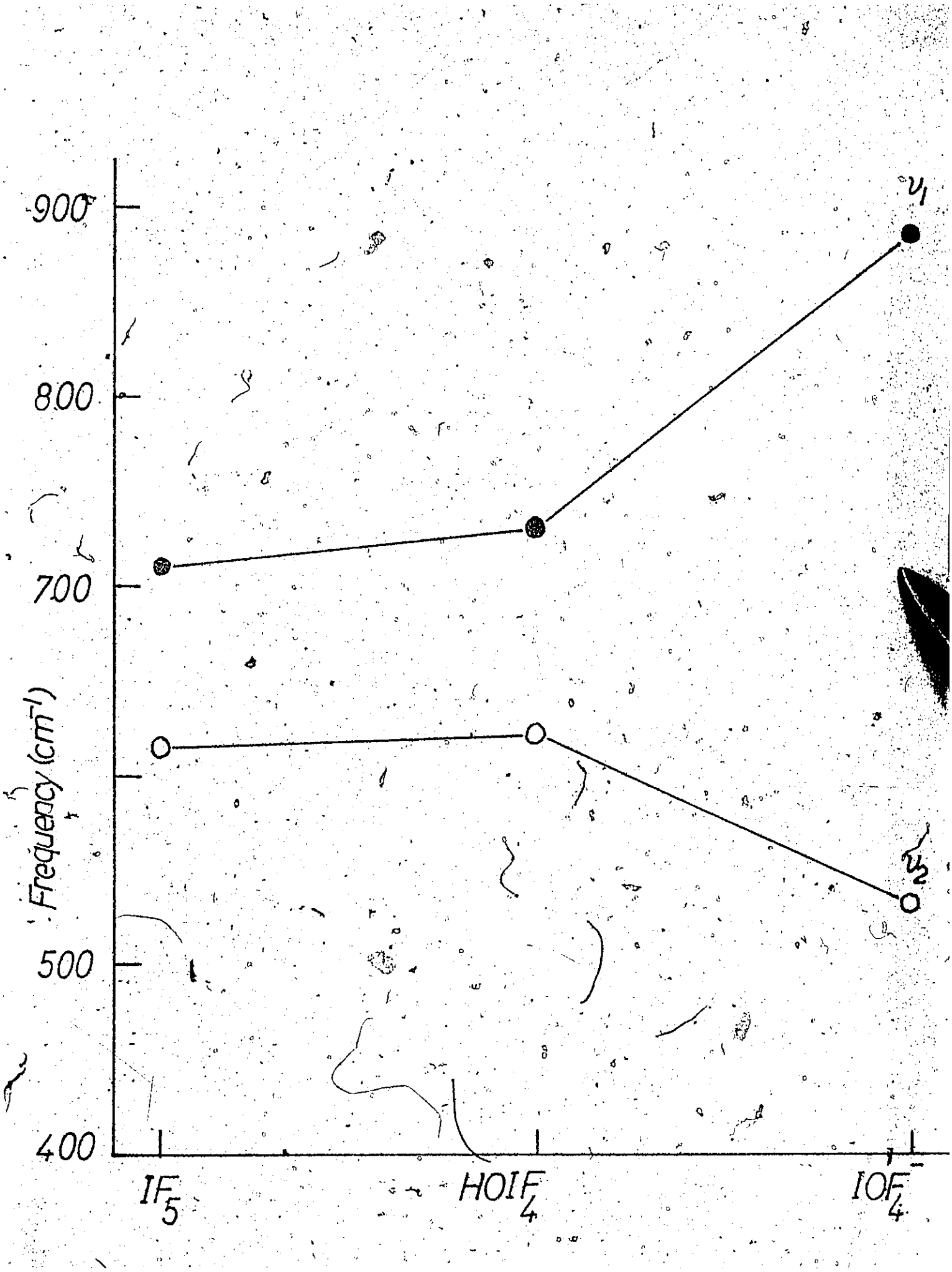
900
800
700
500
400
Frequency (cm⁻¹)
ν1
ν2
IF5
HOIF4
IOF4⁻

(iv) AO_2F_2E Species

The observed frequencies in the vibrational spectra of the C_{2v} species XeO_2F_2, $IO_2F_2^-$ and $TeO_2F_2^{2-}$ are given in Table XXXVIII. XeO_2F_2 is monomeric in the liquid phase[93], and the polarized Raman spectrum of the liquid makes the assignment in Table XXXVIII definitive. The polarized Raman spectrum of $IO_2F_2^-$ in 48% HF confirms the assignment for this ion. Since is was not possible to observe the spectrum of $TeO_2F_2^{2-}$ in solution, some of the modes in the spectrum of this ion were assigned by comparison with XeO_2F_2 and $IO_2F_2^-$. The major difficulty in the assignment for $TeO_2F_2^{2-}$ is $\nu_3(A_1)$ and $\nu_4(A_1)$, since these two modes are impossible to assign in the solid salts. However, a plot of these modes across the series XeO_2F_2, $IO_2F_2^-$ and $TeO_2F_2^{2-}$ makes their assignment in Table XXXVIII reasonably certain. This plot is shown in Figure 31.

The doubling of the (AO_2) stretching modes in these species, $\nu_1(A_1)$ and $\nu_6(B_1)$, is increasingly evident as we move to the left in the periodic chart. The observed multiplicity in both the symmetric and asymmetric (TeO_2) stretching modes in $TeO_2F_2^{2-}$ indicates the increasing degree of polymerization, over oxygen bridges, across the series.

TABLE XXXVIII

Comparison of the Fundamental Frequencies in AO_2F_2E Species(C_{2v})

Class	Mode No.	XeO_2F_2 [a]	$IO_2F_2^-$ [b]	$TeO_2F_2^{2-}$ [c]
A_1	ν_1	850	817	796
			814	781
	ν_2	537	479	404
				385
	ν_3 *	350	360	353
	ν_4 *	205	194	197
A_2	ν_5	224	220	(201) [e]
B_1	ν_6	905	851	760
				755
	ν_7	324	345	330
	ν_8	585	456	305
B_2	ν_9	315	323	279

a ref 93

b 3.0 M HIO_3 in 48% HF, this work

c $Cs_2TeO_2F_2$, this work

e estimated from $\nu_5 + \nu_9$ combination

* these modes plotted in Figure 31

Figure 31

Plot of the Stretching Modes ν_3 & ν_4 in AO_2F_2E Species

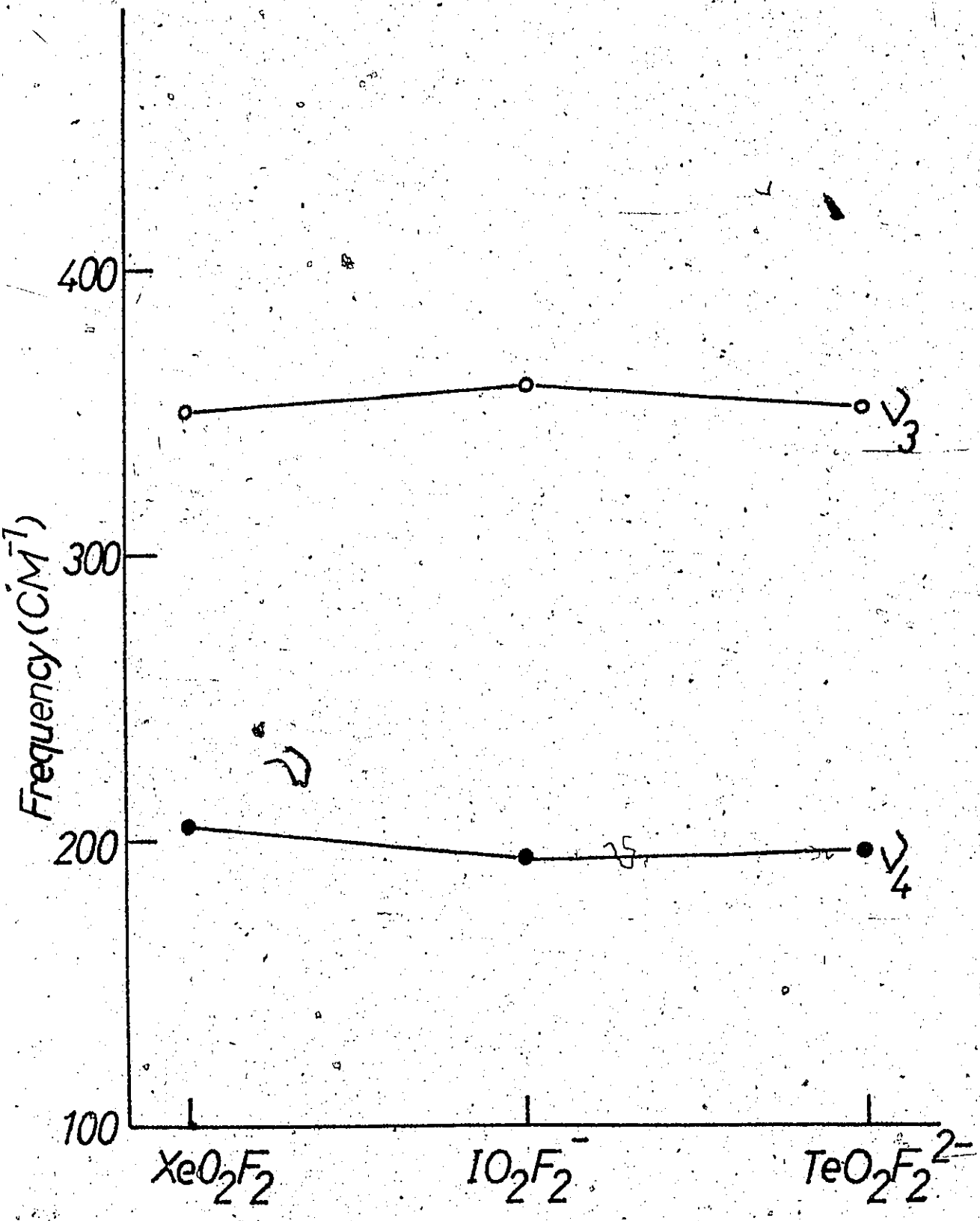
400
300
200
100
Frequency (CM^{-1})
ν_3
ν_4
XeO_2F_2
$IO_2F_2^-$
$TeO_2F_2^{2-}$

CONCLUSIONS

This chapter has shown how the isoelectronic species prepared and studied in this thesis can be correlated by comparison of their vibrational spectra. However, in Chapter I the anomalous structures of some hexahalo species was reviewed. For example, both $TeCl_6^{2-}$ and $TeBr_6^{2-}$ are reported to be octahedral[34]. This is contrary to the predictions of VSEPR theory[3]. In these few paragraphs the stereochemistry of the oxofluoro species prepared and studied in Chapters III, IV and V is reviewed, and attempts are made to rationalise the stereochemical role of the lone valence electron pair.

Prior to this study the oxyfluoride chemistry of tellurium(IV) was little studied. Three new oxofluoro anions have been prepared. Both $TeOF_4^{2-}$ and $Te(OH)F_4^-$ are five coordinate, and $TeO_2F_2^{2-}$ is four coordinate. The $5S^2$ lone valence electron pair exerts a stereochemical influence as predicted by VSEPR theory. All of the attempts to prepare compounds with coordination numbers greater than five failed. The TeF_6^{2-} ion seemingly cannot exist. However, tellurium(VI), the highest oxidation state, shows coordination numbers of up to eight[131].

Thus, tellurium(IV) in all of its known fluoro and oxofluoro species follows the predictions of VSEPR theory. In the anion $TeO_2F_2^{2-}$ evidence has been presented indicating some polymerization over oxygen bridges. In this respect tellurium(IV) is similar to the isoelectronic iodine(V) species, and unlike selenium(IV) which has a marked tendency to form fluorine bridges,

as in the case of SeO_2F^- (see Chapter V).

While the chemistry of iodine(V) resembles that of tellurium(IV) in many ways, the chemistry of iodine resembles that of xenon(VI) more than that of tellurium(IV). Iodine is in a distorted octahedral environment in the IF_6^- ion[23]. Such a distortion is predicted by VSEPR theory[3]. Chapter IV and this chapter outline the comparison of IF_5, $HOIF_4$ and IOF_4^- with the isoelectronic tellurium(IV) species. However, in addition to these species, iodine (V) forms a number of other oxofluoro species, for example IOF_3, which have no isoelectronic tellurium(IV) analogue. In 100% HF, however, the highest coordinated iodine(V) species, like the case of tellurium(IV), is the pentafluoro species IF_5.

Thus, iodine(V) in all of its fluoro and oxofluoro compounds gives evidence for the involvment of the lone valence electron pair in determining the stereochemistry of the compound as suggested by VSEPR theory.

Antimony(III) and selenium(IV) were dealt with together in Chapter V since the study presented there is essentially of an introductory nature. As was mentioned in that chapter, antimony is unique among the elements studied in that there are no known oxofluoro species in its penultimate oxidation state. Aqueous HF solutions failed to give any evidence of any oxofluoroantimonate(III) species. However, in its fluorine chemistry, antimony obeys the predictions of VSEPR theory, the lone valence electron pair being stereochemically active in all cases. As in the case of tellurium all attempts to increase the coordination number of antimony(III)

above five failed. The hexafluoro anion SbF_6^{3-} seemingly cannot exist. In fact the isolation of the bridged $Sb_2F_9^{3-}$ anion illustrates the reluctance of antimony to increase its coordination above the pentafluoro species SbF_5^{2-}.

Selenium(IV) is the least studied of all the above elements. Indeed this study has raised more questions than it has solved. The fluoro and oxofluoro species of selenium(IV) should provide much material for furthur study. Selenium little resembles tellurium in its fluorine chemistry. For example, SeO_2F^- and $SeOF_2$ are both well characterized while TeO_2F^- and $TeOF_2$ are both unknown. Furthermore, for tellurium the highest fluorinated species in 100%HF is TeF_5^- while in the case of selenium it is $SeOF_2$.

The stereochemical influence of the lone valence electron pair in the fluoro and oxofluoro species of selenium(IV) is difficult to determine in the absence of diversity of known species.

REFERENCES

1. N.Bartlett, Proc.Chem.Soc., 218 (1962)
2. N.Bartlett, Endeavour, 10, 3 (1967)
3. R.J.Gillespie, "Molecular Geometry", Van Nostrand-Reinhold, Toronto 1972
4. G.Engel, Z.Krist., 90, 341 (1935)
5. E.E.Aynsley & A.C.Hazell, Chem.Ind., 611 (1963)
6. I.D.Brown, Canad.J.Chem., 42, 2758 (1964)
7. R.M.Gavin, J.Chem.Ed., 46, 413 (1969)
8. C.L.Chernick, Record of Chem.Prog., 24, 139 (1963)
9. H.H.Claassen, G.L.Goodman & H.Kim, J.Chem.Phys., 56, 5042 (1972)
10. H.Kim, H.H.Claassen & E.Pearson, Inorg.Chem., 7, 616 (1968)
11. E.L.Gasner & H.H.Claassen, Inorg.Chem., 6, 1937 (1967)
12. G.R.Jones, R.D.Burbank & W.E.Falconer, J.Chem.Phys., 53, 1605 (1970)
13. K.Hedberg, S.H.Peterson & R.R.Ryan, J.Chem.Phys., 44, 1726 (1970)
14. R.M.Gavin & L.S.Bartell, J.Chem.Phys., 48, 2460 (1968)
15. W.E.Falconer, A.Buchler, J.L.Stauffer & W.Klemperer, J.Chem.Phys., 48, 312 (1968)
16. G.L.Goodman, J.Chem.Phys., 56, 5038 (1972)
17. L.S.Bartell & R.M.Gavin, J.Chem.Phys., 48, 2466 (1968)
18. K.O.Christe, J.P.Guertin & W.Sawodny, Inorg.Chem., 7, 626 (1968)
19. S.P.Beaton, D.W.A.Sharp, A.J.Perkins, I.Shett, H.H.Hyman & K.O.Christe, Inorg.Chem., 7, 2174 (1968)
20. H.Klamm, H.Meinert, P.Reich & K.Witke, Z.Chem., 8, 393 (1968)

21. H.Klamm, H.Meinert, P.Reich & K.Witke, Z.Chem., 8, 469 (1968)

22. S.Bukshpan, J.Soriano & J.Shamir, Phys.Chem.Lett., 4, 241 (1969)

23. K.O.Christe, Inorg.Chem., 11, 1215 (1972)

24. H.Klamm & H.Meinert, Z.Chem., 10, 227 (1970)

25. E.E.Aynsley & G.Hetherington, J.Chem.Soc., 2802 (1953)

26. E.E.Aynsley & W.A.Campbell, J.Chem.Soc., 3290 (1958)

27. F.Seel & H.Massat, Z.Anorg.Allg.Chem., 280, 186 (1955)

28. A.J.Edwards & M.A.Mouty, J.Chem.Soc. A, 703 (1969)

29. C.J.Adams & A.J.Downs, J.Chem.Soc. A, 1534 (1971)

30. C.J.Adams & A.J.Downs, Chem.Comm., 1699 (1970)

31. A.C.Hazell, Acta Chem.Scand., 20, 165 (1966)

32. K.Nakamoto, "Infrared Spectra of Inorganic Compounds" Wiley,1966

33. D.Nakamura, K.Ito & M.Kubo, J.Amer.Chem.Soc., 84, 163 (1962)

34. A.K.Das & I.D.Brown, Can.J.Chem., 44, 939 (1966)

35. E.Martineau & J.B.Milne, J.Chem.Soc. A, 2971 (1970)

36. R.A.Jacobson, Inorg.Chem., 12, 210 (1973)

37. M.C.Poore & D.R.Russell, Chem.Comm., 18 (1971)

38. K.J.Wynne, J.Chem.Ed., 50, 328 (1973)

39. A.J.Edwards, J.Chem.Soc. A, 2751 (1970)

40. D.Moffett, This Thesis p.25

41. D.S.Schroeder & R.A.Jacobson, Inorg.Chem., 12, 515 (1973)

42. J.G.Ballard, T.Birchall, J.B.Milne & D.Moffett, Can.J.Chem., 52, 2373 (1974)

43. A.Bystrom & K.-A.Wilhelmi, Arkiv Kemi, 3, 461 (1951)

44. S.H.Mastin & R.R.Ryan, Inorg.Chem., 10, 1757 (1971)

45. E.E.Aynsley, G.Hetherington & P.L.Robinson, J.Chem.Soc., 1119 (1954)

46. J.L.Hoard & B.N.Dickenson, Z.Krist., 84, 436 (1933)

47. P.J.Hendra & Z.Jovic, J.Chem.Soc. A, 600 (1968)

48. N.Bartlett, F.Einstein, D.F.Stewart & J.Trotter, J.Chem.Soc. A, 1190 (1967)

49. K.Leary, D.H.Templeton, A.Zalkin & N.Bartlett, Inorg.Chem., 12, 1726 (1973)

50. N.Bartlett, B.DeBoer, F.Hollander, F.O.Sadky, D.Templeton & A.Zalkin, Inorg.Chem., 13, 775 (1974)

51. N.Bartlett, M.Gennis, D.D.Gibler, B.K.Morrell & A.Zalkin, Inorg.Chem., 12, 1717 (1973)

52. R.D.Burbank & G.R.Jones, Science, 168, 248 (1970)

53. R.D.Burbank & G.R.Jones, Science, 171, 485 (1971)

54. H.Moissan, Compt.Rend., 135, 563 (1902)

55. A.G.Robiette, R.H.Bradley & P.N.Brier, Chem.Comm., 1567 (1971)

56. G.M.Begun, W.H.Fletcher & D.F.Smith, J.Phys.Chem., 42, 2236 (1965)

57. R.J.Gillespie & H.S.Clase, J.Chem.Phys., 47, 1071 (1967)

58. L.A.Alexander & I.R.Beattie, J.Chem.Soc. A, 3091 (1971)

59. H.Selig & H.Holzmann, Israeli J.Chem., 7, 417 (1969)

60. N.Bartlett, S.Beaton, L.W.Reeves & E.J.Wells, Can.J.Chem., 42, 2531 (1964)

61. G.R.Jones, R.D.Burbank & N.Bartlett, Inorg.Chem., 9, 2264 (1970)

62. J.W.Mellor, "Comprehensive Treatise on Inorganic and Theoretical Chemistry", Longmans London 1931 Vol.XI.

63. A.J.Edwards, M.A.Mouty, R.D.Peacock & A.J.Suddens, J.Chem.Soc., 4087 (1964)

64. N.N.Greenwood, A.C.Sarma & B.P.Straughan, J.Chem.Soc. A, 1446 (1966)

65. A.J.Högborn, Oetvers.Akad.Stockholm, 38, 1 (1882)

66. K.O.Christe, E.C.Curtis, C.J.Shack & D.Pilipovich, Inorg.Chem., 11, 1679 (1972)

67. F.A.Fluckiger, Lieb.Ann., 84, 248 (1871)

68. A.Bystrom & K.-A.Wilhelmi, Arkiv Kemi, 3, 50 (1950)

69. R.R.Ryan & D.T.Cromer, Inorg.Chem., 11, 2311 (1972)

70. T.Birchall & B.DellaVale, Can.J.Chem., 49, 2808 (1971)

71. E.E.Aynsley, R.D.Peacock & P.L.Robinson, J.Chem.Soc., 1231 (1965)

72. B.Cohen & R.D.Peacock, "Advances in Fluorine Chemistry", Eds. Stacey, Tatlow & Sharp, Butterworths, 1972

73. G.M.Begun, W.H.Fletcher & D.F.Smith, J.Chem.Phys., 42, 2336 (1965)

74. J.Martins & E.B.Wilson, J.Mol.Spectry., 26, 410 (1968)

75. R.R.Ryan & L.B.Asprey, Acta Crystallogr., Sect.B, 28, 979 (1972)

76. E.B.R.Prideaux & J.O.Millott, J.Chem.Soc., 520 (1926)

77. A.Englebrecht, W.Loreck & W.Nehoda, Z.Anorg.Allg.Chem., 360, 88 (1968)

78. J.E.Griffiths & G.E.Walrafen, Inorg.Chem., 11, 427 (1972)

79. H.Burger, Z.Anorg.Allg.Chem., 360, 97 (1968)

80. W.A.Mazeika & H.M.Neumann, Inorg.Chem., 5, 309 (1966)

81. D.E.McKee, C.J.Adams & N.Bartlett, Inorg.Chem., 12, 1722 (1973)

82. E.E.Aynsley, R.Nichols & P.L.Robinson, J.Chem.Soc., 623 (1953)

83. J.W.Viers & H.Wallace Baird, Chem.Comm., 1093 (1967)

84. A.J.Edwards & P.Taylor, J.Fluor.Chem., 4, 173 (1974)

85. R.Paetzold & K.Aurich, Z.Anorg.Allg.Chem., 348, 941 (1966)

86. A.W.Cordes, Inorg.Chem., 6, 1204 (1967)

87. J.D.McCullough & R.E.Marsh, Acta Crystallogr., 3, 41 (1950)

88. Bi.-Cheng Wang & A.W.Cordes, Inorg.Chem., 9, 1643 (1970)

89. M.Agerman, L.H.Anderson, I.Lindquist & M.Zackrisson, Acta Chem. Scand., 12, 477 (1958)

90. R.Paetzold & K.Aurich, Z.Anorg.Allg.Chem., 315, 72 (1962)

91. C.R.Wise, J.Amer.Chem.Soc., 45, 1233 (1923)

92. J.L.Huston, J.Phys.Chem., 71, 3339 (1967)

93. H.H.Claassen, E.L.Gasner, H,Kim & J.L.Huston, J.Chem.Phys., 49, 253 (1968)

94. L.Helmholtz & M.T.Rodgers, J.Amer.Chem.Soc., 62, 1537 (1940)

95. H.A.Carter & F.Aubke, Inorg.Chem., 10, 2296 (1971)

96. J.Pitts, S.Kongpricha & A.W.Jache, Inorg.Chem., 4, 256 (1965)

97. G.Mitra & P.C.Kundu, Sci.Cult., 22, 119 (1956)

98. E.B.R.Prideaux & J.O.Millott, J.Chem.Soc., 167 (1926)

99. S.Witehowa, T.Witek & T.Paryjezak, Z.Chem., 2, 55 (1962)

100. R.J.Gillespie, B.Landra & G.L.Schrobilgen, Chem.Comm., 607 (1972)

101. E.E.Aynsley, J.Chem.Soc., 2425 (1958)

102. E.E.Aynsley & M.L.Hair, J.Chem.Soc., 3747 (1958)

103. M.Schmeisser & K.Lang, Angew.Chem., 67, 156 (1955)

104. P.A.Giguere & M.Falk, Spectrochem.Acta, 16, 1 (1960)

105. A.J.Edwards & G.R.Jones, J.Chem.Soc. A, 2858 (1969)

106. R.Paetzold & K.Aurich, Z.Anorg.Allg.Chem., 335, 281 (1965)

107. E.A.Robinson, D.S.Lavery & S.Weller, Spectrochim.Acta, 25A, 151 (1969)

108. D.F.Smith, J.Amer.Chem.Soc., 85, 816 (1963)

109. J.G.Mahm, I.Sheft & C.L.Chernick, J.Amer.Chem.Soc., 85, 110 (1963)

110. H.H.Claassen & G.Knapp, J.Amer.Chem.Soc., 86, 2341 (1964)

111. F.A.Cotton & G.Wilkinson, "Advanced Inorganic Chemistry", Interscience 1966

112. J.D.Durig, O.D.Bonner & W.H.Breazeale, J.Phys.Chem., 69, 3886 (1965)

113. W.E.Dasent & T.C.Waddington, J.Chem.Soc., 2429 (1960)

114. A.D.Pethybridge & J.E.Prue, Trans.Farad.Soc., 63, 2019 (1967)

115. G.Hood, A.C.Jones & C.A.Reilly, J.Phys.Chem., 63, 101 (1959)

116. J.G.Dewbar, J.Chem.Soc., 4111 (1965)

117. M.T.Rodgers & L.Helmholtz, J.Amer.Chem.Soc., 63, 278 (1941)

118. K.W.Bagnall, "Chemistry of Selenium, Tellurium and Polonium", Elsevier, 1966.

119. H.Siebert, Z.Anorg.Allg.Chem., 301, 162 (1959)

120. J.D.McCullough, J.Amer.Chem.Soc., 59, 789 (1937)

121. G.E.Walrafen, J.Chem.Phys., 36, 90 (1961)

122. R.Paetzold & K.Amoulong, Z.Anorg.Allg.Chem., 317, 166 (1962)

123. N.T.McDevitt & W.L.Baun, Spectrochim.Acta, 20, 779 (1964)

124. "Bailsteins Handbuch der Organischen Chemie", Vol IV, Springer-Verlag, 1963, p 199, System No. 336

125. J.Hayami, N.Ono & A.Kaji, Tetrahedron Lett., 1385 (1968)

126. R.F.Weinland & D.Koppen, Z.Anorg.Allg.Chem., 22, 256 (1901)

127. A.I.Vogel, "Quantitative Inorganic Analysis", 3rd Edition, Longmans, 1966

128. N.Bartlett, S.Beaton, L.W.Reeves & E.J.Wells, Can.J.Chem., 42, 2532 (1964)

129. E.E.Aynsley, R.D.Peacock & P.L.Robinson, J.Chem.Soc., 1231 (1952)

130. R.Paetzold & K.Aurich, Z.Anorg.Allg.Chem., 315, 72 (1962)

131. H.Selig, S.Sarig & S.Abramowitz, Inorg.Chem., 13, 1508 (1974)

132. A.Englebrecht & F.Sladsky, Angew.Chem., 76, 379 (1964)

133. L.Kolditz & I.Fitz, Z.Anorg.Allg.Chem., 349, 184 (1967)

134. L.Kolditz & I.Fitz, Z.Anorg.Allg.Chem., 349, 175 (1967)

135. L.Kolditz, Pure Appl.Chem., 13, 511 (1966)

136. H.H.Claassen, C.L.Chernick & J.G.Malm, J.Amer.Chem.Soc., 85, 1927 (1963)

137. J.Leiciejewicz, Z.Krist., 116, 345 (1961)

138. V.Lorenzelli, T.Dupuis & J.LeComte, Compt.Rend., 259, 1057 (1964)

139. H.Siebert, "Anwendungen der Schwingungsspektroskopie in der anorganischen Chemie", Springer -Verlag, 1966

140. K.O.Christe, E.C.Curtis & R.D.Wilson, J.Inorg.Nucl.Chem., in press

141. D.E.Irish, "Raman Spectroscopy of Complex Ions in Solution" in "Raman Spectroscopy", ed. H.A.Szymanski, Plenum, 1967

142. W.J. Hamer & Y.Wu, J.Res.Nat.Bur.Stds., 74A, 761 (1970)

143. International Critical Tables, McGraw-Hill, 1928, Vol.III: pp.54 and 55

144. K.Fredenhagen & N.Wellmann, Z.Physik.Chem., A162, 454 (1932)

145. A.Finch, P.N.Bates & M.A.Jenkinson, J.Fluorine Chem., 2, 111 (1972)

146. H.D.Lutz, H.J.Kluppel & R.Kho, Angew.Chem.Int.Ed., 10, 183 (1971)

147. A.C.Pavia & P.A.Giguere, J.Chem.Phys., 52, 3551 (1970)

148. W.E.Dasent & T.C.Waddington, J.Chem.Soc., 2429 (1960)

149. K.Fredenhagen, Z.Anorg.Allg.Chem., 218, 161 (1934)

150. H.Klamm & H.Meinert, Z.Chem., 10, 270 (1970)

151. H.Meinert & Udo Gross, Z.Chem., 9, 190 (1969)

152. K.O.Christe & D.Natmann, Inorg.Chem., 12, 59 (1973)

153. L.Alexander & I.R.Beattie, J.Chem.Soc. A, 1745 (1972)

154. G.Oates & J.M.Winfield, Inorg.Nucl.Chem.Lett., 8, 1093 (1973)

155. M.Falk & P.A.Giguere, Can.J.Chem., 36, 1680 (1968)

156. E.L.Muetterties & W.D.Philips, J.Amer.Chem.Soc., 81, 1084 (1959)